Phenotypic impact of keratin 8/18 downregulation in colonic *in vitro* 3D cultures

Jimmy Fagersund, 1901610

Jimmy.fagersund@abo.fi

Supervisors:

Mina Tayyab, doctorate candidate

Docent Malin Åkerfelt

Associate Professor Diana Toivola

CB00BR56 Master's thesis in Cell Biology, 30 sp

Master's Programme in Biosciences, Department of Biosciences, Faculty of Science and Engineering, Åbo Akademi University

2022

Abstract

The second deadliest and third most common type of cancer is colorectal cancer (CRC). The disease mechanism is to a large extent unknown and the number of cases is on the rise in westernized countries. Interestingly, keratins [subfamily of intermediate filaments] have shown to be involved in development of both colitis and colorectal cancer. Keratins (K) occur as two different subtypes (type I and II) which form obligate heteropolymeric filaments that influence essential cellular functions such as proliferation, cell death and differentiation. Further insight is needed for the functionality of keratins; especially when it comes to colitis and CRC development. Traditional 2D culture and animal models have been utilized extensively in keratin research, but neither is ideal. *In vitro* 3D modelling is an alternative approach. By suspending cells in extracellular matrix, the cells are given an *in vivo*-like microenvironment. The aim for this project was to achieve standardized 3D models, substituting 2D culture and mouse models, and compare phenotypical differences between 2D and 3D culture caused by K8/K18 loss. Both 2D culture and 3D culture of Caco-2 cells and organoids were used to study viability, morphology, proliferation, apoptotic signaling and differentiation; and if any changes occur as a response of K8/K18 downregulation. K18 shRNA Caco-2 cells showed a slower proliferation but no viability difference in 2D culture, simultaneously as they possessed K8 and K80-positive aggregates. In 3D culture, the same cells showed an eccentric lumen formation and hampered growth. Moreover, the K18 shRNA cells showed increased protein levels of villin (in both 2D/3D). Surprisingly, K8 knockout Caco-2 cells merely showed modest differences in morphology, viability and proliferation. Finding K8-positive aggregates in K18 knockdown cells suggests that they could have caused the observed phenotypes. Further assessment is needed to determine if the aggregates are cancer-specific or if they could be an undescribed *in vivo* phenotype. The results show behavioral differences between 2D culture and 3D culture, such as proliferation and morphology, which suggests that *in vitro* 3D cultures could be a better approach to conventional 2D culture.

Table of contents

1. Introduction

The human colon is the most distal segments of the gastrointestinal tract and its basic function is to absorb residual fluids and electrolytes prior to defecation. Moreover, the colon possesses a unique architecture in a precarious position adjacent to the intestinal microbiota, which makes it susceptible to disease. The colonic epithelium has the highest turnover rate in the human body. It takes 3-5 days for the epithelium to be fully renewed (Alberts et al., 2003). Slow-dividing stem cells at the bottom of the crypt give rise to fast-proliferating transit-amplifying cells. Transit-amplifying cells are then terminally differentiated into enterocytes, goblet cells and other cell types. The epithelium is arranged in crypts and the apical epithelial layer is protected by a thick mucus layer which is inhabited by microbes (Barker et al., 2008). Bacterial species in the healthy intestinal microbiota are often represented by Firmicutes and Bacteroidetes (Zhang and Li, 2014). It is a delicate predicament, as the epithelium and mucus constitute the sole barrier against infection. Idiopathic and chronic inflammation of the colon, i.e. inflammatory bowel disease (IBD), is a disease that is suggested to be caused by epithelial dysfunction, dysbiosis and abnormal immune response (Kumar et al., 2018). Furthermore, long-term chronic inflammation is a risk factor to develop colorectal cancer (CRC). Both IBD and CRC are prevalent in developed countries and are on the rise in developing countries (Bray et al., 2018; Molodecky et al., 2012). Screening for CRC is complicated, as symptoms are rarely specific and tumorigenesis can go unnoticed for a long time (Kumar et al., 2018). There is need for further understanding of IBD and CRC pathogenesis.

Keratins (K) are intermediate filament proteins that can be found in epithelial tissue, such as the colonic epithelium. They provide the epithelium with mechanical resilience but are also involved in multiple essential functions, such as migration, proliferation, apoptosis and differentiation (Toivola et al., 2015). In the human colon, the main type II keratin is K8, as K18, K19 and K20 are the main type I keratins (Polari et al., 2020). Keratin proteins of both types are needed to form the obligate heteropolymeric filaments in the cytoplasm. K8 is one of the most studied keratins and is pivotal for colon homeostasis (Polari et al., 2020). Full body knockout (KO) mice ($K8^{-/-}$) experience a colitis-like disease picture that manifests with fragile and hyperplastic lesions coupled with diarrhea and chronic inflammation (Baribault et al.,

1994). On a molecular level, the loss of K8 has been shown to cause altered ion transport, increased hyperproliferation, decreased rate of apoptosis (Asghar et al., 2015) and abnormal differentiation patterns (Lähdeniemi et al., 2017) of the colonic epithelium by affecting Notch signaling, ion transporter localization and levels of anti-apoptotic proteins. In addition, loss of K8 has also been shown to provide an increased susceptibility to tumorigenesis in colon cancer models of mice (Misiorek et al., 2016).

Animal models have been an indispensable asset when studying the role of keratin in the intestine and several other organs (Polari et al., 2020). At the same time, there is an increasing need for alternative approaches, as the use of laboratory animals is expensive, laborious and ethically questionable. In addition, there is need for a 3D platform suitable for studying the role of keratins in the context of colonic health and CRC development.

In recent years, organoid research and usage of *in vitro* 3D models have increased in popularity. It can partially be accredited to Hans Clever's research group, who was first in presenting a protocol for culturing adult stem cells (ASC) from small intestine *in vitro* (Sato et al., 2009). Since then, various *in vitro* models have surged as the extracellular environment seen *in vivo* can be mimicked by providing adequate extracellular matrix and growth factors (Corrò et al., 2020). Nevertheless, there are currently few 3D assays that allow high-throughput analysis of 3D cultures. This would be useful in acquiring a large sample size for studying morphology, phenotypes, and drug screening of organoids. Moreover, there is a need for standardized 3D culture assays (Härmä et al., 2014). Härmä et al. have developed a 3D platform that is standardized, automatized, and optimized for tumor spheroid culture. The spheroids are first stained with live cell dyes and then imaged using automatized confocal microscopy. The images are consequently processed using the AMIDA (automated morphometric image data analysis) software. The approach allows assessment of morphometric and phenotypical parameters of 3D cultures and is also complemented by quality control and statistical tools (Härmä et al., 2014). We wanted to implement this methodology for studying keratins in a colonic context.

The purpose of this project was to take a novel approach to study K18/K8 by culturing transgenic Caco-2 cells and colon-derived organoids from conditional K8 KO mice. We examined (in both 2D/3D) cellular parameters such as viability, morphology,

proliferation, rate of apoptosis and differentiation capacity, and compared them in 2D versus 3D culture. In addition, we assessed alterations in keratin composition as a result of K18/K8 downregulation.

The results showed that loss of K18 in Caco-2 cells caused several phenotypes in viability, proliferation and 3D morphology. In addition, the Caco-2 K18 shRNA (knockdown) cells possessed aggregates containing K8 and less-described K80. Caco-2 K8 KO cells showed less phenotypical differences but could be useful for *in vitro* applications and perhaps reveal other novel phenotypes upon exposure to stress. Our results show that cell behavior differs between 2D and 3D culture in several aspects, such as proliferation, viability and morphology, which suggests that *in vitro* 3D cultures could be a better alternative to conventional 2D culture.

2. Literature overview

2.1 Colon

2.1.1 Anatomy and physiological function

The colon is a major part of the large intestine in the gastrointestinal tract. In humans, it is approximately 1.5 m in length and 6.5 cm in diameter and can be divided into four constitutive segments: ascending, transverse, descending and sigmoid colon (fig. 1; left). The colon receives the luminal content from the small intestine and mediates the transport of the feces to the rectum prior to defection (Saladin, 2008). As the small intestine is primarily responsible for nutritional uptake, the colon is the organ that manages the intake of water and salt prior to fecal excretion. (Saladin, 2008). The colon can take up approximately 1.5 l fluid daily under physiological conditions. The colonic epithelium possesses ion transporters which allow electrolyte uptake, thus making the colon a specialist regarding water and electrolyte absorption (Kunzelmann and Mall, 2002). The colonic wall can be divided into four different tissue layers (fig. 1; right) The innermost layer of the intestinal wall forms the border between the luminal content and the colonic wall is called the mucosa, containing the simple columnar epithelium and lamina propria. The following profound layers are the submucosa, the muscle layers (muscularis) and the serosa (or peritoneum) (Kierszenbaum and Tres, 2016).

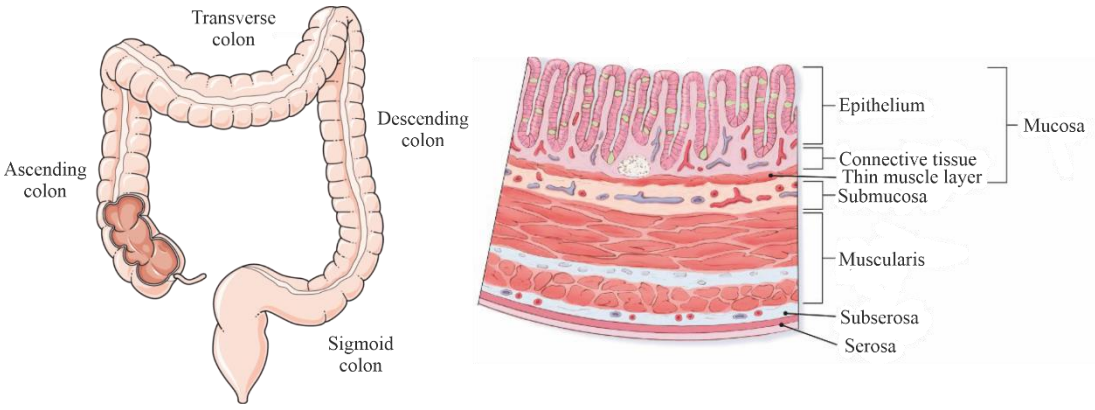

Figure 1. Anatomy of the colon and the colonic wall. Images modified from Servier Medical Art (licensed under a Creative Common Attribution 3.0 Unported License) and American

Cancer Society (<www.cancer.org/cancer/colon-rectal-cancer/about/what-is-colorectal-cancer>. Accessed 15.10.2021).

2.1.2 The colonic crypt

The colon mucosa has a simple columnar epithelium that is arranged into crypts (fig. 2; left). In contrast to the epithelial architecture of the small intestine with protruding villi and cavernous crypts coupled with extensive folding, the colonic epithelium is merely arranged into longer glandular crypts coupled with substantial mucous secretion. The intestinal epithelium has one of the highest turnover rates in the human body (3-5 days) and is continuously renewed to persevere and maintain the intestinal barrier (Sugimoto et al., 2018; Alberts et al., 2003). The colonic stem cells are slow-dividing multipotent stem cells located at the bottom of the crypts. By asymmetric cell division, the stem cells can produce highly proliferative transit-amplifying cells simultaneously as one daughter cell remains as a stem cell. The transit-amplifying cells then move towards the top of the crypt as they are proliferating and are then terminally differentiated to produce all the different cell types of the colon epithelium (fig. 2; right). As the differentiated cells reach the surface epithelium, they are progressively discarded or shredded off by a process called anoikis (Barker et al., 2008).

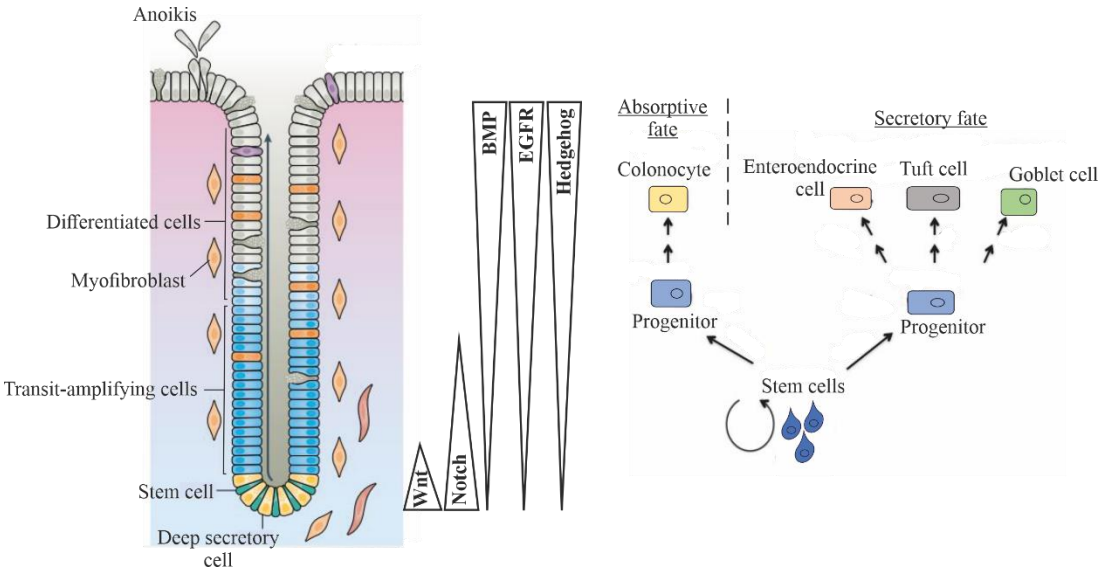

Figure 2. The colonic epithelium and its morphological gradients and epithelial differentiation. (**Left**) The slow-dividing stem cells at the bottom of the colonic crypt produce fast-diving transit-amplifying cells which produce all the differentiated cell types of the epithelium. Cells migrate from apically from the crypt bottom and shred off (anoikis) into the

luminal space, as they are continuously renewed. (**Middle**) Morphological gradients (or signaling pathways) that govern cell fate determination. Wnt/β-catenin (Wnt) and Notch signaling pathways help maintain stem cells while Bone morphogenetic protein/transforming growth factor β (BMP) signaling pathway, Epidermal growth factor receptor (EGFR) signaling pathway and Hedgehog signaling pathway promotes differentiation. (**Right**) Stem cells produce absorptive and secretory progenitors that produce all the differentiated cell types of the colon epithelium. Figure partially modified from Beumer & Clevers, 2021.

2.1.3 Stem cells and the stem cell niche

The intestinal stem cells can be recognized as they express a stem cell marker called leucine-rich-repeat-containing G protein-coupled receptor 5, also known as Lgr5 (Barker et al., 2007). In the small intestine, these cells are intermingled with Paneth cells. Paneth cells secrete antimicrobial peptides, but also provide the stem cells with appropriate signals to maintain the stemness of the lgr5-positive cells. The stem cell niche is characterized by high levels of Wnt ligands and Notch ligands (fig. 2). provided by Paneth cells. The Paneth cells are long-lived cells that can survive up to 2 months and are localized to the niche (Beumer and Clevers, 2021). Interestingly, Paneth cells are restricted to the small intestine and do not normally occur in the colon (Kierszenbaum and Tres, 2016). Also, there still seems to be an ambiguity in the current literature concerning how the colonic stem cell niche works, as it is often vaguely referred to as the intestinal stem cell niche. Sasaki et al. have suggested that Reg4-positive Deep secretory cells (DSC) are the equivalent to Paneth cells in the colon (Sasaki et al., 2016). Wu et al. have also suggested that a newly identified subset of stromal cells provide Wnt stimulation in the colon crypts (Wu et al., 2021). Nonetheless, the niche is a complex compartment influenced by the surrounding microenvironment and stromal cells. It remains to be fully defined and acknowledged by the scientific community.

2.1.4 Differentiated cell types

Progenitor cells, which are leaving the intestinal stem cell niche, start proliferating upon loss of Wnt signals (fig. 2; middle). Ephrin B receptors (expressed by DSCs) and Eph B ligands (expressed by differentiating cells) interaction creates a repellent force

that pushes cells towards the surface epithelium (Alberts et al., 2003). Notch signaling determines which cells will differentiate into the absorptive and secretory lineages as they are leaving the crypt (fig. 2; right) Absorptive cells, or colonocytes, are the main differentiated cell type of the absorptive lineage. They are responsible for the water and nutrient absorption and the most abundant cell type of the epithelium. The cell types of the secretory lineage are goblet cells, tuft cells and enteroendocrine cells (Beumer and Clevers, 2021). Goblet cells are the cells that produce mucus which lubricates the mucosal wall. They are the most abundant cell type of the secretory cell lineage and can be identified by protein markers such as mucin 2. Mucins are high-molecular hygroscopic glycoproteins that provide the gel-like properties to the mucus (Kim and Ho, 2010). Enteroendocrine cells (EECs) are chemosensory cells that constitute <1% of the epithelial cells and can secrete various hormones to modulate functions, such as nutrient absorption, immune response, and bowel movement (Yu et al., 2020). The least characterized cell type of the secretory lineage are tuft cells. They constitute a small fraction of the cells in the colon epithelium and are proposed to have a sensory role. Nevertheless, the role of tuft cells still needs to be elucidated (Gerbe and Jay, 2016).

As cellular signaling is indispensable for colonic homeostasis and differentiation, the following chapters will give an overview of the fundamental signaling pathways in the colon (Notch, Wnt/β-catenin, BMP/TGF-β and Hedgehog signaling pathways).

2.1.5 Notch signaling

The earliest studies of Notch dates back to the 1910s, when “notched wings” in mutated *D. melanogaster* was observed in a genetics study. As the phenotype was later shown to be associated with a novel signaling pathway, it would also provide the name for Notch signaling (Siebel and Lendahl, 2017). In contrast to conventional signaling pathways that are initiated based on membrane-bound receptor and free ligand interaction, both Notch ligands and receptors are membrane-bound and, thus, Notch signaling functions via cell-to-cell interaction. There are two different variants of Notch signaling pathways: the canonical and the non-canonical. For simplicity, only the canonical Notch signaling is covered in this chapter.

In mammals, there are four different Notch receptors (Notch 1-4) and Notch ligands: delta-like (Dll1, Dll3 and Dll4) and Jagged (Jag1 and Jag2) (Sjöqvist and Andersson, 2019). Structurally, these proteins are large single-pass transmembrane proteins with several intra- and extracellular domains (fig. 3). Upon initiation of Notch signaling, there is a signal-receiving cell and signal-sending cell. The cell with more ligands than receptors constitute the signal-sending cell and vice versa. Ligand-binding to the receptor causes two consecutive proteolytic cleavages of the receptor. Gamma-secretase executes the second cleavage which releases the Notch Intracellular Domain (NICD) which, consequently, translocates to the cell nucleus. NICD binds to transcriptional regulator CSL, which causes further binding of co-activators to form a transcriptional complex that regulates transcription of Notch target genes (Siebel and Lendahl, 2017). Nevertheless, this overview merely scratches the surface of the complexity as several other mechanisms exist that regulate receptor-ligand affinity, signal transduction, and amplification of the Notch signaling pathway.

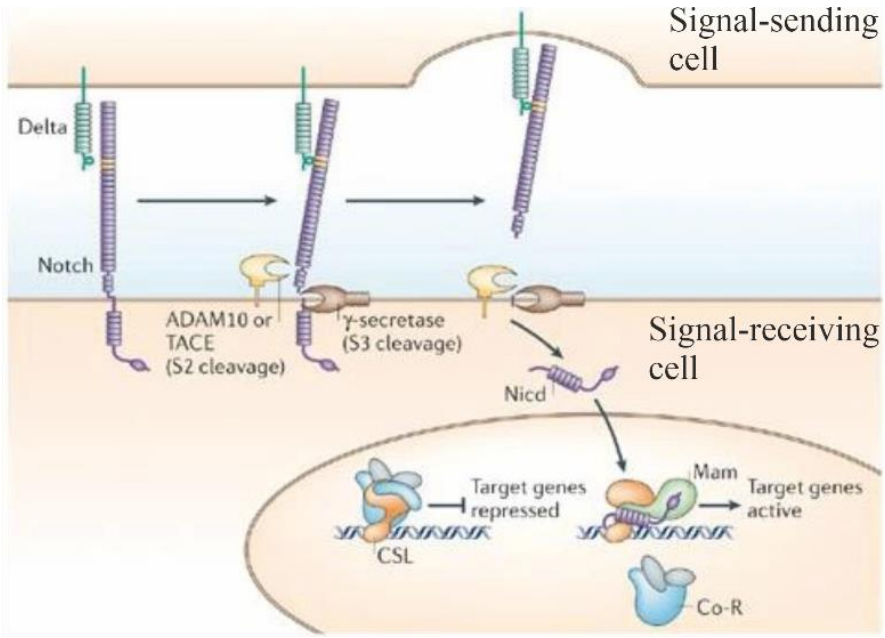

Figure 3. The canonical Notch pathway is mediated via cell-to-cell interaction. A signal-sending cell presents its ligand (e.g. Delta) to a Notch receptor of a signal-receiving cell. The binding causes two consecutive cleavages (S2 cleavage and S3 cleavage) of the Notch receptor. S2 cleavage is mediated by ADAM10 or TACE (TNF-α-converting enzyme) metalloprotease, which provides the substrate for S3-cleavage. The S3-cleavage by γ-secretase releases the Notch intracellular domain (NICD) to translocate to the nucleus. NICD can then

regulate target gene expression by binding to co-activators (such as Mam or Mastermind) or co-repressors (co-R). CSL (DNA-binding transcription factor) facilitate the formation of the transcription complex. Figure is modified from Bray, 2006.

Notch signaling, in an intestinal context, functions by maintaining homeostasis and differentiation of the epithelium. Both Wnt and Notch signaling pathways are indispensable to maintain the stem cell pools in the crypts. Upon leaving the stem cell niche, high levels of Notch1 promote cells to differentiate into the absorptive lineage, as low levels of Notch1 drive cell differentiation into the secretory lineage (Siebel and Lendahl, 2017).

2.1.6 Wnt/β-catenin signaling pathway

Wnt/β-catenin signaling is a highly conserved signaling pathway, as seen from studies with *Xenopus* and *Drosophila*. *Int-1* gene (later named the *Wnt1* gene) was identified 1982 as a potential pro-oncogene. Contemporarily, the wingless (wg) gene was identified as a modulator that controls segment polarity during larvae development in *D. melanogaster* (Clevers and Nusse, 2012). Wnt1 and wingless would later become recognized as homologs.

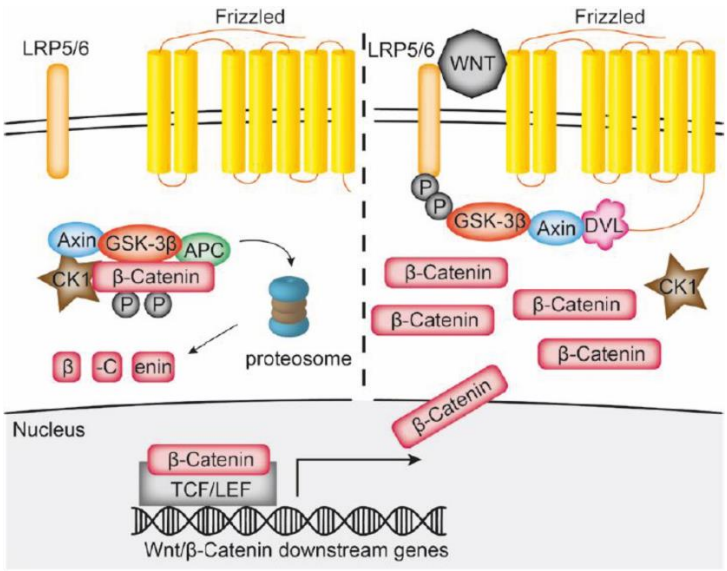

Figure 4. The canonical Wnt signaling pathway. In absence of Wnt ligands, β-catenin is continuously degraded. When Wnt is bound to Frizzled and LRP5/6 receptors, Dishevelled is recruited to the receptor complex and sequesters GSK-3β and Axin from the degradation complex. β-catenin can then translocate to the nucleus and regulate transcription of Wnt/β-

catenin target genes. Abbreviations: Low-density lipoprotein receptor-related protein 5/6 (LRP5/6), Glycogen synthase kinase 3β (GSK-3β), Adenomatous polyposis coli (APC), casein kinase-1 (CK1), Dishevelled (DVL), T-cell factor-1 (TCF), Lymphoid enhancer-binding factor-1 (LEF). Figure is modified from Kassumeh et al, 2021.

Wnt/β-catenin signaling pathway is also referred to as the canonical signaling pathway, as there are also other Wnt signaling pathways that work in different cytological contexts (Clevers and Nusse, 2012). The canonical signaling pathway governs over β-catenin-dependent target genes that are involved in functions, such as stem cell renewal, proliferation and cell differentiation (Steinhart and Angers, 2018) during embryonal development and tissue homeostasis (MacDonald et al., 2009). Wnt proteins are secret growth factors (or morphogens) that function by paracrine or autocrine fashion. In absence of Wnt signals, intracellular β-catenin is continuously translated and consequently targeted for proteasomal degradation (fig. 4). The degradation is mediated by a "degradation complex" composed of proteins: Axin, Adenomatous polyposis coli protein (APC), casein kinase (CK1) and glycogen synthase kinase 3 (GSK3) (MacDonald et al., 2009). Wnt protein binds to an appropriate Frizzled family protein receptor and its co-receptor low-density lipoprotein receptor related protein 5/6 (LRP 5/6) at the cell surface. Receptor activation (Wnt-Frizzled-LRP5/6) causes recruitment of cytoplasmic Dishevelled and GSK3-Axin complex. Sequestration of Axin renders the destruction complex non-function, thus inhibiting degradation of β-catenin. β-catenin is then translocated to the nucleus where it functions as a co-activator by binding to DNA-binding protein of the T-cell factor-1/lymphoid enhancer-binding factor-1 (TCF/LEF) family (fig. 4). Target genes of Wnt/β-catenin signaling cell type and context-dependent, but generally believed to target genes associated with cell cycle progression and stem cell maintenance (Steinhart and Angers, 2018).

In a colonic context, Wnt signaling is restricted to the stem cell niche at the bottom of the crypt with a morphological gradient. In the small intestine, Paneth cells provide Wnt growth factors, as in the colon, Wnt is suggested to be secreted from mesenchymal cells (Beumer and Clevers, 2021). Recently, Wu et al. identified a subset of stromal cells that secrete Wnt agoinst R-spondin 1 in the colonic stem cell niche. It is also suggested that these cells participate in a regeneration of damaged intestine

(Wu et al., 2021). Wnt/β-catenin signaling pathway has gotten considerable attention as mutated APC causes constant Wnt stimulation and contributes to hyperproliferation and CRC development (Schneikert and Behrens, 2007). Similarly, transgenic mice harboring a stabilized form of β-catenin gave rise to intestinal adenomas (Harada et al., 1999). Therefore, Wnt signaling is essential for normal colon physiology but also play a role in cancer development.

2.1.7 Bone morphogenetic protein/Transforming growth factor β signaling pathway

Bone morphogenetic proteins (BMPs) are secreted growth factors that are important for bone and cartilage formation, hence the name. They are important during embryonal development and needed for adult tissue homeostasis. BMPs belong to the superfamily of Transforming Growth Factor-β proteins that encompass many growth factors, such as TGF-βs, activins and inhibins (Wang et al., 2014). A simplistic overview of the BMP/TGF-β signaling pathway can be described as following:

Membrane-bound type I and type II serine/threonine kinase receptors dimerize upon binding to a BMP ligand. Receptor activation triggers formation of a heterotetrameric complex which, consequently, allows the type II receptor to phosphorylate the type I receptor at the intracellular domains. Phosphorylation of the intracellular domain of the type I receptor allows further phosphorylation of intracellular downstream targets called receptor-regulated Smads (R-Smads). R-Smads form complexes with co-mediator smads (co-Smad) which are then translocated to the nucleus and regulate gene expression of target genes (Wang et al., 2014).

In the colon epithelium, BMPs (BMP2 and BMP4) are secreted from mesenchymal cells located apically in the mucosa, simultaneously as BMP inhibitors (e.g. Noggins) are secreted from the stromal cells at the bottom of the crypt. Phosphorylated Smads (i.e. BMP stimulation) repress stem cell-associated genes and restrict the stem cell pool to the bottom of the crypt (Beumer and Clevers, 2021). Interestingly, it has been acknowledged that inactivation of the BMP/TGF-β signaling pathway is associated with the majority of sporadic CRC cases (Kodach et al., 2008).

2.1.8 Hedgehog signaling pathway

In concordance to aforementioned pathways, Hedgehog signaling pathway is no exception, as it plays an integral role in cell growth and differentiation in various types of adult tissue. It has been hypothesized that abnormal Hedgehog signaling could contribute to hyperplasia and even dysplastic changes in the gastrointestinal tract, as well as other tissue types (Wu et al., 2017). In the mammalian gastrointestinal tract, there are two secreted Hedgehog growth factors: Sonic Hedgehog (Shh) and Indian Hedgehog (Ihh). These growth factors bind to the transmembrane receptor Patched 1 (Ptc1), which activates transmembrane receptors Ptc and Smo. In absence of the growth factors, Ptc is remained dormant by Smo via an unknown mechanism. Receptor activation causes subsequent activation of Smo (a G protein-coupled receptor-like transmembrane protein) which conveys the signal intracellularly. Smo can activate several downstream targets through Gli family proteins (Gli 1-3) which function as the last mediators of the signaling cascade. Gli proteins are incorporated in suppressor complexes within the cytoplasm, but released and translocated to the nucleus upon activation by Hedgehog growth factors. Aberrant activation of Hedgehog signaling is associated with tumorigenesis in various tissues, but it is still unclear if excessive Hedgehog signaling contributes to CRC development (Wu et al., 2017).

2.2 Colon diseases

2.2.1 Inflammatory bowel disease

Inflammatory bowel disease (IBD) is a multifactorial disease that results from complex interplay between gut microbiota and patients with genetic predisposition that consequently results in abnormal immune response in the mucosa. Ulcerative colitis (UC) and Crohn's disease (CD) constitute the two subtypes of IBD, where the former is limited to colon and rectum and restricted to mucosa and submucosa. Based on a systematic review, the highest reported prevalence of UC and CD were 505 and 322 per 100,000 persons, respectively, in Europe between 1930 and 2008. Moreover,

a majority of the studies showed an increasing incidence over time, especially in westernized regions, e.g. Europe and North America (Molodecky et al., 2012).

CD can manifest as skip lesions throughout the gastrointestinal tract in combination with transmural inflammation. The intestine is often the most affected site. Although the pathogenesis for IBD still needs to be elucidated, many researchers believe it is a synergy of epithelial dysfunction, abnormal immune response and dysbiosis (i.e. unfavorable bacterial flora) (Kumar et al., 2018). Environmental factors that can contribute to development of IBD are high-fat and sugary foods, tobacco smoking, psychological stress and medications. In terms of genetic factors that contribute to IBD development, approximately 30 risk loci have been identified that are shared between UC and CD. Analysis of the genes in question shows that they play integral parts in epithelial barrier function, innate and adaptive immunity, regulation of immune response, cell migration and autophagy, thus, encompassing several mechanisms essential for intestinal homeostasis (Guan, 2019). Mutated nucleotide-binding oligomerization domain 2 (*NOD2*) is found in approximately 30% of CD patients and was also the CD-associated gene discovered. Functional NOD2 protein is believed to be an intracellular sensor of bacterial components, e.g. identifying peptidoglycan fragments derived from bacterial cell wall, and further initiating a pro-inflammatory response. In addition, NOD2 is also thought to be involved in autophagy. Autophagy is the cellular recycling process that degrades organelles and cytosolic content, but is also involved in infection control by removing intracellular bacteria. Single nucleotide polymorphisms of Autophagy-related 16-like 1 (*ATG16L1*) is another risk locus for IBD. ATG16L1 is normally, together with NOD2, important for the autophagy machinery and therefore a defense against bacterial infection (Guan, 2019). There are less known UC-associated genes in comparison with CD-associated genes. However, there are multiple class II major histocompatibility (MHC class II) variants that have been predominantly linked to UC, which can interfere with the immune function (Cho and Brant, 2011).

Several studies have examined the intestinal microbiota of healthy patients in comparison with the ones of UC and DC patients. Common traits in the microbiota of IBD patients were a reduced diversity of bacterial species in fecal samples and a more unstable microbiota compared to healthy individuals. Firmicutes and Bacteroidetes are generally the predominating phyla of bacterial species in the intestinal microbiota of

healthy patients. Absence of Firmicutes and Bacteroidetes is associated with both subtypes of IBD. While an overrepresentation of enterobacteria has been observed in CD patients, an increased abundance of *Escherichia coli* (*E. coli*) and lack of Clostridium species have been observed in UC patients (Zhang and Li, 2014).

2.2.2 Colorectal cancer

Colorectal cancer (CRC) is the third most common cancer subtype but ranks second in mortality. In 2020, there was over 1.9 million new CRC cases and approximately 940,000 deaths globally (fig. 5)(Sung et al., 2021). Westernized areas, such as Europe and North America, represent the areas with highest reported incidences. Old age, IBD, smoking, obesity, diabetes, excessive alcohol consumption and high intake of red and processed meats are environmental factors that can predispose for CRC. On the contrary, moderate levels of exercise have shown to have a preventive effect against the disease development.

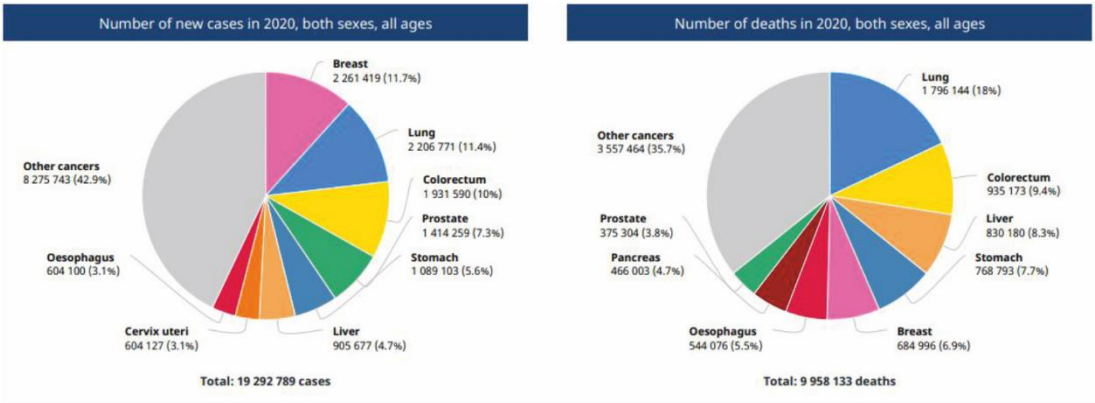

Figure 5. Number of cancer cases and cancer deaths. The left circle graph represents the number of new cancer cases (2020) for both sexes and all ages. The right circle graph represents the global number of deaths by cancer in 2020 (both sexes, all ages). Figure was acquired from Globocan 2020 (Sung et al., 2021).

CRC is a progressive disease that can develop over 10 years time, hence, the median age for diagnosis is approximately 70 years. The tumors generally start out as dysplastic lesions that acquire pro-tumorigenic mutations that exacerbate the disease further into *in situ* adenoma and, consequently, malignant adenocarcinoma. This slow

multistep development of CRC is called the adenoma-carcinoma sequence. For example, mutation of the *APC* gene is an early genetic alteration that occurs in over 70% of all colorectal adenomas (Brenner et al., 2014). CRC development can either occur sporadically or concomitant with inherited cancer syndromes. The hereditary form constitutes 3-5% of all CRC cases, the most common types are Lynch syndrome and familial adenomatous polyposis coli (FAP) (Brenner et al., 2014). FAP is characterized by an autosomal dominant inheritance of mutated *APC* gene. FAP manifests a high abundance (> 1,000) of polyps throughout the colon and can be observed prior to 30 years of age (Kumar et al., 2018). Lynch syndrome is characterized by an abundance of poorly differentiated tumors (usually located to the right side of the colon) as a consequence of dysfunctional DNA mismatch repair system. The diagnosis of Lynch syndrome is based on identification of inherited mutations, where *MLH1* or *MSH2* mismatch-repair genes are the most commonly mutated. Mutation of *MutL homolog 1* (*MLH1*) and *MutS homolog 2* (*MSH2*) can cause changes in lengths of repetitive DNA sequences known as microsatellites. Microsatellite instability (MSI) can, consequently, create wide-spread genetic alterations that contribute to an increased mutational burden in CRC development (Sinicrope, 2018). Furthermore, persistent chronic inflammation associated with IBD increases the risk for developing CRC. The risk is higher 8-10 years after the initiation of IBD and frequent inflammation also promotes carcinogenesis (Kumar et al., 2018). CRC is generally known as a heterogenous disease with a repertoire of genetic and epigenetic abnormalities that progressively promote cancer development. In addition to *APC* and DNA mismatch repair genes, other common abnormalities are mutated tumor suppressor gene *TP53* and CpG island hypermethylation phenotype (CIMP) (Kumar et al., 2018).

2.3 Cytoskeleton

2.3.1 Overview of the cytoskeleton

The cytoskeleton is considered the structural framework of the cell and provides its shape. The cytoskeleton of the mammalian cell consists of a tripartite set of filaments that are functionally indispensable for normal cell function. The three sets of filaments are microfilaments, intermediate filaments, and microtubules. Although, septins have gotten recognition as the fourth group of cytoskeletal filaments in recent years.

Microfilaments are the thinnest filaments formed from globular actin (G-actin) monomers that consequently are polymerized into filamentous actin (F-actin). The monomers are ATP-dependent for assembly and rely on actin-binding proteins to facilitate their assembly, stability, and disassembly. In terms of functionality, actin filaments are responsible for generation of mechanical forces that modulate cell shape and cell motility (Fletcher and Mullins, 2010).

Similar to microfilaments, microtubules are also built from nucleotide-dependent dimers, possess a directionality and rely on accessory proteins for filament stabilization and dynamics. Microtubules are the stiffest filaments among the cytoskeletal filaments and a single microtubule can span the full length of a typical animal cell. The branched network of microtubules function as highway for intracellular transport during interphase and play an integral part in formation of the mitotic spindle during mitosis (Fletcher and Mullins, 2010). Septins are non-polar hetero-oligomers that can further polymerize into larger filaments of various conformation, such as rings or lattices. Together with microfilaments and microtubules, septins have a scaffolding role in e.g. cell morphogenesis and small-scale bending of membranes. They are also involved in cellular functions such as cell division and cell migration (Woods and Gladfelter, 2021).

2.3.2 Intermediate filaments

Named after their intermediate diameter relative to microfilaments and microtubules, intermediate filaments (IFs) are highly conserved family of proteins in all vertebrae.

A single IF protein structurally consists of two highly conserved central α-helical domains (central rod) that is flanked by two variable open N- and C-terminal domains (head and tail) (Eriksson et al., 2009). The central rods have an integral role in interaction between IF monomers and forming apolar IF tetramers. Consequently, eight tetramers are further associated into octameric structural unit via lateral interaction, that corresponds to a single unit length filament (ULF) (fig. 6). The formation and growth of mature filament are based on longitudinal associations of ULFs which represents the 10 nm thick intermediate filaments (Etienne-Manneville, 2018). IFs are the most flexible and elastic out of three sets of cytoskeletal filaments, capable being stretched 3.6-fold its own length (Kreplak et al., 2005). IFs distinguish themselves from microfilaments and microtubules, as they are independent of nucleotides for assembly, lack directionality and are independent of cofactors for assembly *in vitro* (Etienne-Manneville, 2018).

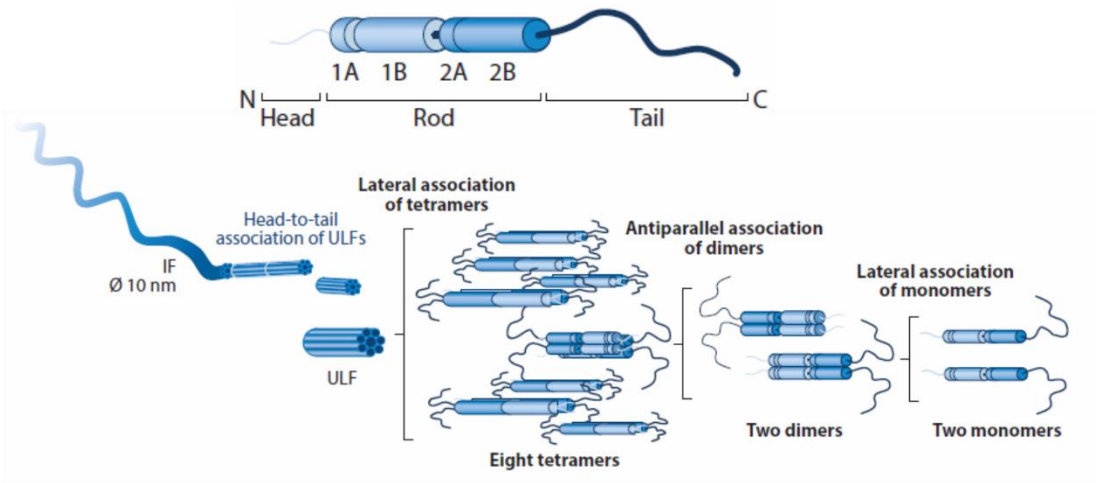

Figure 6. General structure of IFs and their assembly. (**Top**) An IF protein can be divided into three different domains: head, rod and tail domains. The rod domain is the most conserved domain and consists of 4 sub-helices (1A, 1B, 2A and 2B) separated by linker regions. (**Bottom**) IF-monomers initially form parallel dimers and then further two dimers associate into an antiparallel tetramer. Consequently, eight tetramers form a unit-length filament (ULF) which associate into the mature longitudinal filaments. Figure is modified from Etienne-Manneville, 2018.

Classification of IF proteins is based structure and sequence homology and IFs are divided into six (I-VI) different classes. Type I and II IFs represent acidic and neutral/basic keratins respectively, where type I and II keratins form obligate heterodimers in 1:1 stochiometric ratio. Keratins are generally expressed in epithelial

cells. Type III IFs include proteins such as vimentin, desmin, glial fibrillary acidic protein (GFAP), peripherin and syncoilin. Vimentin is expressed in mesenchymal cells (e.g. fibroblasts) while desmin and syncoilin are associated with muscle cells. GFAP can be found in e.g. astrocytes. Type IV IFs consist of α-internexin and nestin (expressed in neural tissue), and synemin is expressed in muscle cells, but in less abundance than desmin (Etienne-Manneville, 2018). Nuclear lamins constitute the fifth IF-group. Lamin proteins collectively form a structural meshwork at the inner side of the nuclear envelope (Xie and Burke, 2016). The sixth and final group represent IF proteins filensin and phakinin, which constitute their own distinct group of lens-specific proteins (Goulielmos et al., 1996).

From a time perspective, IFs had first been observed by using brightfield microscopy coupled with silver staining in the 1930s. In the mid-to-late 1970, researchers were able to isolate, solubilize and purify several IF proteins. They were also studied using electron microscopy, which consequently would give rise to the classification of IF proteins and a reputation of being architectural proteins that provide structural integrity to the cell. This would remain as the prevailing view into the 1990s and would soon after starting to get more recognition as multifunctional and versatile family of proteins, especially as IFs have shown involvement in several diseases (Eriksson et al., 2009).

2.3.3 Keratins

Keratins (K) constitute a major group of IFs that are abundantly expressed in epithelia (Toivola et al., 2015). These proteins are structurally shaped as rods with a central α-helical domain and terminal head/tail domains (further described in *2.3.4*). Type I/II keratins form non-covalent obligate heteropolymeric filaments. In humans, keratins are derived from 54 unique functional genes and they can be divided into type I (K9-40) and type II (K1-8, K71-86) keratins (Toivola et al., 2015). An important attribute of keratins is that specific keratins are paired primarily in a epithelial cell and differentiation state-selective manner (Omary et al., 2009). For example, the basal cells of the epidermis express K5/K14 pairs, as differentiated keratinocytes express

K1/K10. The most abundant keratins in epithelial tissues are K7, K8 (type II) and K18, K19, K20 and K23 (type I) (Omary et al., 2009).

2.3.4 Post-translational modifications of keratins

The versatility of keratin can partially be attributed to that these proteins are extensively modified by post-translational modifications (PTMs). Keratins consist of the conventional IF three-domain structure (central rod domain flanked by head and tail domains). The rod domain can be further divided into sub-helices (1A, 1B, 2A and 2B) separated by three linker domains (L1, L12 and L2). The sub-helices possess little variation in amino acid sequence and are highly conserved, whereas the head and tail domains possess considerable variation between different keratins. Phosphorylation and ubiquitination are PTMs that have been extensively studied, while studies on sumoylation, glycosylation and acetylation are on the rise. Assembly and disassembly of keratins are heavily dependent on PTMs, such as phosphorylation of Ser/Thr residues at head and tail domains. Phosphorylation is considered an integral PTM in terms of solubility and filament dynamics, and is associated with several physiological and disease mechanisms (Snider and Omary, 2014). Ubiquitination is the process of labelling proteins with an ubiquitin group, which is utilized in cytosolic degradation systems (Grumati and Dikic, 2018). In the context of keratins, ubiquitination is suggested to target partnerless keratins as a stabilizing function, but also implemented in targeting of mutated keratins for degradation. Ubiquitination sites are currently unknown for keratins (Snider and Omary, 2014).

2.3.5 Keratin function

Keratins are important for the structural integrity of epithelia, as they build up an intracellular meshwork that spans the cell. The filaments are connected to neighboring cells via desmosomes, and are also linked to the extracellular matrix via hemidesmosomes (Polari et al., 2020). Furthermore, keratins are also involved in more dynamic functions such as cell signaling, cell migration, differentiation and protecting the cell from various type of cellular stress (Loschke et al., 2015).

There are plenty of studies showing that keratins have an impactful influence over cellular signaling pathways (Eriksson et al., 2009). K8 and K18 partners have been shown to protect hepatocytes from pro-apoptotic signals, as K8-null hepatocytes are more sensitive to Fas-mediated apoptosis compared WT hepatocytes (Gilbert et al., 2001). In terms of stress, keratins have a cytoprotective mechanism that allows them to function as a "phosphate sink", meaning that they sequester unwarranted phosphorylation from pro-apoptotic proteins and stress-activated kinases (Ku and Omary, 2006). They are upregulated in response to mechanical and non-mechanical stresses, such as toxins, heat, hypoxic and oxidative stress (Toivola et al., 2010). It is also suggested that keratins can indirectly modulate mitotic regulators via 14-3-3 protein interaction and, thus cell proliferation (Liao and Omary, 1996), but the exact mechanism is still unknown.

2.3.6 Keratins and keratinopathies of the colon

In mice, K8, K18 and K19 are the three most abundant keratins of the colon epithelium, whereas K7 and K20 have a lower abundance. In terms of distribution, K8, K18 and K19 are evenly found throughout the length of the crypt epithelium (Zhou et al., 2003). K20 is primarily present in the upper part of the crypt and associated with differentiated cells. K7 is only expressed in mice and located at the base of the crypts (Zhou et al., 2003). As an exception, K7 has been observed in colon tumors from humans (Polari et al., 2020). Cancer cells tend to maintain the keratin profile of the tissue of origin after dissemination. Therefore, keratins function as tumor cell markers for determining the origin of metastatic tumors in clinical histopathology (Moll et al., 2008). Loss of K8 has shown an IBD-like phenotype in mice and one study also showed that a subset of IBD patients had missense mutations of K8 (Owens and Lane, 2004). $K8^{-/-}$ mice have several colon-specific phenotypes, such as epithelial hyperproliferation (increased crypt length), decreased apoptosis, diarrhea, and inflammation. Heterozygous $K8^{+/-}$ mice have no inflammation but are more sensitive to chemically induced colitis, and have a slight increase in crypt length. The latter suggests that the hyperproliferation is gene dosage-dependent of K8 levels (Asghar et al., 2015). Diarrhea is caused by impaired chloride ion transport which, consequently,

hampers water uptake in the colon (Asghar et al., 2016). In the small intestine of $K8^{-/-}$ mice, filamentous actin and other apical membrane proteins have been seen to mislocalize, which has led to the suggestion that keratins could be involved in maintenance of epithelial polarization and protein targeting (Owens and Lane, 2004). The gut microbiota may also play a part, as antibiotic treatment has shown to ameliorate inflammation in $K8^{-/-}$ mice (Habtezion et al., 2005).

Recently, it was shown that K8/K18 co-immunoprecipitated together with pro-caspase 1 in colon epithelial scrapings, thus illustrating that keratins interact with NOD-, LRR- and pyrin domain-containing protein 3 (NLRP3) inflammasome formation and perhaps have an inflammation-modulating role in colon epithelium (Misiorek et al., 2016). Furthermore, it has also been shown that $K8^{-/-}$ causes loss of Notch1 activation and, consequently, shifts dividing cells towards a secretory cell fate as enterocytes are diminished (Lähdeniemi et al., 2017).

Not only are keratins associated with mentioned phenotypes, but they are also linked to tumorigenesis in the colon. Tumors do not develop spontaneously in $K8^{-/-}$ mouse colon. By giving $K8^{-/-}$ mice azoxymethane (carcinogen; AOM) injections or crossing them with tumor-susceptible $Apc^{+/Min}$ mice, they developed a significant number of tumors in the distal colon while $K8^{+/+}$ and $K8^{+/-}$ mice did not develop any tumors. This suggests that K8 potentially functions as a tumor suppressor (Misiorek et al., 2016). As $K8^{-/-}$ mice have a high embryo lethality and several extraintestinal manifestations, two conditional K8 KO mouse models were developed by Stenvall et al., which subsequently showed similar colon-specific phenotypes by loss of K8 (Stenvall et al., 2021).

2.3.7 Role of K18

Although K18 is one of the main type I keratins (together with K19), neither $K18^{-/-}$ mice nor $K19^{-/-}$ mice possess any distinct phenotypes in the colon (Magin et al., 1998). The primary observation that has been made is that old $K18^{-/-}$ mice develop K8-positive aggregates in hepatocytes. Hepatocytes only express K8 and K18. The aggregates were characterized and contained K8, ubiquitin and M_M120-1 (Mallory body antigen). In other words, the aggregates resembled MDBs that are associated

with alcoholic hepatitis (Magin et al., 1998). Characteristic components of MDBs are K8/K18 filaments, ubiquitin and p62 (also known as sequestosome 1); and they are thought to arise from chronic stress, extensive protein misfolding causing proteasomal overload and increased K8:K18 ratio. The pathological role of MDBs is still unresolved (Zatloukal et al., 2007). K18 is regarded as a goblet cell marker, as these cells possess prominent K18 staining and the keratin filaments are, exclusively in goblet cells, reduced to thick bundles and cytoplasmic dots in mice that are overexpressing hK18 R89C (Zhou et al., 2003).

2.4 *In vitro* models

2.4.1 Overview

In the recent decade, three-dimensional (3D) *in vitro* cultures have emerged as a novel approach to study cells and tissue biology. An *in vitro* model refers to the modelling of cells or tissue outside the living organism, i.e. in glass. Various primary cell lines and cancer cell lines have traditionally been heavily utilized in cell biological research, especially by culturing cells on flat two-dimensional (2D) surfaces. 2D culture and animal models have been extensively utilized but confers limitations. Single cell functionality cannot represent the collective dynamics of cells in tissue and lacks the cellular microenvironment present *in vivo* (Simian and Bissell, 2017). Although animal models have been tremendously useful to understand mammalian physiology and diseases, all physiological scenarios in animal models cannot be extrapolated to human physiology (Benam et al., 2015). Relative to conventional 2D cell culturing of single cell lines, the rise of 3D culture has paved a new path for bioscience.

2.4.2 Various types of *in vitro* 3D cultures

3D culture encapsulates a broad spectrum of culturing methods that substitutes conventional 2D culture in search for more authentic cell culture settings, such as ECM-based 3D culture, scaffold-free culture and more advanced techniques (e.g.

microfluidics). Scaffold-free culture refers to cells suspended freely in media without any attachment where they are diving and forming cellular aggregates (clusters of cells). Scaffold-based techniques entail culturing of cells in purified extracellular matrices, which can be composed of both natural and synthetic components. Polyethylene glycol (PEG) and polylactic acid (PLA) are examples of synthetic materials used as matrix. Natural proteins such as laminin, collagen, fibrinogen and hyaluronic acid are often used in hydrogels. Matrigel, a commercially available ECM-extract purified from Engelbreth-Holm-Swarm mouse sarcoma, has been available for 40 years and been heavily utilized for 3D culture. Nevertheless, the Matrigel composition has not been fully defined and batch variations are associated with the product (Aisenbrey and Murphy, 2020). Matrigel contains proteins such as collagen IV and laminin, in addition to a plethora of different growth factors (Reidy et al., 2021).

In a historic perspective, Bissell et al. were one of the pioneers in studying how ECM regulates gene expression in the early 1980s (Simian and Bissell, 2017). The research field received an upswing when Sato et al. were the first to culture organoids derived from intestinal ASCs (Sato et al., 2009). There are several examples of cells that can be used for 3D culture, such as immortalized cancer cells or primary cells (e.g. ASCs or induced pluripotent stem cells). Generally, a spheroid refers to a 3D structure derived from single or cluster of immortalized cancer cells when cultured in e.g. Matrigel or collagen. An organoid refers to a 3D structure derived from stem cells and generally obtains a *in vivo*-like morphology when cultured in e.g. Matrigel.

2.4.3 Principles of ECM-based 3D culture

When a cell is suspended in an ECM, the architecture is fundamentally altered. For example, epithelial cells opt for a round morphology composed of a polarized cell membrane with a hollow lumen in the center of the spheroid.

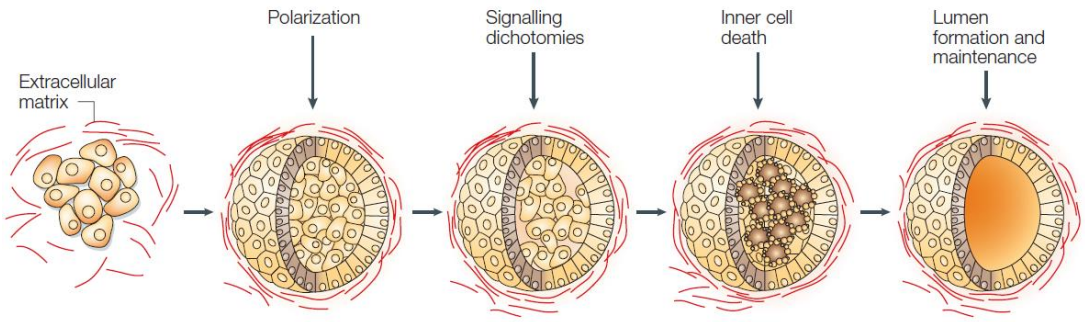

Figure 7. Schematic morphological development of spheroids. Epithelial cells suspended in extracellular matrix (ECM) initially start to divide and cluster together. After a couple of days, apicobasal polarization starts to become apparent. Concomitantly, the cells within the spheroid start to divide into two separate populations: the cells directly attached to the ECM and the inner cells of the spheroid. After a couple of days, the inner cells will start to diminish via anoikis as they are lacking attachment. Non-aggressive cell lines usually maintain their lumens, while aggressive cell lines start showing invasive tendencies. Modified from Debnath and Brugge, 2005.

It takes several days for the spheroids to grow in size before they start to polarize, i.e. forming an exterior basal cell layer towards the ECM (fig. 7). Without any signaling input or attachment to the ECM, the inner cells will start to dissipate (given they are not resistant to cell death) and form a lumen (Debnath and Brugge, 2005). The dimensionality of spheroids influences spatial distribution of cell surface receptors and their interaction with neighboring cells, which leads to differences in cellular signaling response compared to 2D culture. Gene and protein expression, proliferation, apoptosis and differentiation are all fundamental processes which are altered in 2D culture (Härmä et al., 2010). As 3D-culture simulates an *in vivo*-like microenvironment, the morphology and the aforementioned processes are therefore more similar to what has been observed *in vivo*. A reduced cell proliferation has been documented in a wide range of cell lines when cultured in 3D. But there are cell lines which get a higher proliferation rate when they are cultured in 3D relative to 2D, and the choice of ECM can influence the proliferation rate in 3D (Edmondson et al., 2014). In terms of viability, most studies have showed that there is no significant difference throughout the first 5 days. In some instances, the viability is reduced after prolonged culture as some parts of the spheroids suffer from oxygen deprivation and waste accumulation. It has also been suggested that cells cultured in 3D culture are

metabolically more similar to tissue in the organ of origin compared to the same cells cultured in 2D (Lagies et al., 2020).

In 2D culture, all the cells are provided oxygen and nutrients in a uniform manner. 3D cultures are composed structurally different zones where nutrients and oxygen are unevenly distributed within the spheroids. This heterogeneity in access to nutrient and oxygen causes the spheroidal cells to be in different nutritional states, i.e. different cell cycle stages (Edmondson et al., 2014).

In terms of differentiation, non-cancerous immortalized cell lines have shown to be able to differentiate in 3D culture in a larger extent compared to 2D culture (Jensen and Teng, 2020). It is occasionally refer to spontaneous or structural differentiation as some cell lines show *in vivo*-like organization in ECM (Debnath et al., 2003), but differentiation capacity can vary between cell lines (Härmä et al., 2010). For example, colon cancer cell line HCT116 is regarded as a highly aggressive cell line with a low capacity to differentiate. On the other hand, colon cancer cell line HT29 is suggested to have an intermediate capacity to differentiate into enterocytes and mucin-expressing cells (Yeung et al., 2010). It has also been shown that the threshold for drug-induced apoptosis is lower in 2D culture, whereas cells in 3D culture are more resilient against drug-induced apoptosis (Jensen and Teng, 2020).

There are two major aspects that makes *in vitro* 3D models advantageous: (1) they can be experimentally examined by biochemical assays and examined under a microscope (fig. 8), and (2) they mimic the structural features of epithelia *in vivo* (Debnath and Brugge, 2005).

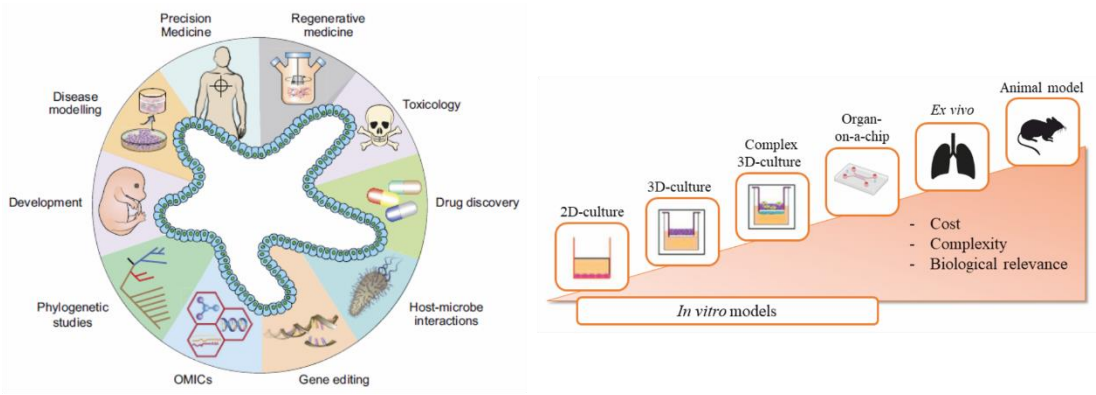

Figure 8. 3D cultures (organoids/spheroids) can be implemented in a wide range of studies (**left**) such as drug discovery, system biology (OMICs) and development. (**Right**) The spectrum of available models stretches from traditional 2D culture to animal models. Complexity and cost rise higher up in the chart, but the models are also more biologically relevant. Figure is modified from Corrò et al. 2020 and Lacroix et al. 2018.

2.4.4 *In vitro* perspective of colonic cell lines

Caco-2 and HT-29 are two commonly used immortalized colon cell lines, whereas there is a plethora of several other commercially available colon-derived cell lines as well. Caco-2 and HT-29 cells were isolated 1974 and 1964, respectively. Both cell lines are derived from human adenocarcinoma. These cell lines gained a reputation as they showed features of differentiation similar to intestinal cells seen *in vivo*, which had not been seen in cell lines derived from the healthy small intestine or colon (Rousset, 1986) at the current time period.

In terms of genetic aberrations, both Caco-2 and HT-29 cells possess wildtype KRAS and EGFR. The HT-29 cells possess V600E BRAF mutation and therefore deemed more aggressive (Luca et al., 2013). Both cells lines have an adherent epithelial morphology in 2D culture while Caco-2 cells opt for a round polarized morphology and HT-29 cells opt for a mass morphology when cultured for 7-10 days in Matrigel (Luca et al., 2013). Caco-2 cells have been suggested to differentiate spontaneously when cultured in 2D culture, as well as HT-29 cells under certain culture conditions.

Although the degree of differentiation is still ambiguous for both 2D and 3D culture. There are also other previous studies that have cultured Caco-2 cells in 3D culture (Jaffe et al., 2008; Patankar et al., 2019), although there are some difference in spheroid morphology which could be accredited to genotypic and phenotypic drift. Nevertheless, one needs to acknowledge that cancer cell lines and normal cells show great disparity in phenotype and should be considered when using them for an *in vitro* model.

2.4.5 Intestinal organoids and their culture conditions

In terms of usage of primary tissue, Hans Clever's lab was one of the first to develop a protocol to isolate and culture colon crypts in 3D culture (Sato et al., 2009). After a couple of days in culture, the crypts adopt 3D morphological structures called colon organoids or mini-guts. These organoids are defined as self-organizing basal-luminal oriented balls of epithelium with a crypt-like morphology. Their approach to culture colon organoids has since then promoted the usage of organoids in research. Not only is it possible to culture organoids long-term, but also use them for e.g. drug screening, personalized medicine and even store them in biobanks (Drost and Clevers, 2018).

Their protocol was the first report of using ASCs for growing organoids (Corrò et al., 2020). Their approach was to provide the stem cells with growth factors that mimicked the homeostatic signaling landscape in small intestine. R-spondin (Wnt agonist) was used as a substitute for Wnt signals occurring in the stem cell niche and have been observed to cause hyperplasia *in vivo*. Media was also supplemented with EGF and Noggin. EGF is linked with intestinal proliferation and Noggin is BMP inhibitor that has been shown to cause de novo crypt formation in vivo (Sato et al., 2009). Collectively, these factors are termed ENR after the used growth factors (EGF/Noggin/R-spondin). They opted to use Matrigel, as it is a laminin-rich ECM that supports the ASC with adequate adhesion and prevents anoikis (Sato et al., 2009).

Since then, culture protocols for colonic organoids (from both mouse and human), human adenoma and adenocarcinoma have been published as well. Both human and mouse colon have been cultured with addition of recombinant Wnt3A, as the colon organoids does not produce enough Wnt signals to maintain the colonic stem cells.

Organoid culture of mouse adenoma and human adenocarcinoma do not require Noggin and R-spondin, but some of the organoids halted in proliferation upon withdrawal of EGF (Sato et al., 2011).

2.4.6 Advancements in the research field

In vitro modelling of the colon has also advanced further from solely using homotypic organoids. Some researchers suggest that *in vitro* models need further complexity by incorporating fibroblasts (Åkerfelt et al., 2015), vasculature and innervation to achieve a more *in vivo*-like model (Benam et al., 2015). Not to mention addition of immune cells, which potentially could give some insight into IBD pathogenesis. Puschhof et al. have also published a protocol for coculturing intestinal organoids with microbes, which further includes the aspect of host-microbiota relationship (Puschhof et al., 2021). Microfluidics, i.e. organ-on-a-chip technologies, have been implemented for both the small intestine (Kasendra et al., 2018) and the colon (Sontheimer-Phelps et al., 2020). Utilization of organ-on-a-chip technologies are advantageous as they take the fluidal aspect into account without dismissing the ECM component to the systems (Reidy et al., 2021). Nevertheless, a highly complex *in vitro* model system is not necessarily optimal for answering all biological questions.

3. Aims of the project

Keratins are highly abundant proteins in the intestinal epithelium and loss of K8 has shown to have profound consequences on colonic homeostasis: hyperproliferation, apoptotic resistance, inflammation, diarrhea and an increased propensity for development of CRC. While colonic diseases such as IBD and CRC are on the rise globally, the pathogeneses for these diseases are still today largely unknown. As the extracellular microenvironment is receiving progressively more attention in the popularized usage of ECM-based 3D models and provides a new approach to understanding keratins in the colon, our aim was to establish colonic *in vitro* 3D models to study phenotypic effects of loss of K8/K18 and compare to K8/K18 expressing cells. Simultaneously, the project will give a comparative view of using both 2D and 3D culture of Caco-2 cells and crypt-derived organoids cultured in 3D.

We will use several transgenic variants of colon-derived cancer cell line Caco-2 (K18 shRNA and K8 KO cells) and organoids derived from a conditional K8 KO model to study several fundamental parameters in both 2D and 3D culture. By a streamlined approach, we will monitor the 2D and 3D cultures in the Incucyte imaging system, whereas after the culture period we will assess viability (WST-8 assay) and morphology (via automated live-cell imaging and morphological analysis). Moreover, protein levels, such as keratins, proliferation, differentiation and apoptosis markers, will be assessed via western blotting and immunofluorescence stains to determine any phenotypic changes caused by K18/K8 downregulation. Our hypothesis is that the *in vivo* phenotypes are translated into our *in vitro* 3D models, at least to a partial extent. We hypothesize that K18 downregulation should lower K8 protein levels.

In short, the aim was to setup 3D cultures of Caco-2 cells and elucidate phenotypical differences in K18 knockdown and K8 KO compared to unaltered controls, in both 2D and 3D culture. The specific aims were to assess the impact of K18/K8 loss in 2D and 3D culture for:

I. Cell proliferation, viability and morphology
II. Partner keratin level changes
III. Apoptosis and differentiation

4. Materials and methods

4.1 Immortalized colon cell lines

Cell lines used were Caco-2 (ATCC® HTB-37™) and HT-29 (ATCC® HTB-38™); both cell lines are derived from human colorectal adenocarcinoma. Each respective cell line has been transfected with a stable lentivirus vector pLVTHM (Addgene; #12247). The pLVTHM vector expresses short-harpin RNA (shRNA) combined with an enhanced green fluorescent protein (eGFP) reporter (Wiznerowicz and Trono, 2003). The constructs were created by inserting a scrambled sequence and K18 shRNA sequence into the vectors using MluI and ClaI restriction enzymes. The K18 shRNA is processed into siRNA upon expression and knock down K18 mRNA levels by RNA interference. The scrambled vector does not affect K18 mRNA levels as the sequence is scrambled, thus, non-complementary to target mRNA. In other words, we utilized a K18 shRNA (knockdown) and a Scramble (control) for each cell line. The vector constructs were ordered from and generated by Life Technologies.

Furthermore, Caco-2 K8 KO cell line was created through CRISPR-mediated knockout method using a specific guide-RNA that cuts out the *KRT8* gene. Consequently, the altered gene ideally causes altered mRNA production and incomplete protein production of K8. The production of the cell line was assisted by the Genome Editing Core at Turku Bioscience. The cells were produced in 2022 and CRISPR WT clone #9 and KO clone #3 were used.

The cell lines were cultured in Dulbecco's modified eagles' medium (1x DMEM; Gibco; #41965-039) supplemented with 10% fetal bovine serum (FBS; Serana; S-FBS-SA-015), 2 mM L-glutamine (Lonza; BE17-605E/U1), 100 U/ml penicillin and 100 µg/ml streptomycin (Gibco; #15140-122). The HT-29 cell lines were utilized between passages 1-5 and the Caco-2 cells were maintained between passages 1-30. The culture medium was changed every 2-3 days.

4.2 Conditional K8 KO mouse model

To generate mouse-derived organoids, colon crypts were isolated from a conditional knockout mouse model (Stenvall et al., 2021) which utilizes the cre-loxP recombination system. A cre-recombinase sequence was coupled to the promoter of the villin 1 gene, thus resulting in a coupled-expression of cre-recombinase protein together with endogenous villin protein in villin-expressing cells. Subsequently, the recombinase mediates deletion of the K8 gene which is flanked by loxP-sites in the DNA. Furthermore, the mouse strain used possesses an inducible cre-ERT2 recombinase. This specific recombinase is localized in the cytoplasm by default, but also coupled with a mutated estrogen receptor. By administering tamoxifen (a synthetic estrogen analogue), the cre-ERT2 will be translocated to the nucleus of the cell and, consequently, delete the loxP-flanked segment. Tamoxifen can be used in both *in vivo* (intraperitoneal injection) and *in vitro* (tamoxifen-supplemented medium) to knock out K8. The latter approach was utilized for our experiments.

4.3 Crypt isolation

The colon crypts were isolated by sacrificing the mice by CO_2 inhalation and removal of the colon (colectomy). To minimize any premature degradation, most of the procedures were carried out on ice. Feces, fat tissue and blood vessels were removed and the colon was washed thoroughly. The colon was cut into small 3 mm segments and suspended in ice-cold 1x PBS. To further wash the colon segment, the segments were washed by vortexing for five seconds, 1x PBS was removed using a strainer and fresh ice-cold 1x PBS was added. This washing step was repeated for a minimum of 15 times. After the washing, the clean colon segments were resuspended in 1x PBS supplemented with 5 mM ethylenediaminetetraacetic acid (EDTA) and put on a rocker for 20 minutes at RT. The EDTA is a chelating agent that facilitates the detachment of crypts from the tissue. The colon segments were then transferred to a new tube with fresh ice-cold 1x PBS. Consequently, the crypts were fractioned out by vigorous shaking of the tube. The crypts were eluted through a strainer and the colon pieces were resuspended in 1x PBS and the fractioning was repeated eight times. The

fractions with good quality crypts, i.e. containing long crypts and small amounts of debris, were pooled together and centrifuged at 290 x g for five minutes at +4 ºC. The supernatant was discarded and the pellet of crypts was resuspended in DMEM/F-12 culturing medium (Stem cell technologies; #36254). The number of crypts was approximated by counting the crypts in a droplet under a light microscope. Centrifugation was repeated and the crypt concentration was adjusted to desired concentration.

4.4 Flow cytometry

The eGFP-expressing cells were isolated by fluorescence activated cell sorting using Sony SH800 cell sorter. Standard Caco-2, Caco-2 Scramble and Caco-2 K18 shRNA cells were collected in medium suspension (DMEM) prior to cell sorting. Standard Caco-2 cells were used to configure the gating based on forward scatter (FSC) and side scatter (SSC) to exclude apoptotic cells and any cell duplicates. After configuration, the Caco-2 Scramble and K18 shRNA cells lines were sorted based on eGFP fluorescence intensity to achieve two cell populations with strong eGFP expression. Isolated cells were collected in separate centrifuge tubes and plated to a 48-well plate to allow the cells to proliferate and amplify the numbers of sorted cells.

4.5 3D culture

For the 3D culture experiments, a miniaturized platform that is optimal for drug screening and studying morphological and phenotypical changes over time was utilized. This platform was developed by Härmä et al. 2014 and allowed us to examine a large set of 3D structures without sacrificing detailed imagery of the 3D morphology (Härmä et al., 2014). The majority of the 3D experiments were done using this platform (excluding 3D culture harvested for western blotting) and usage of 96-well angiogenesis µ-plates (Ibidi; #89646). These plates were used since they allow the organoids/spheroids to be embedded in a sandwich-type of manner without a meniscus formation, i.e. all spheroids are positioned in the same optical plane.

In preparation of the 3D culture, extracellular matrix (ECM) of choice (e.g. Matrigel) was diluted to 50% (1:1 ratio) in DMEM (4 mg/ml Matrigel) and added to the center of the inner well of each plate well. The "lower gel" was then allowed to polymerize in +37 ºC for 30-60 minutes. The cells were then suspended in 25% Matrigel diluted in DMEM and plated on top of the lower gels. The cells usually reside in the upper gel and become sandwiched between the two layers of ECM. The upper layer was then allowed to polymerize for 3-4 hours or overnight before culturing medium was added to the wells. Matrigel (Corning; #356231) and collagen (BD bioscience; #354236) were the extracellular matrices used in these experiments. A collagen stock was mixed and used for the experiments (*see Buffers and recipes*). To avoid any risk of the wells drying out, the outer most rows of the plates and reservoirs at the edges of the plate were filled with 1x PBS. The medium was changed every second day for the first week and after that the medium was changed daily. The spheroids were cultured for around 10-15 days, and the plate was continuously monitored in Incucyte ZOOM (Essen bioscience).

The same principle was applied to crypts, as the ECM was suspended in DMEM/F-12 medium and Intesticult™ organoid growth medium (Stem cell technologies; #06005) was added on top of the gels. Crypts were generally cultured for approximately seven days.

4.6 Proliferation measurements for 2D cultures

To assess the difference in rate of proliferation between the cell lines, Incucyte S3 Live-cell analysis system (Sartorius) was used. Incucyte is a high-content imaging system that allows real-time monitoring of cells throughout experiments. The system collects phase-contrast and fluorescent images every two hours. The system can also generate quantitative data for cell proliferation by setting up an analysis definition (fig. 9) in the Incucyte software. The confluency can be measured for every well at each time point of acquisition and presented as a confluency curve. In this case, 2,000 cells/well (for both cell lines) were plated in µclear 96-well plates (Greiner; #655090) and cultured in the Incucyte S3 for approximately four days.

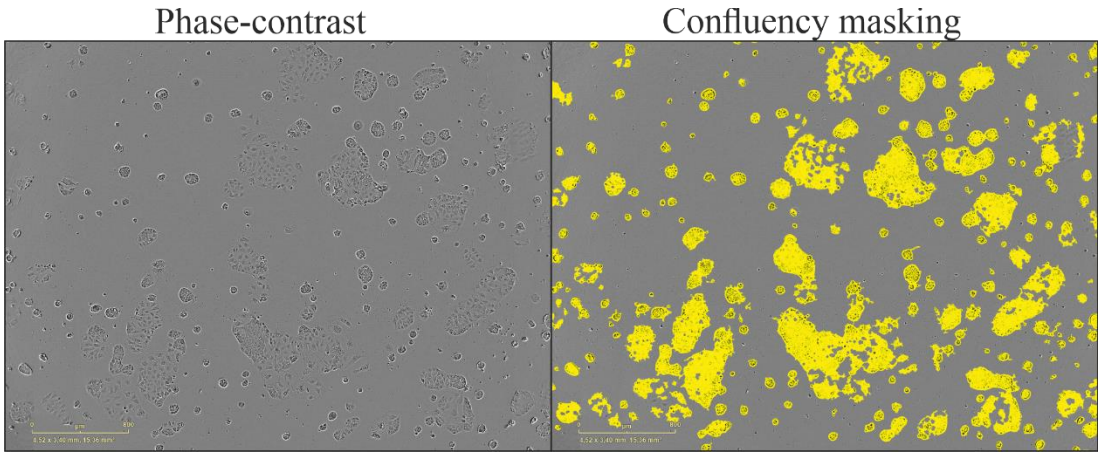

Figure 9. Analysis tools incorporated in the Incucyte software allows whole-well measurements of confluency. The work definition can be setup by 3-5 practice images and adjusting to an appropriate setting that provides adequate confluency masking/segmentation (yellow). Scale bars are 800 µm.

4.7 Viability assay for 2D and 3D culture

At the end of each experiment, the WST-8 assay (Dojindo Molecular Technologies; CK04) was used to assess dehydrogenase activity between the two cell lines in both 2D and 3D cultures. In other words, dehydrogenase activity reflects on how viable and metabolically active the cells or spheroids are. In practice, the 10x WST-8 reagent was added to the medium in the wells of interest in a 1:10 dilution ratio. The plates were incubated at +37 ºC for a minimum of 30 minutes. During incubation, electron transporters within the cells reduces the WST-8 tetrazolium salt to produce an orange formazan dye (fig. 10; left). The dye was then quantified spectrophotometrically at 450 nm using a Wallac 1420 VICTOR2™ microplate reader (Perkin Elmer).

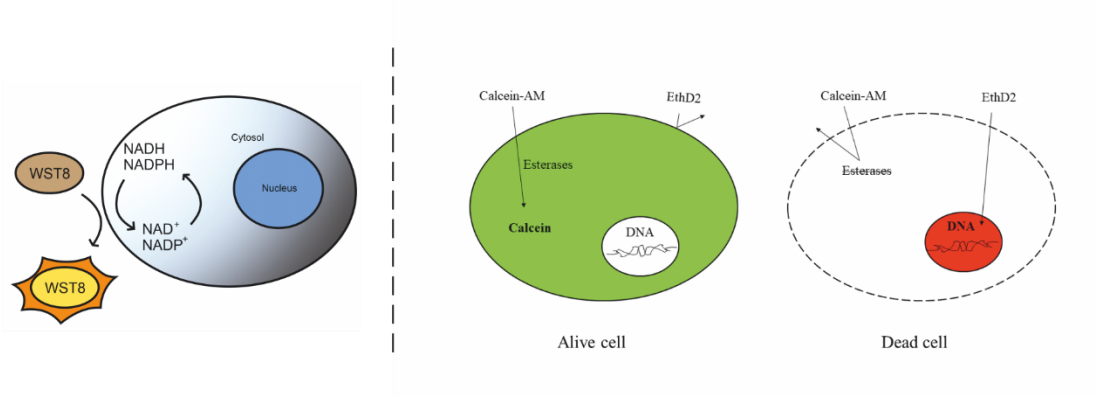

Figure 10. Mechanisms of WST8 reagent, Calcein and Ethidium-homodimer 2 stains. (Left) WST-8 tetrazolium salt is reduced by electron transporters in metabolically active cells, which creates an orange formazan dye which can be quantified. (**Right**) Calcein-AM is permeable to viable cells and is retained in the cell cytoplasm via esterase. Ethidium homodimer-2 (EthD2) cannot pass through the cell membrane of intact cells and only stains DNA of dead (or apoptotic) cells.

4.8 Live cell staining and automated confocal microscopy

As a complementary approach to the WST-8 assay, the cells were stained with Calcein AM (Invitrogen; C3099) and Ethidium homodimer-2 (EthD2; Invitrogen; E3599) to elucidate the ratio of viable and dead cells. Calcein AM is a cell-permeant compound that is retained in the cytoplasm once it is hydrolyzed, a green fluorescent dye is emitted. EthD2 stains DNA red but is non-permeant to the cell membrane (fig. 10; right), thus solely capable of staining apoptotic cells. The medium was aspirated and stains were diluted 1:1,000 in DMEM, distributed to the wells of interest and incubated for 30 minutes prior to imaging. The same principle was applied for 3D cultures.

The essence of the 3D platform was to utilize fluorescent dyes at the endpoint of the culture period to clearly display the morphology of spheroids and organoids. To acquire z-stacks of the 3D-cultures, Zeiss Axiovert-200M microscope equipped with Yokogawa CSU22 spinning disc confocal unit and a Zeiss Plan-Neofluar 5x objective was used. As the 96-well angiogenesis µ-plates are optimized to reduce meniscus formation, a relatively narrow z-stack (below 800 µm) can be acquired for several positions using an automated stage. The z-stacks were then merged into maximum

projections and the fluorescence intensities were normalized with Slidebook 6 (Intelligent imaging innovations) to remove background noise.

4.7 Automated morphometric image data analysis (AMIDA)

The normalized maximum projections were then processed and analyzed using the AMIDA (**A**utomated **M**orphometric **I**mage **D**ata **A**nalysis) program. AMIDA is a free-to-use analysis tool developed by the HSC laboratory and is utilized for the analysis of morphological parameters of 3D cultures (Härmä et al., 2014). The spheroids/organoids were first segmented (i.e. contoured), numerated and quantified based on cancer-relevant and morphological parameters (fig. 11). To ensure proper segmentation, the software allows manual adjustment of two settings: sensitivity and threshold. Sensitivity (range 2-50) adjusts the splitting of segmented regions in the analyzed image, as a higher sensitivity value leads to larger segmented regions. Threshold (range 1-5) controls the cut-off value of the histogram, which means that a higher threshold value leads to more stringent segmentation and generally identifies more structures.

Based on the segmentation, AMIDA produces morphological data of all the segmented structures. These morphological data or parameters can be arranged into three different classes: general, morphological, and functional parameters. The first class consists of parameters such as size and relative distance between structures. Morphological parameters entail features associated with the phenotype e.g. roundness, roughness of the contour and invasiveness (appendages). Functional parameters are measured separately for each RGB channel and account for measurements such as signal density, number of cells per structure and polarization within the structure (hollowness). The cumulative data is processed and visualized as box plots using R-studio.

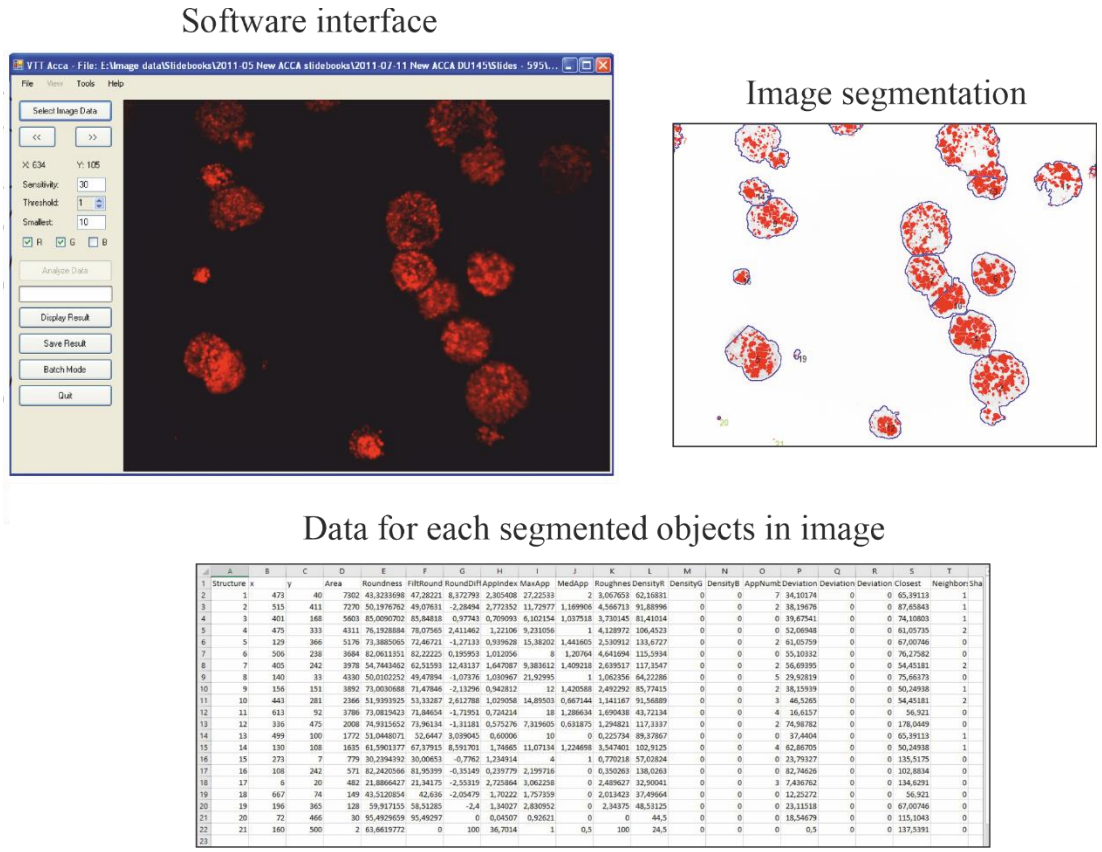

Figure 11. Automated Morphometric Image Data Analysis (AMIDA) software overview. Parameters (sensitivity and threshold) can be adjusted in the software interface. After the finished analysis, the software output will be segmented images and attached numerical data for each segmented object in each analyzed image.

4.8 Immunofluorescent staining of 2D and 3D cultures

In order to study proteins of interest in cells grown in 2D, the cells were fixed and stained using indirect immunofluorescence (IF) staining. The samples were fixed using either 1% paraformaldehyde (PFA) or pure acetone. Cells were plated on 10 mm glass coverslips in 24-well plates prior to fixation. For PFA fixation, cells were fixed using 1% PFA for 10 minutes and washed 3 x 3 minutes with 1x phosphate-buffered saline (1x PBS; Biotop; #09-94000-100). Consequently, the cells were permeabilized using 0.025% triton X-100 (Sigma-Aldrich; T8787) in 1x PBS for 3 x 3 minutes followed by a five-minute incubation with 0.2% NP-40 (diluted in 1x PBS; Roche; #11754599001). The permeabilization was then finished by washing 3 x 3 minutes with 0.025% triton X-100. Acetone fixation was alternatively used. In brief, the cells were treated with pure ice-cold acetone for 10 minutes and briefly left to airdry.

Acetone melts plastic; therefore, the glass coverslips were acetone-fixated in a glass petri dish. Acetone also functions as a permeabilizing agent, so there is no need for additional permeabilization. After respective fixation, the same procedure for blocking and staining was followed.

The cells were first blocked with serum-free blocking buffer (3% bovine serum albumin in 1x PBS) for 20 minutes and then blocked with blocking buffer supplemented with 2% goat and donkey serum for 30 minutes. After blocking, the cells were incubated overnight at +4 ºC with primary antibodies (*see supplemental table 1*) suspended in blocking buffer with serum. After incubation, the primary antibody suspension was removed, and the cells were washed with 1x PBS for 3 x 5 minutes. The cells were then briefly blocked with 3% BSA with serum for 10 minutes, followed by incubation in blocking buffer supplemented with secondary antibodies, i.e. fluorophore-conjugated antibodies (*see supplemental table 2*) that target the primary antibodies. The cells were incubated at room-temperature (RT) for 45 minutes and kept in dark. Finally, the cells were washed 3 x 5 minutes with 1x PBS, where the second wash was supplemented with Draq5 (nuclear stain; 1:500; Thermo scientific; #62251). The coverslips were then mounted to superfrost Ultra plus™ Adhesion slides (Thermo scientific #10417002) using ProLong™ Gold Antifade Mountant (Thermo scientific, #P10144).

To study proteins of interest in spheroids grown in 3D, the medium was aspirated and cold 1% PFA (optionally 4% PFA) was added to all the wells and fixed for 20 minutes. The PFA was then gently aspirated from the wells and consequently washed 3 x 5 minutes with wash buffer (1x PBS with 0.2% Triton X-100 and 0.05% Tween). The remaining wells (that were not used for WST8-assay or live-cell imaging) were used for IF staining. The wash buffer was aspirated and permeabilization buffer (1x PBS with 0.5% Triton X-100; optionally 0.7%) was added for 20 minutes. The spheroids were then washed once with wash buffer for five minutes and unspecific antibody-binding was prevented by adding blocking buffer (1x PBS with 2.5% BSA and 2% donkey/goat serum) for 30 minutes. The primary antibody (generally 1:100 dilution) was then suspended in blocking buffer and added to the spheroids. The primary antibody was incubated at +4 ºC overnight. The next day, the primary antibody suspension was removed, and the spheroids were washed 3 x 5 minutes with wash buffer. The secondary antibody (generally 1:200 dilution) suspended in blocking

buffer was added to the spheroids and incubated for 90 minutes at RT in the dark. If used, Draq5 (nuclear stain) was added simultaneously at a 1:500 dilution. The secondary antibody was removed, and the spheroids were washed 3 x 5 minutes with 1 x PBS. Whenever DAPI (nuclear stain) was used, it was added to the second wash in a 1:5,000 dilution for 15 minutes, followed by 2 x 5-minute washes with 1 x PBS. The plate was then stored in the dark at +4 ºC.

The IF-stained cultures were imaged using Zeiss Axiovert-200M confocal microscope. The same microscope was also used for automated live-cell imaging described in 4.7. In addition, a 3i Marianas CSU-W1 spinning disc confocal microscope was used. The microscope was equipped with 405-, 488-, 561- and 640-nm lasers and main objectives used were Zeiss Plan-Apochromat (20x, NA 0.8) and Zeiss LD Plan-Neofluar (40x, NA 0.6). Image processing was done using slidebook 6.0 software and ImageJ.

4.8 Harvesting for western blotting and Bichoninic acid assay

To quantify the protein content of Caco-2 cells in 2D and 3D cultures, the cells were harvested, homogenized and protein levels were standardized prior to western blotting. The Caco-2 cells were cultured to approximately 90% confluency on 100 mm cell culture dishes and washed three times with 1x PBS. Homogenizing buffer (0.187 M Tris-HCl pH 6.8; 3% SDS; 5 mM EDTA) was added to the cultures and adherent cells were scraped off using Nunc™ Cell Scrapers (#179693; Thermo Scientific). For 3D cultures, 24-well plates were coated with 50% Matrigel (diluted in DMEM) and allowed to polymerize at +37 ºC for 2-3 hours. The Caco-2 cells were then suspended in 25% Matrigel (diluted in DMEM) and allowed to briefly polymerize to increase the viscosity of the cell suspension mixture. The matrix-cell suspension was then distributed to the Matrigel-coated wells and allowed to polymerize overnight before DMEM was added to the wells. The spheroids were cultured for 11-14 days, and medium was changed daily. The 3D gels were then washed three times using cold 1x PBS and the gels were depolymerized by adding cold 5 mM EDTA-PBS and resuspended a couple of times to facilitate the detachment of the spheroids. The spheroid suspension was then transferred to a centrifuge tube. Additional EDTA-PBS

was added, and the tubes were put on a rocker for 45 minutes in +4 ºC to completely depolymerize the Matrigel. The tubes were then centrifuged at 200 x g for five minutes at +4 ºC. The supernatant was carefully aspirated, and homogenizing buffer was added to the spheroid pellet. The lysates were made in triplicates.

The lysates (from both 2D and 3D culture) were then supplemented with cOmplete™ Protease Inhibitor Cocktail (Roche; #04693116001) and 1 mM phenylmethylsulfonyl fluoride (Sigma-Aldrich; #11359061001) to inhibit any protein degradation. The lysates were incubated at +95 ºC for five minutes and then mechanically pressed through a 27G needle (Terumo) with a 1ml syringe to lyse any cell remnants. The lysates were then stored at -80 ºC.

To standardize the protein levels of 2D and 3D lysate samples, bicinchoninic acid assay (BCA) was used. BCA is a colorimetric assay that measures reduction of Cu^{2+} to Cu^{1+} in an alkaline solution. Bicinchoninic acid reagent chelates Cu^{1+} and forms a complex that absorbs light at 562 nm. This reaction is directly proportional to the protein content of the samples. Samples and protein standards (protein albumin in a range from 50 ug/ml to 1,000 ug/ml) were distributed in triplicates to a 96-well microplate and mixed with a working reagent according to Pierce™ BCA protein assay kit (Thermo scientific, #23225). The plate was incubated at +37 ºC for 30 minutes and then stored in the dark at RT for five minutes prior to measuring. The microplate was measured spectrophotometrically at 562 nm using a Wallac 1420 VICTOR2™ microplate reader (Perkin Elmer). The protein concentrations of the samples were standardized to 5 µg/10 µl by diluting with laemmli buffer.

4.9 Western blotting

To quantify protein levels of interest in the lysate samples, sodium dodecyl sulfate – polyacrylamide gel electrophoresis (SDS-PAGE) was used to separate proteins based on molecular weight. The negatively charged proteins travel through the gel as an electric current is applied to the gel. The proteins are denatured by the SDS and given a negative charge that is proportional to the length of the proteins. Thus, the proteins are solely separated based on molecular weight. The gels were cast at different concentrations (ranging from 6-15%), as smaller proteins require a higher

concentration gel since smaller proteins travel faster in gel and vice versa. iBright™ prestained protein ladder (Invitrogen; #LC5615) was used as reference to accurately approximate the molecular weight of the blotted proteins of interest. The lysate samples were incubated at +95 ºC for five minutes and vortexed before they were loaded to the gel. SDS-PAGEs were generally run at 100 V for 90-150 minutes.

After the separation of the proteins, they were transferred from the gel to a polyvinylidene fluoride (PVDF) membrane. The proteins were transferred by an electric current from the gel into the membrane which immobilizes the proteins and facilitates detection of the separated proteins from the lysate samples. The transfer was done at 100 V for one hour in +4 ºC. After the transfer, the membrane was blocked with blocking buffer (5% milk in PBS-0.2% tween) to avoid any unspecific binding of antibodies.

Indirect immunoblotting was used to identify the proteins of interest. A primary antibody targeting the protein of interest and subsequently a horse radish peroxidase-linked (HRP-linked) secondary antibody was used to detect the host-specific primary antibody. The HRP-linked secondary antibody can then be detected using a detection agent that produces chemiluminescence upon oxidation by HRP, which can then be quantified.

After the blocking of the membrane, the blocking buffer was removed by washing for 3 x 5 minutes with PBS-0.2% tween. The primary antibodies (suspended 1:1,000 in 0.5% BSA-PBS with 0.02% NaN_2) were added to the membrane and incubated in +4 ºC overnight. The primary antibody suspension was then removed, and the washing step was repeated. The secondary antibodies (suspended 1:10,000 in blocking buffer) were then added to the membrane and incubated for one hour at RT. The washing step was repeated, and Amersham ECL Western Blotting Detection agent (GE healthcare, #45-000-878) was added to the membrane prior to detection. The western blots were visualized using the iBrightTM CL1500 imaging system (Thermo scientific). The chemiluminescence of the blots were then measured using ImageJ. The data was then quantified in Excel and the figures were made in GraphPad Prism 7.

4.10 Statistical analysis

For western blot quantifications a non-parametric student's *t*-test was used to assess statistical significance between each cell line in both 2D and 3D lysate samples. The morphological data from AMIDA was analyzed using a Bonferroni-corrected non-parametric Mann-Whitney U-test. Measurements of cell confluency (cell proliferation) was analyzed using two-way ANOVA. AMIDA results were analyzed in R-studio and the other statistical assessments were done in either GraphPad Prism 6 or Excel.

5. Results

5.1 Loss of K18 in the knockdown cell line was optimized using fluorescent activated cell sorting to remove K18 expressing cells

To answer the question whether loss of keratins has an impact on various phenotypes and cell functions in our colonic *in vitro* models, we needed to assess what the initial levels of K18 were in the K18 shRNA cell lines. As these cell lines only had been produced and not extensively utilized, there was a need to assess the knockdown efficiency before proceeding with further experiments. The western blotting of the cell lysate of the Caco-2 and HT-29 cells showed that K18 protein levels were weaker in the K18 shRNA lines in comparison with the Scramble controls (fig. 12A). The quantification further showed that there was significant downregulation of K18 in both cell lines, as the Caco-2 and HT-29 cells showed K18 levels of approximately 40% and 60% respectively (fig. 12B). K8 was also downregulated as the K18 was knocked down, although it was not quantified. K20 was present in the HT-29 cells and slightly decreased in K18 shRNA, while it was not expressed in the Caco-2 cells (fig. 12A).

As a complementary approach to elucidate whether individual cells only had a partial knockdown or if there was heterogeneity within the cell line, the Caco-2 cells were fixed with 4% PFA and stained for K18. The Scramble Caco-2 cells showed a co-expression of both K18 and the eGFP reporter from the construct (fig. 12C). This suggested that there was one coherent population of control cells that possessed the construct and K18 protein expression, although some cell-to-cell variation in eGFP signal was observed. On the contrary, there were two different cell populations within the Caco-2 K18 shRNA cells (fig. 12D). A majority of the cells expressed the eGFP reporter and showed low levels or no K18 protein. There was also a second population that lacked the eGFP reporter and still possessed K18 protein (fig. 12E). The Scramble cell line had a stronger eGFP signal relative to the K18 shRNA cell line (fig. 12C and 1D).

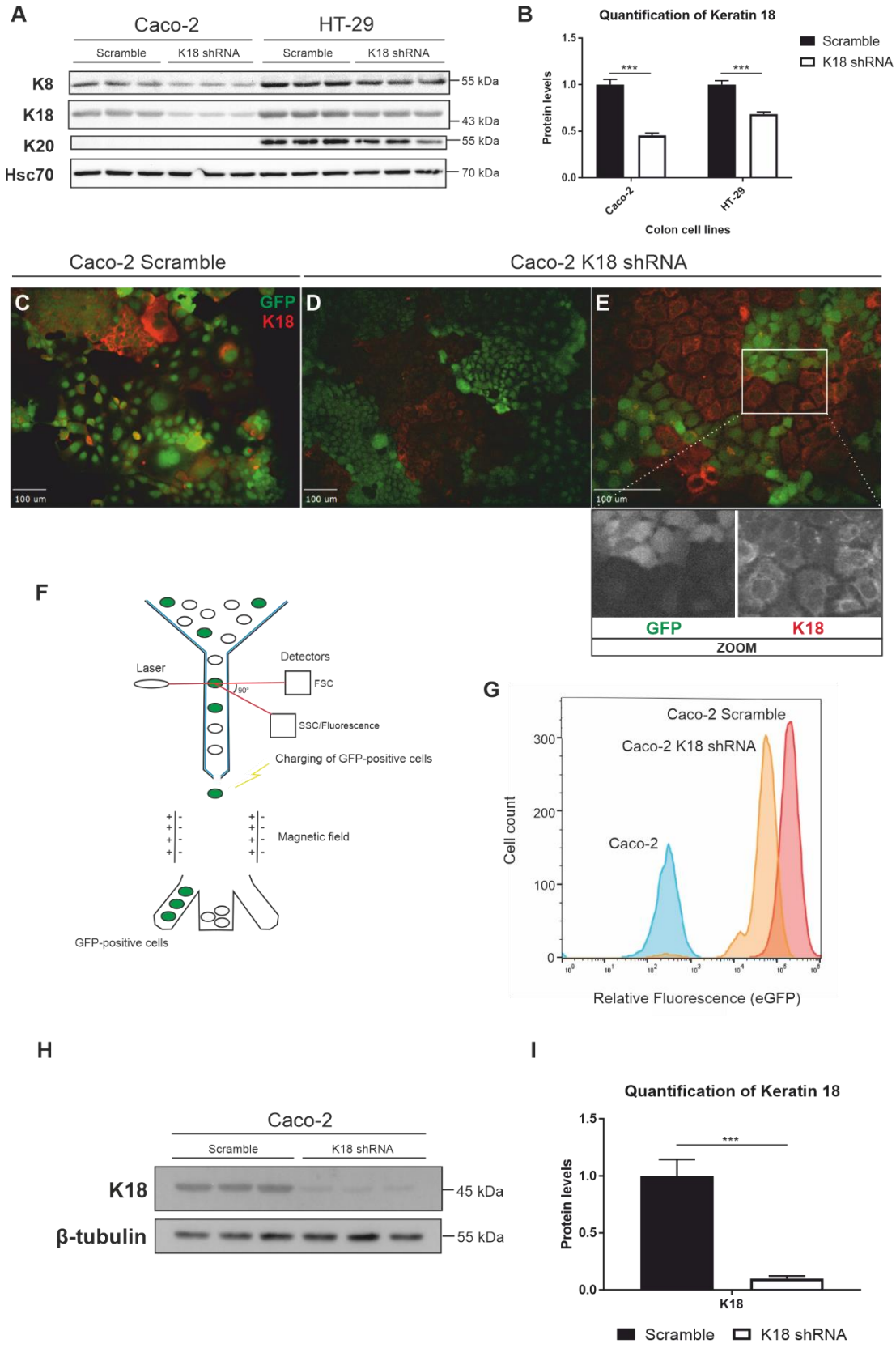

Figure 12. Caco-2 K18 shRNA cells were cell sorted to isolate bona fide K18 shRNA cells. (**A**) K8, K18, K20 protein levels were examined in lysates from the two immortalized colon cell lines. The Scramble samples were provided with a scrambled sequence within the

PLVTHM construct to function as a control for the K18 shRNA samples. Hsc70 was used as loading control. (**B**) Relative quantification of K18 levels in the control and K18 shRNA cell lines. Band intensities were quantified using ImageJ and normalized against loading control Hsc70. Data is shown as staple diagrams and whiskers shows standard deviation. (**C-D**) The localization of K18 was also examined using immunofluorescent staining and confocal microscopy. The PLVTHM construct express eGFP together with the shRNA, thus marking cells that possess the Scramble or K18 shRNA construct. K18 is shown in red and eGFP in green. (**E**) Higher magnification showing the two distinct cell populations. Region of interest (ROI) shows eGFP and K18 in separate channels. (**F**) The illustration presents the principal overview of fluorescent activated cell sorting (FACS) and how the eGFP-positive cells were isolated from each the Caco-2 cells. (**G**) Histogram of the different Caco-2 populations used for FACS. Standard Caco-2 cells were used to set up parameters for the cell morphology, as the Caco-2 Scramble and K18 shRNA cell lines were isolated based on their relative fluorescence. X-axis shows the cells relative fluorescent signal (eGFP) and Y-axis shows the number of cells isolated. (**H**, **I**) Assessment of K18 levels in the Caco-2 cell lines after cell sorting, as presented in **A** and **B**. Scale bars are 100 μm. Significance was determined using student's t-test (*** $P < 0.001$).

This problem was conveniently solved, as the bona fide K18 shRNA cells express an eGFP reporter. This allowed isolation of the K18 shRNA cells using flow cytometry. The basic principle of flow cytometry, or in this case fluorescence activated cell sorting, is that single cells from the cell line can be isolated based on whether they have fluorescence or not. The cells were maintained in suspension and then passed through a laser coupled with detectors that could quickly differentiate between fluorescent and non-fluorescent cells (fig. 12F). Downstream from the detectors, the flow cytometer provided an electric charge to eGFP-positive cells. The positively charged cells were then isolated from the non-charged (non-fluorescent) cells as they pass through a magnetic field. Standard Caco-2 cells were used to calibrate the gating off cells, as we wanted to exclude doublets and apoptotic cells. The histogram shows the population of standard non-fluorescent Caco-2 cells and the isolated populations from the Scramble and K18 shRNA cell lines. The histogram confirmed our observation that the scrambled cells had a stronger eGFP signal relative to the knockdown cells (fig. 12G). Approximately 7,500 GFP-positive cells were isolated from both cell types. When the two newly sorted cell lines had been cultured for some

time, the K18 protein levels were re-examined by western blotting (fig. 12H). The quantification of K18 after the cell sorting showed that approximately 10% of the original K18 protein levels remained (fig. 12I). Thus, we had acquired an adequate level of K18 knockdown to continue with further experiments. The HT-29 cells were not cell sorted nor further used due to time and prioritization.

5.2 The K18 shRNA cells showed a slower proliferation and no difference in viability compared to Scramble cells in 2D culture

We wanted to compare whether there were any apparent differences between the Scramble and K18 shRNA cells in terms of viability and proliferation in 2D and 3D culture. Firstly, we examined these questions in 2D culture setting. Caco-2 K18 shRNA cells and Scramble control cells were plated (day 0) equally on 96-well plates, and, consequently, monitored for four days in the Incucyte S3 live-cell analysis system. At the endpoint of the experiment, the viability was measured using a viability assay (WST-8) (fig. 13A). The image set acquired from the Incucyte showed that the cells were equal in terms of confluency at the beginning of the experiment and that the Caco-2 Scramble cells had a higher confluency after four days (fig. 13B). In terms of cell morphology, the Scramble cells were more prone to spread out in the wells as the K18 shRNA cells grew more tightly together (fig. 13B). However, there was no viability difference in terms of dehydrogenase activity at the end of the experiment after four days (fig. 13D).

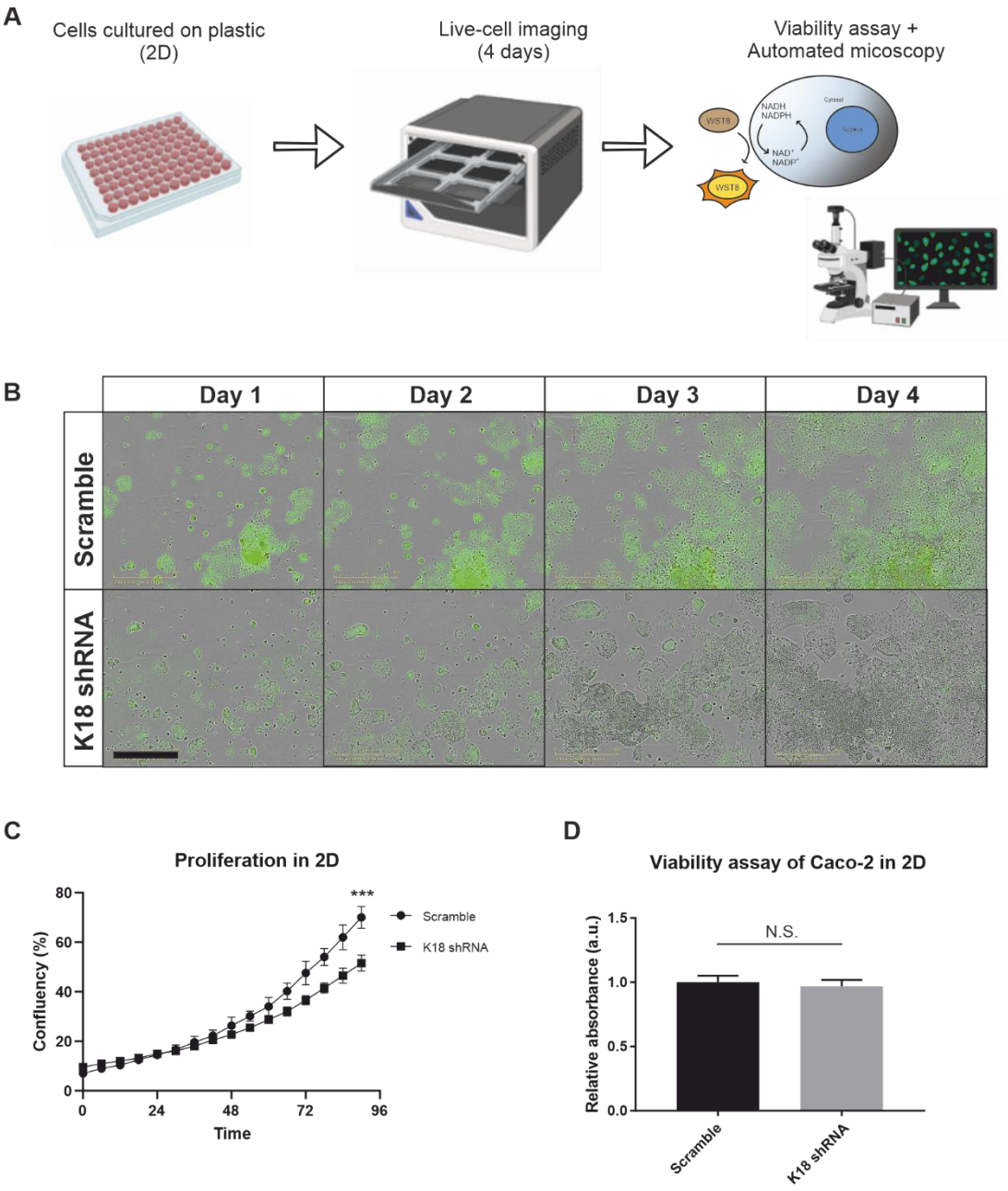

Figure 13. Assessment of proliferation and viability of Caco-2 K18 shRNA cells in 2D culture. (**A**) Illustration of the workflow of how the 2D experiments are executed. The cells are plated on plastic (2D) on 96-well plates. The plates are then placed in Incucyte S3 live-cell analysis system throughout the whole incubation period, where images were acquired every two hours. At the endpoint of the experiment, WST-8 assay was used to measure reduction of WST-8 tetrazolium salt to an orange formazan dye. The reduction of WST-8 is dependent on electron transporters, thus reflecting the cellular dehydrogenase activity. The plate was also assessed using automated live-cell imaging and staining (not shown). (**B**) Representative image sets of the Caco-2 Scramble and K18 shRNA cell lines acquired from Incucyte S3. The images show both the phase-contrast images combined with green fluorescence channel, acquired at same position throughout four days. The scale bar is 800

µm. (**C**) Proliferation curves of the scrambled and K18 shRNA cell lines. The curves show the average confluency of 15 wells/cell line imaged for four days. The confluency was calculated based on the analysis tool included in the Incucyte S3 software. Two-way analysis of variance (ANOVA) was used to assess the statistical significance. (**D**) The viability difference between the two cell lines was determined after four days using WST-8 assay. The average absorbance from each cell lines were compared using a spectrophotometer. The absorbance of the K18 shRNA cells was normalized against the Scramble control and student's t-test was used to assess statistical significance (***P < 0.001; N.S. = non-significant).

5.3 Loss of K18 in Caco-2 cells display K8 and K80-positive aggregates in 2D culture

Caco-2 cells were fixed with acetone and stained for various keratins to assess the keratin profile in 2D culture. By staining for K18 in the Scramble and K18 shRNA cell line, we observed that the control cell line possessed prominent cytoplasmic keratin filaments, while K18 was absent in the knockdown cell line (fig. 14A). K8 formed a clear filamentous network in the control cell line, while in the K18 shRNA there was a less dense filamentous network coupled with K8-positive aggregates (fig. 14B). K80 was localized to the cytoplasm in a non-filamentous conformation in the control cells, but also present in the aggregates of the K18 shRNA cells (fig. 14C). Nevertheless, K8 and K80 stains were done separately and therefore co-localization is not guaranteed. These intracellular aggregates suggests that the protein degradation system is dysfunctional and could affect various cellular functions.

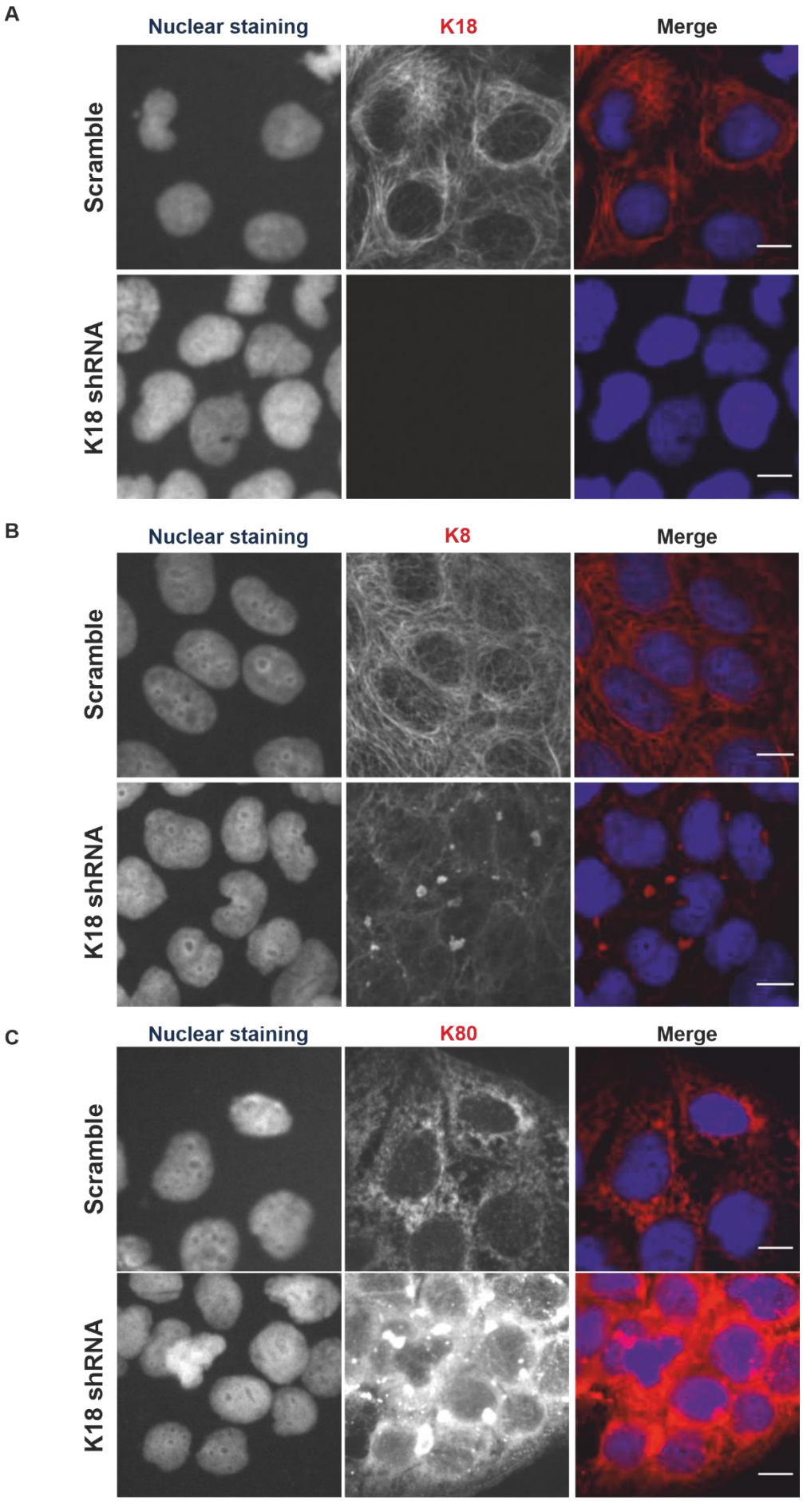
A
Nuclear staining
K18
Merge
Scramble
K18 shRNA
B
Nuclear staining
K8
Merge
Scramble
K18 shRNA
C
Nuclear staining
K80
Merge
Scramble
K18 shRNA

Figure 14. K18 knockdown in Caco-2 cells causes formation of K8 and K80-positive aggregates. (**A**) Confocal images of Caco-2 Scramble and K18 shRNA cells grown in 2D. The cells were stained with anti-K18 antibody (red) together with Draq5 as nuclear stain (blue). Each channel is shown separately and together as a merged image. The Caco-2 cell lines were also stained with (**B**) anti-K8 antibody or (**C**) anti-K80 antibody. Scale bars are 5 µm.

5.4 Lumen formation and hampered growth characterize K18 shRNA spheroids

The essence of the project was to assess whether we can observe any phenotypes in 3D that could show any resemblance to keratin loss *in vivo*. Therefore, we plated the Scramble and K18 shRNA cells in the miniaturized 3D culture with two different ECM compositions (Matrigel and a 1:1 mixture of Matrigel and type I collagen). At the endpoint of the experiment, viability was assessed using WST-8 viability assay and spheroid morphology was examined by live-cell staining, automated confocal microscopy combined with AMIDA software analysis. The first three days of the 3D cultures were primarily dedicated to establishment and growth of the single cells into smaller spheroids (fig. 15) The Caco-2 cells formed round cell clusters that had not yet adapted to a basal-apical polarization. At approximately day 5, it was noticeable that the K18 shRNA spheroids were growing more slowly in size than the control spheroids. In addition, there was also spheroids within both cell lines that started to form lumens at approximately the same time point. Around day 9, several of the spheroids of both cell lines had adapted a basal-apical polarity. Interestingly, there were some observable differences between the spheroids lacking K18 and the control spheroids. The Caco-2 Scramble spheroids had a more “promiscuous” morphology compared to K18 shRNA spheroids. The Scramble spheroids had a turbid and rougher structure whereas the knockdown spheroids had larger and clearer lumens (fig. 16A). Another noticeable difference was that the K18 shRNA spheroids had a more eccentric lumen formation, as some of the spheroids formed multiple lumens (fig. 15).

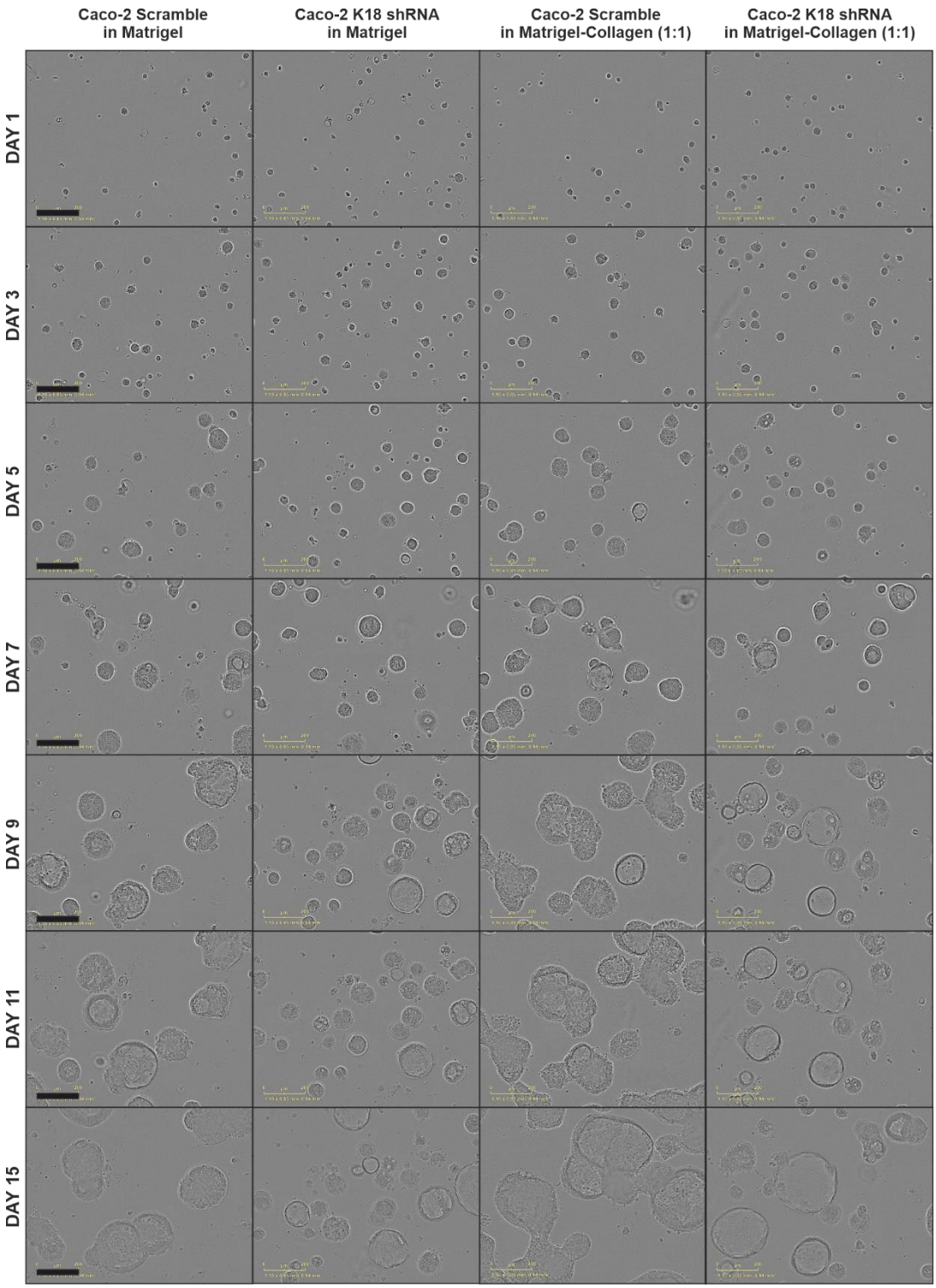

Figure 15. Monitoring of Caco-2 Scramble and K18 shRNA spheroids grown in two different matrix compositions for 15 days. Caco-2 Scramble and K18 shRNA cells were cultured in the 3D at equal cell numbers and two different ECM compositions: Matrigel and Matrigel/collagen 1:1 mix. The 3D-plate was monitored in Incucyte ZOOM for 15 days. Image panel presents the spheroid growth until day 11 and the last day of the experiment (day 15). The images were acquired using phase contrast and 5x objective. Scale bars are 200 µm.

In context to the two different matrix compositions, the spheroids grown in Matrigel:Collagen (1:1) mix were prone to cluster together, especially the Scramble spheroids (fig. 15). At the endpoint of the experiment (day 15), the viability of the spheroids was assessed using WST-8 assay, which showed a significantly higher metabolic activity of the Scramble spheroids relative to the K18 shRNA spheroids in both ECMs (fig. 16B). There was also a difference between Scramble spheroids in the two matrices, as the absorbance was higher in the Matrigel: Collagen mix compared to Matrigel solely (fig. 16B). As higher absorbance corresponded to higher dehydrogenase activity, the Scramble spheroids are more metabolically active than K18 shRNA spheroids. In corporation of collagen into the ECM promotes additional metabolic activity and growth (fig. 16B).

The spinning disc confocal images (fig. 16C) showed that the staining (together with endogenous eGFP) provides enough signal for adequate AMIDA analysis of the spheroids. The stains are essential as they facilitate segmentation of the spheroids, which then provides the numerical data for spheroid morphology. Although the segmentation was never immaculate, it provides data that accurately correspond to the max projections. Spheroids of the Scramble control and the K18 shRNA grown in Matrigel were assessed and compared. The spheroids in Matrigel:Collagen were excluded as the z-stacks were out of focus. The cumulative morphological data of all the spheroids confirmed that the Scramble spheroids were significantly larger compared to the K18 shRNA spheroids, although the Scramble spheroids showed a broad variation in size (Area) (fig. 16D). Similarly, the K18 shRNA spheroids were more round (Roundness) compared to the Scramble that showed a wide heterogeneity. Both cell lines showed a broad variation in roughness of the spheroids, but the K18 shRNA spheroids had more even membrane surface compared to the controls. By looking at the hollowness, K18 shRNA spheroids were less hollow on average than the control spheroids (Hollowness). Nevertheless, the K18 shRNA population also possessed a broad variation in hollowness (fig. 16D) and a small fraction of spheroids which were prominently large and hollow.

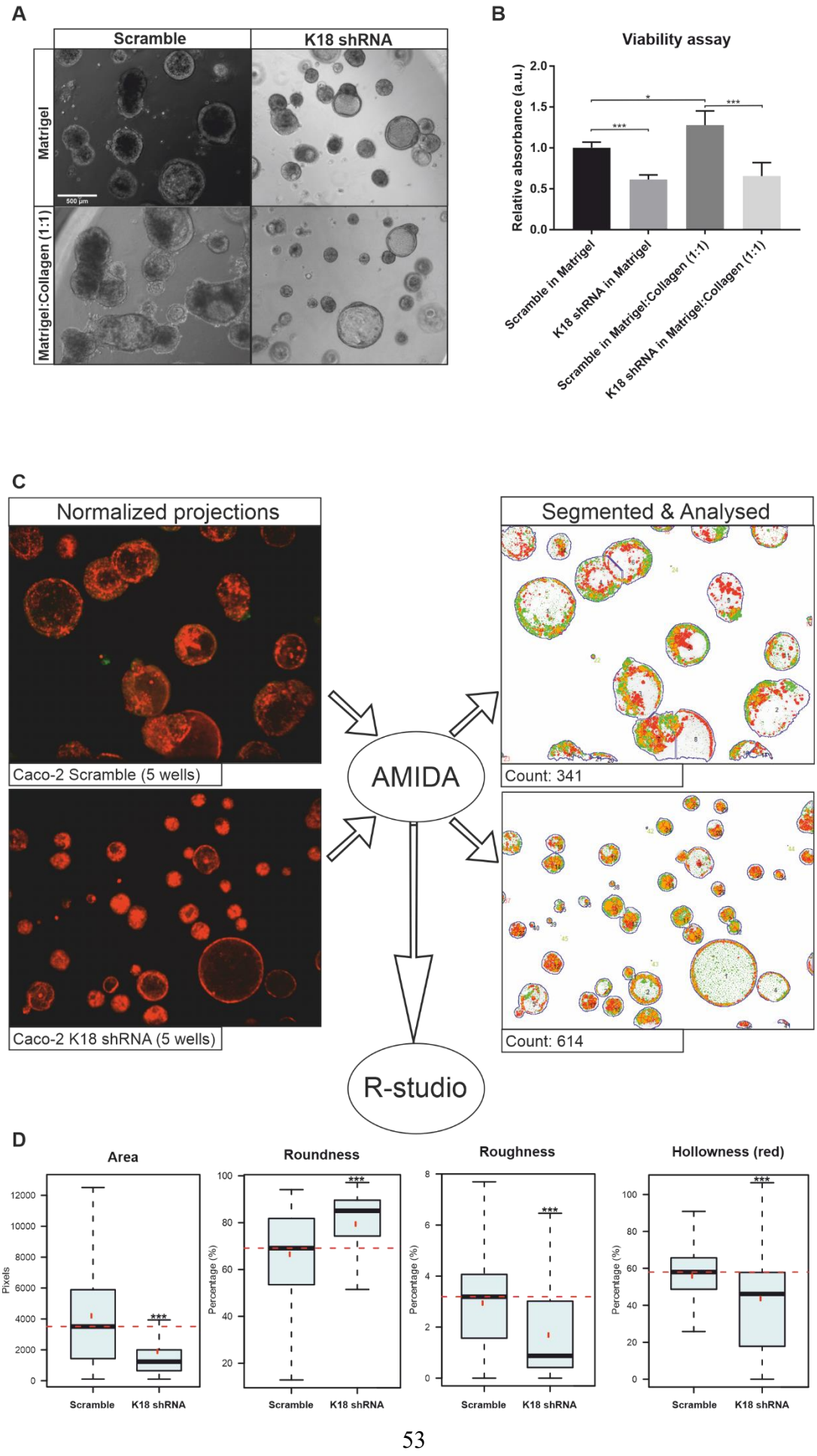
A
Scramble
K18 shRNA
Matrigel
Matrigel:Collagen (1:1)
500 µm
B
Viability assay
Relative absorbance (a.u.)
2.0
1.5
1.0
0.5
0.0
*
***
***
Scramble in Matrigel
K18 shRNA in Matrigel
Scramble in Matrigel:Collagen (1:1)
K18 shRNA in Matrigel:Collagen (1:1)
C
Normalized projections
Caco-2 Scramble (5 wells)
Caco-2 K18 shRNA (5 wells)
AMIDA
R-studio
Segmented & Analysed
Count: 341
Count: 614
D
Area
Pixels
12000
10000
8000
6000
4000
2000
0
***
Scramble
K18 shRNA
Roundness
Percentage (%)
100
80
60
40
20
***
Scramble
K18 shRNA
Roughness
Percentage (%)
8
6
4
2
0
***
Scramble
K18 shRNA
Hollowness (red)
Percentage (%)
100
80
60
40
20
0
***
Scramble
K18 shRNA

Figure 16. Loss of K18 in Caco-2 spheroids showed differences in both viability and morphology. At the endpoint of the 3D experiment, viability was assessed by WST-8 assay and automated confocal microscopy of stained Caco-2 spheroids to use for morphological analysis. (**A**) Phase-contrast images from day 12 of the experiment. Scale bar is 500 µm. (**B**) Relative absorbance (WST-8 assay) of the two cell lines in two different ECM-compositions. K18 shRNA cells were normalized against Scramble cells in the same ECM. Scramble control in Matrigel:Collagen (1:1) was normalized against Scramble in Matrigel. Whiskers show standard deviation and statistical significance was measured using student's t-test (P*<0.05; P***<0.001). (**C**) Z-stacks of Caco-2 spheroids stained with 1 µM lysotracker were acquired using automated confocal microscope. Z-stacks were merged into max projections. The AMIDA software provides segmentations of the projections (based on red/green fluorescence) and the parametric data is processed via R-studio scripts. (**D**) The morphological data (area, roundness, roughness and hollowness) from AMIDA is presented as box plots. Area was measured in pixels, as the rest of shown parameters were measured in percentage. The boxes encapsulate the 25th-to-75th percentiles and the black line marks the median value. Whiskers represents the max/min values within the spheroid populations. Red lines mark the average value of the controls, standard deviation is also annotated (red mark).

5.5 Increased villin expression is associated with downregulation of K18 in both 3D and 2D cultures of Caco-2 cells

To characterize differentiation, rate of apoptosis and proliferation in K18 shRNA Caco-2 in both 3D and 2D culture, we used western blotting to quantify proteins associated with these functions. In addition, we were interested to see if there are any alterations in the keratin profiles. The Caco-2 cells were grown to 80% confluency in 2D and the 3D cultures were grown for approximately 11 days before harvest.

K18 shRNA Caco-2 cells showed a significant downregulation of K18 in both 3D (~50%) and 2D cultures respectively (~10%). Assessing other type I keratins, we observed that K19 levels were extensively upregulated (fig. 17A & 17D). 2D culture showed a 2-fold increase of K19 and 3D culture showed a 2.5-fold increase (fig. 17A & 17D). The remainders of the assessed type I keratins (K20 and K23) showed no differences in protein levels (fig. 17A & 17D) based on the quantification of the bands and normalization against loading control. The complementary type II keratins (K8,

K7 and K80) showed no difference in their protein levels, with exception of K7 in 2D and 3D culture and K80 in 2D culture (fig. 17A & 17D).

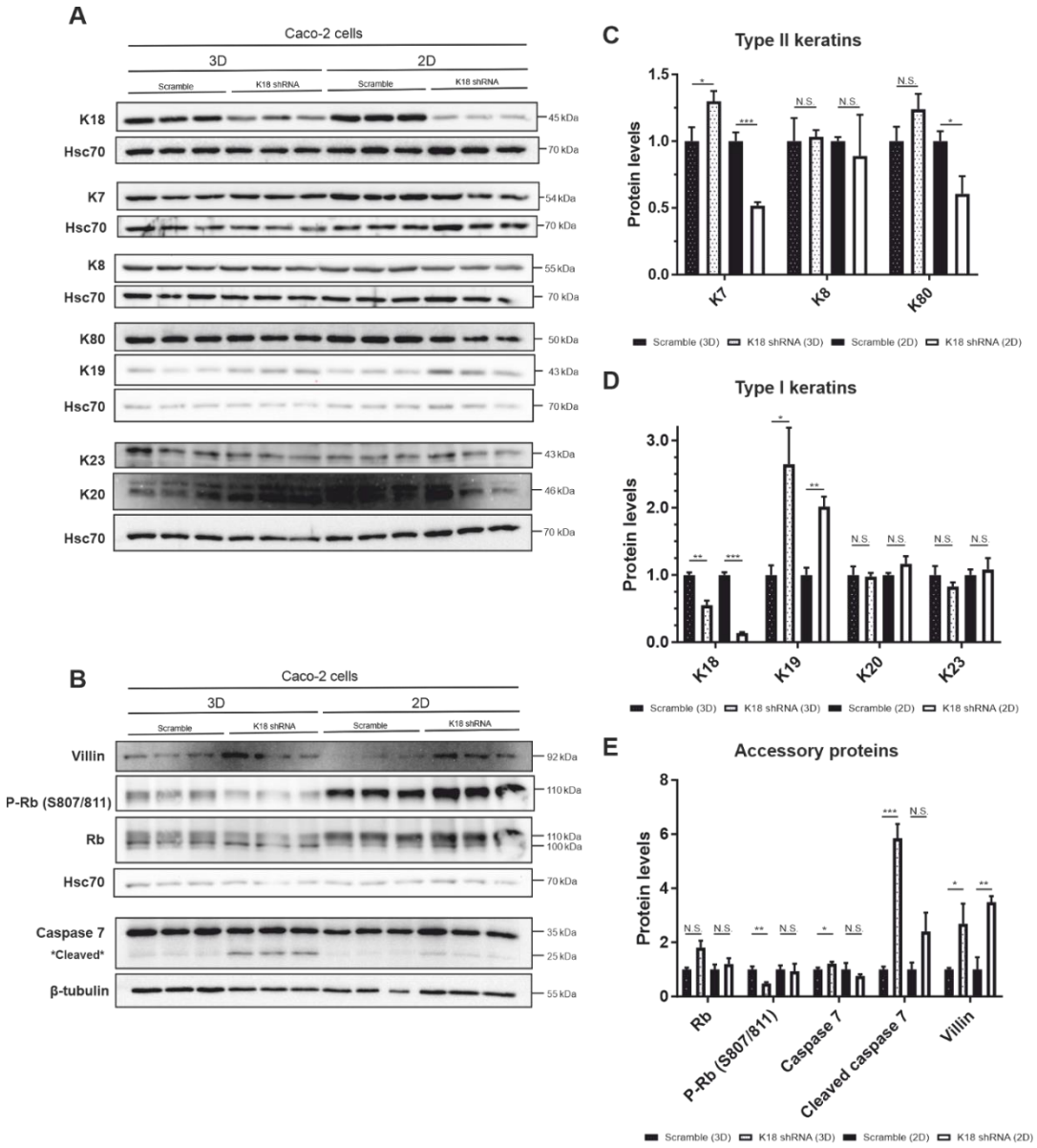

Figure 17. Western blotting of type II/I keratins and accessory proteins in 3D and 2D culture of Caco-2 cells. Caco-2 cells (Scramble and K18 shRNA) were grown in Matrigel (3D) for 11 days and then harvested for western blotting. For 2D culture, the cells were grown to approximately 80% confluency. (**A, B**) Western blots of type I, type II keratins and accessory proteins from Scramble and K18 shRNA cells cultured in both 3D and 2D culture. Samples were collected in triplicates and proteins levels were standardized between samples. Proteins from the same PVDF-membrane are coupled with corresponding loading control. (**C, D, E**) Quantification of western blots presented in A and B. Protein levels were normalized

against corresponding loading control. The average of the Scramble and K18 shRNA triplicates were compared against each other in 3D and 2D culture. Whiskers represent standard deviation (*P < 0.05; **P < 0.01; ***P < 0.001; N.S. = non-significant).

Interestingly, the K18 shRNA Caco-2 had significantly higher levels of villin (enterocyte marker) in both 3D and 2D (fig. 17B). The quantification (fig. 17E) also suggested that it is more accentuated in 2D relative to 3D. Apoptosis marker caspase 7 was also significantly more cleaved in the K18 shRNA cells and more prominent in the cells grown in 3D (fig. 17B). Retinoblastoma protein (Rb) phosphorylation is a marker for mitogenic signaling. By the quantification, there was a difference in phosphorylated (S807/811) Rb in 3D culture but not in 2D (fig. 17E). Moreover, phosphorylated Rb was more prominent in 2D culture compared to 3D culture (fig. 17B).

Furthermore, immunofluorescent staining was used as complementary approach to assess differentiation in 3D culture. We assessed differentiation in both spheroids (Caco-2 Scramble + K18 shRNA) and crypt-derived organoids from the conditional K8 KO mouse model (K8 WT + K8 KO). Tamoxifen-treatment was used to induce K8 loss in the organoids, while controls were treated with ethanol. We assessed K8 in organoids to determine if there are any similarities to what has been observed *in vivo* (Lähdeniemi et al., 2017) (increased ratio of secretory cells to absorptive cells). The anti-villin and anti-mucin 2 antibodies were not providing adequate signal in the spheroids (fig. 18A & 18B). On the other hand, the nuclear stain of the organoids revealed a neatly organized single layer of cells and hollow organoids (fig. 18C & 18D). Administration of tamoxifen also removed the K8 from the organoids, even though there was extracellular material outside the organoids that was K8-positive. Examining the differentiation markers (villin and mucin 2) it was difficult to pinpoint if there was a trend that would show an increased mucin 2 expression in K8 KO spheroids (fig. 18D).

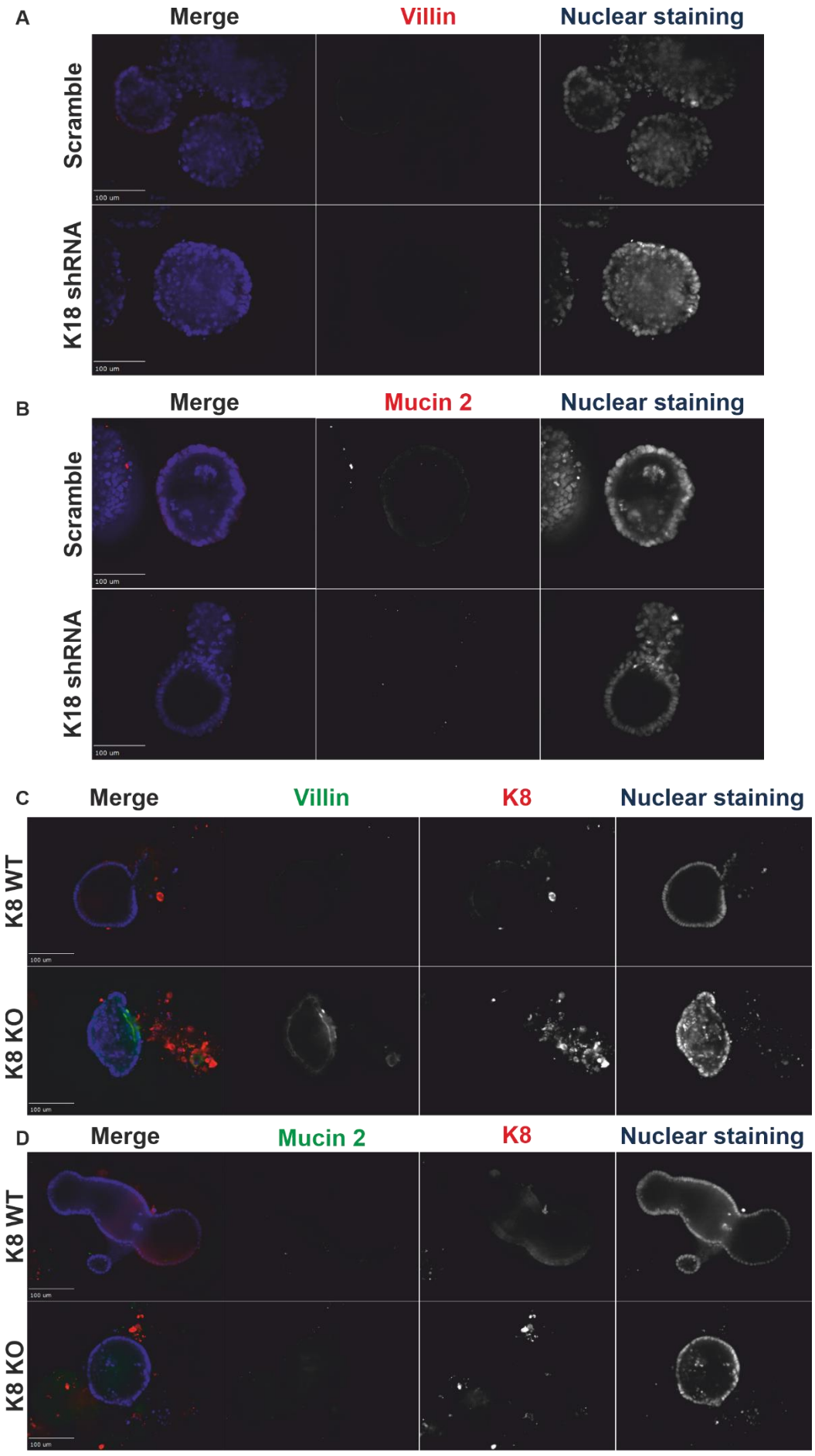
A
Merge
Villin
Nuclear staining
Scramble
K18 shRNA
100 um
B
Merge
Mucin 2
Nuclear staining
Scramble
K18 shRNA
100 um
C
Merge
Villin
K8
Nuclear staining
K8 WT
K8 KO
100 um
D
Merge
Mucin 2
K8
Nuclear staining
K8 WT
K8 KO
100 um

Figure 18. Low signal of differentiation markers in Caco-2 spheroids and K8 conditional knockout organoids. Immunofluorescent stainings with villin and mucin 2 were used to assess differentiation in Caco-2 K18 shRNA spheroids and K8 conditional knockout (KO) organoids. (**A**) Scramble and K18 shRNA spheroids were grown for 11 days and later stained with anti-villin antibody and Draq5 nuclear stain and are presented in separate channels (grey scale) and as a merged image. (**B**) Scramble and K18 shRNA spheroids stained with anti-mucin 2 antibody and Draq5 nuclear stain are presented in separate channels (grey scale) and as a merged image. (**C**) Murine-derived colon organoids were cultured for 7 days and consequently fixed with 4% PFA. All organoids were stained with both anti-K8, Draq5, anti-villin (**C**) and anti-mucin 2 (**D**) to differentiate between cell types. Scale bars are 100 µm.

5.6 Loss of K8 in spheroids showed modest differences in phenotype

CRISPR K8 KO Caco-2 cells were used to examine whether loss of K8 causes any variation in partner keratin levels, any similar phenotypical effects as downregulation of K18 showed in 2D and 3D cultures or if there were any phenotypes that are similar to what has been observed in the K8 KO mouse colon (hyperproliferation, decreased apoptosis, altered differentiation). Based on the western blots, basal levels of K8 in the Caco-2 K8 KO are around 10% compared to WT cells (fig. 19A & 19B). The cells did not possess any keratin aggregation as an effect of knocking out K8, at least based on IF stains (supplemental fig. 2A). However, it caused significant downregulation of type I keratins K18 and K19 (fig. 19A). Also type II keratins such as K7 and K80 were also significantly less abundant in Caco-2 K8 KO cells, excluding K7 levels in 3D (fig. 19B). The differences in keratin levels were relatively similar in comparison of 2D and 3D culture.

The K18 shRNA spheroids showed an increased villin protein expression in the earlier experiment (fig. 17B), which suggest they possessed more enterocytes, thus more differentiated. Villin protein levels in the K8 KO cells/spheroids were examined, but there were no differences between the two genotypes in either 2D or 3D culture (fig. 19A & 19B). We also blotted for Full length Notch 1 (FLN1) and Notch intracellular domain (NICD) in K8 KO cells/spheroids to assess differentiation pattern and if it follows the theory that knocking out K8 promotes the secretory lineage fate more. Although there was no signal for NICD, Notch extracellular domain (NECD) was used

as a decent substitute. The K8 KO cells, in both 2D/3D, showed less cleavage of Notch1 extracellular domain, which suggest that the cell line conform to the same differentiation pattern seen in mice. Although the FLN1 had a weak signal, and the WB quantification only showed a significant increase of NECD in 2D (fig. 19B). There were not any significant differences in villin expression (fig. 19B). Immunofluorescent stains showed a clear ablation of K8 from the K8 KO spheroids (fig. 19C). Proliferation marker Ki-67 showed a rather unspecific staining, thus not suitable to draw any substantial conclusions. Interestingly, tight junction marker Zona occludens-1 (ZO-1) showed a weaker signal in K8 KO spheroids, localized to the basal membrane in the K8 KO spheroids. This could potentially suggest there was a compromised barrier as a result of K8 loss (fig. 19C).

Furthermore, the Caco-2 K8 KO cells were cultured in 3D, monitored until day 14 in the Incucyte S3 and then assessed using viability assay and morphological analysis. The image set acquired throughout the 14 days showed no prominent differences in general morphology between K8 WT and K8 KO (supplemental fig. 3). The spheroids of both genotypes had a dark core, suggesting that they still were not completely hollow after 14 days growth (supplemental fig. 3). The WST-8 assay showed no difference in viability between WT and K8 KO in 3D culture (fig. 20B). Relatively to the K18 shRNA spheroids, K8 KO spheroid growth (Area) did not differ prominently from its WT counterpart (fig. 20C). The morphological analysis showed a significant difference in size, hollowness and roundness between spheroids grown in Matrigel; as the K8 KO spheroids are smaller, less hollow and more round (fig. 20C). Same discrepancies were also be observed for spheroids cultured in 1:1 Matrigel and collagen.

Taken together, the results showed prominent differences between conventional 2D culture and 3D culture in terms of proliferation, viability and morphology. This suggests that 3D culture is a superior modelling approach compared to 2D culturing, as there are prominent differences that may go unnoticed in 2D (e.g. viability or morphology).

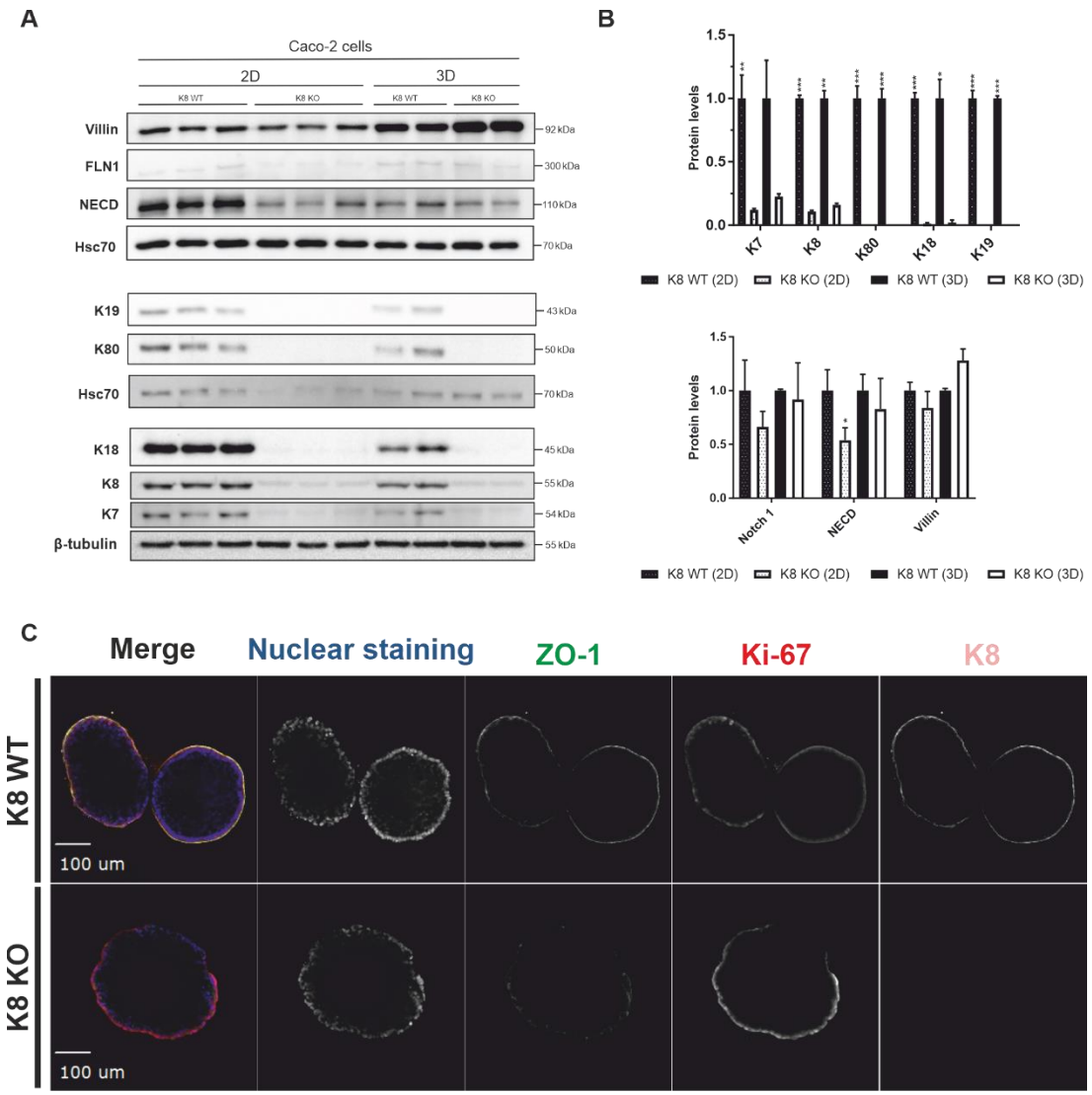

Figure 19. Loss of K8 is apparent based on Western blots and immunofluorescent stains. (**A**) Western blots for keratins and differentiation markers. Lysates were made from Caco-2 K8 WT and KO grown in 2D (up to 80% confluency) and 3D culture (grown for 14 days in Matrigel). 2D and 3D samples were made in triplicates and duplicates respectively. Protein levels were standardized between samples and proteins from the same PVDF-membrane were coupled with corresponding loading control. (**B**) Quantification of WBs. Keratin levels and differentiation markers are shown separately. The averages of WT and K8 KO samples were compared against each other in 3D and 2D culture separately. Whiskers represent standard deviation (*P < 0.05; **P < 0.01; ***P < 0.001; N.S. = non-significant). (**C**) K8 WT and KO spheroids were stained for K8, Ki-67, Zona occludens-1 (ZO-1) and DAPI (nuclear stain) and shown in separate channels and together as a merged image. Scale bars are 100 µm.

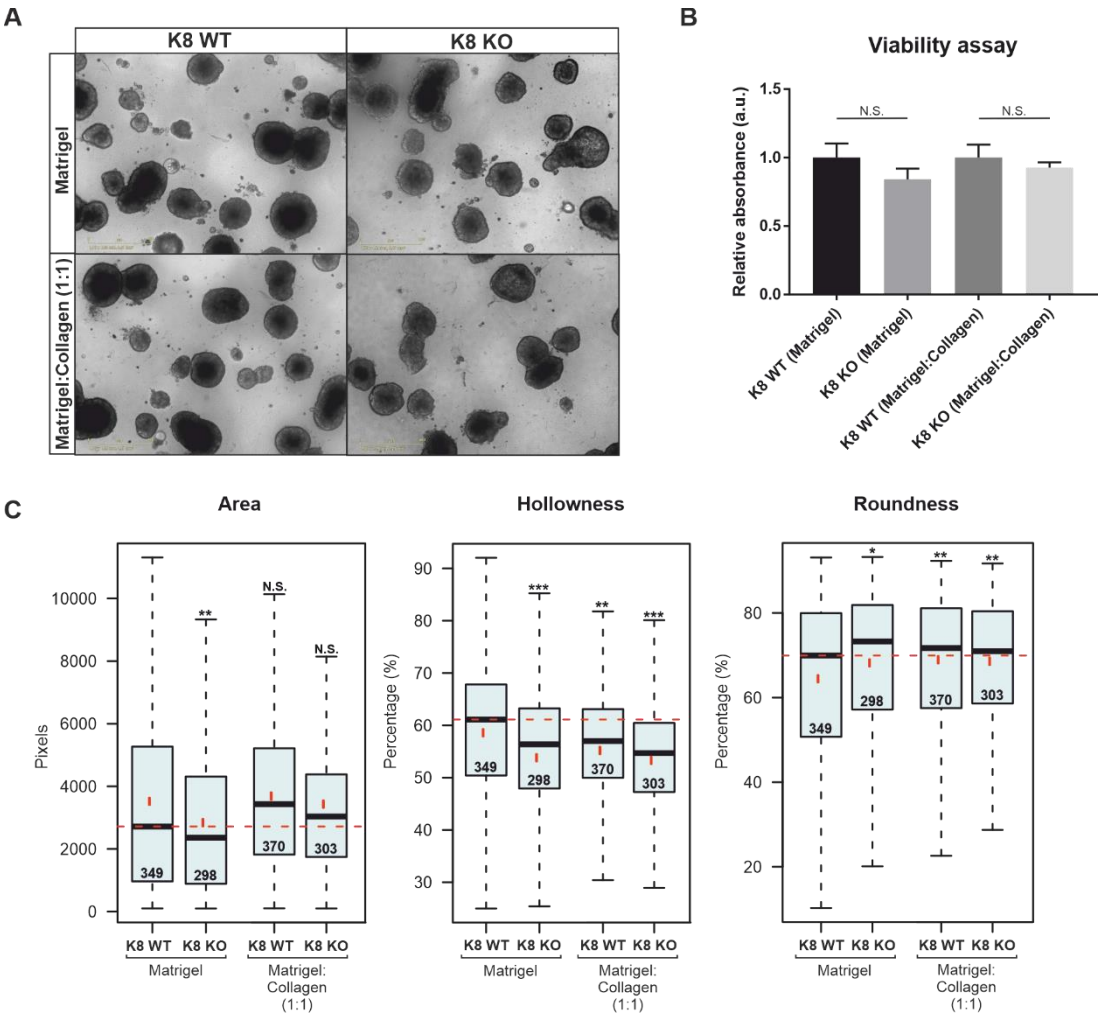

Figure 20. Caco-2 K8 KO spheroids showed subtle morphological alterations without any viability differences. Caco-2 WT and K8 KO were grown in Matrigel and Matrigel:Collagen (1:1 mix) for 14 days and monitored using Incucyte S3. (**A**) Phase-contrast images (10x magnification) of respective genotype in the two different matrices acquired at the final day of the experiment (day 14). (**B**) Viability was assessed using WST-8 assay. Each sample group represents the average absorbance of five wells. X-axis shows relative absorbance (a.u.) and whiskers show standard deviation. (**C**) Morphological data (area, hollowness and roundness) from AMIDA. Area was measured in pixels, as the rest of shown parameters were measured in percentage. The boxes encapsulate the 25th-to-75th percentiles and the black line marks the median value. Whiskers represents the max/min values within the spheroid populations. Red lines mark the average value of the controls, standard deviation is also annotated (red mark). Statistical significance was assess using a Bonferroni-corrected non-parametric Mann-Whitney U-test (P*<0.05; P**<0.01; P***<0.001; N.S. = non-significant).

6. Discussion

The whole premise of this project was to explore the possibilities of using *in vitro* 3D cultures, as these applications have been on the rise in recent years (Corrò et al., 2020). This trend can partially be accredited to the fact that 3D culture has shown to provide more realistic properties, as the cells are grown in an ECM compared to growing cells in a cell culture dish on plastic (Jensen and Teng, 2020). Furthermore, studying keratins in the colon has to a large extent been limited to *in vivo* experimental designs, especially when it comes to elucidating complex cellular mechanisms in physiological contexts (Polari et al., 2020). The role of K18/K8 was studied on several cellular parameters in conventional 2D culture (summarized in table. 1) and embedding Caco-2 cells and isolated mouse crypts into ECMs (3D culture; summarized in table 2). We specifically examined viability, morphology, proliferation, rate of apoptosis and differentiation. In addition, we also assessed alterations in keratin partner composition after downregulation K18 and K8, respectively.

6.1 The impact of K18 or K8 decrease on residual keratin levels in Caco-2 cells

The main keratins present in murine and human colon have to a large extent been documented (Polari et al., 2020), but little to no information is available on keratin profiles in Caco-2 cells (derived from human adenocarcinoma) and how they are affected by downregulation of K18 or K8. Therefore, we assessed keratin levels by western blotting. K8, K18, K19 are for certain high in abundance. K7 is present at lower levels compared to aforementioned keratins. However, there is some uncertainty regarding the K20, as an old K20 antibody provided signal for the HT-29 cell line, but not for Caco-2 cells (fig. 12A). The most recently used K20 antibody (guinea-pig host) provided signal (fig. 17A), but one could question the specificity of the antibody in this case since it has not yet been extensively tested. The relatively recently described and not well studied K80 and K23 could also be further examined to determine the specificity of the antibodies and if the bands are in fact representative (fig. 17A) – e.g. using purified proteins as positive controls. As a result of substantial downregulation of K18 via shRNA, levels of K19 were upregulated (fig. 17D) likely as a compensatory

mechanism for lower levels of K18. But for the rest of the keratins, there was not a consistent significant up- or downregulation in either 2D culture or spheroids (3D culture). The CRISPR K8 KO Caco-2 cells showed significant loss of K8 as well as the rest of the assessed keratins (K7, K18, K19, K80), except for K7 in 3D culture (fig. 20B). One can conclude that CRISPR is a more adequate tool for gene-silencing compared to RNA interference, at least based on the two cell lines used in this project. Rather than targeting the gene expression via mRNA degradation, in the K8 KO cell line, the gene is completely removed and therefore renders the mRNA expression unrealizable altogether.

6.2 K8/K80-positive aggregates as a result of K18 downregulation

The original hypothesis was that downregulation of K18 would cause a subsequent downregulation of K8 in the K18 shRNA Caco-2 cells. The K8 levels were decreased, but only to an insignificant extent. Nevertheless, there were intracellular aggregates observed in the cells. The aggregates were shown to be positively stained by K8 and K80 using immunofluorescence (fig. 14). It has previously been shown in K18 knockout mice that there is no apparent *in vivo* phenotype of K18 loss in the colon (Magin et al., 1998), however the colon was one among several organs examined and could have been more thoroughly studied. The only observed phenotype of K18 KO mice was K8-aggregates in the liver upon old age, which is similar to what was observed in our colonic K18 shRNA Caco-2 cells. One could speculate: why are K8 aggregates observed in K18 shRNA Caco-2 cells while there are no aggregates observed in the colon of K18 KO mice? Caco-2 is a colorectal adenocarcinoma cell line, which suggests that the aggregate formation might be cancer-related. Moreover, aggregation of ubiquitin-conjugated K8 fragments have been frequently observed in both advanced and early stages of colorectal carcinoma development (Nishibori et al., 1996). Another possible hypothesis is that the keratin aggregation in K18 shRNA Caco-2 cells is a result of imbalanced K8/K18 ratio. Keratin aggregation have been observed upon upregulated expression of K8 (e.g. during stress) and the ratio is skewed towards K8 > K18 (Toivola et al., 2015). Downregulation of K18 causes a similar change in the ratio. Similarly, a high K8/K18 ratio has been suggested to be linked to hepatocellular carcinoma (Golob-Schwarzl et al., 2018). MBDs generally

consist of K8/K18 proteins, ubiquitin and p62. Ubiquitin and p62 belong to the proteasomal degradation system, where the aggregates are targeted for degradation but unable to be degraded (Zatloukal et al., 2007). Whether or not the aggregates observed in K18 shRNA Caco-2 cells are bona fide MDBs needs to be elucidated.

The role of K80 has not been extensively described. Li et al. propose that K80 has a pro-tumorigenic role in colorectal carcinoma by promoting migration and invasion via AKT pathway activation (Li et al., 2018). Here it was also shown that K80 is incorporated in keratin aggregates together with K8 in K18 knockdown Caco-2 cells. However, its role still needs to be further examined.

6.3 Proliferation, viability and morphology

General parameters such as proliferation, viability and morphology of 2D and 3D culture were examined to study if loss of K18 or K8 caused any differences. The hypothesis was that hyperproliferation caused by K8 KO *in vivo* would also be observed in the cells, especially in 3D culture. The K8 KO Caco-2 cells showed no difference in viability compared to Scramble cells in neither 2D nor 3D culture (fig. 20B; 2D data not shown). The K18 shRNA cells did not show any difference in 2D culture, but there were significant viability differences for the K18 shRNA cells grown in 3D culture, as they were less viable. This could potentially be caused by the K8/K80-aggregates formed. We assessed the proliferation by examining confluency (in 2D culture) and spheroid size (in 3D culture). In addition, we examined the proliferation marker Rb and its level of phosphorylation which corresponds to active proliferative signaling. Based on confluency in 2D culture solely, we observed decreased and increased confluency in K18 shRNA (fig. 13C) and K8 KO (supplemental fig. 2B) cells, respectively. Zupancic et al. did a similar experiment where they assessed growth rate of HT-29 cells with mutated K8 or K18 cDNA constructs (Zupancic et al., 2014). They observed a hampered growth in mutated K18 (S230T mutation) cells and an increased growth in mutated K8 (K464N and G62C) cells. Their observations are aligned with our results, although mutation and complete loss of K18/K8 may have different cytological effects.

By growing the K18 shRNA cells in 3D culture, mostly smaller spheroids could be observed compared to the K8 WT control, which suggests a decreased growth in 3D culture. However, it is worth pointing out that the Scramble spheroids tended to migrate and merge with neighboring spheroids, which was not observed as often among the K18 shRNA spheroids. There were few notable differences in spheroid size or morphology between Caco-2 K8 WT and K8 KO, even though there are more profound phenotypes caused by K8 loss compared to K18 loss *in vivo* (Asghar et al., 2015; Magin et al., 1998). One hypothesis is that the cancer cell line could be deceiving, as hyperproliferation and apoptotic resistance are also hallmarks of cancer (Hanahan and Weinberg, 2011). Thus, the K8-associated phenotype is likely more prominent in a non-cancerous model system (e.g. non-transformed cell line or animal model).

Interestingly, as the difference in phosphorylated Rb levels is mostly insignificant between Scramble and K18 shRNA in both 2D and 3D culture, the phosphorylated Rb is higher in 2D culture compared to 3D culture (fig. 17B). Proliferation can decrease in 3D compared to 2D, but this is not a universal rule for all cells, as growth rate in 3D is relative to cell line and choice of ECM (Jensen and Teng, 2020). Nevertheless, the proliferative signaling might be more active during the earlier stage of spheroid development, as they tend to differentiate after longer time periods. Therefore, it is possible that a discrepancy in proliferation (caused by either K18 or K8 loss) could be observed at an earlier time point of the 3D cultures.

By acquiring maximum projections of the 3D spheroids stained with lysotracker, AMIDA was able to adequately create segmentations and provide morphological data, while Calcein and EthD2 did not stain the spheroids sufficiently for such analysis. The K18 shRNA spheroids (cultured for 12 days) differed from the control spheroids by being significantly smaller, rounder and less rough. A majority of these spheroids were less hollow relative to Scramble spheroids with a broad variation. The K8 KO spheroids (cultured for 14 days) did not differ by observing the spheroids under the microscope, as AMIDA showed that they were significantly smaller, less hollow and rounder. The differences were marginal, but the large sample size rendered them significant. Furthermore, a fraction of the K18 shRNA spheroids showed an eccentric lumen formation, as they seemed to have multiple lumens. A similar phenotype has been seen in Caco-2 spheroids when Rho-GTPase Cdc42 was depleted. Loss of Cdc42

was shown to disrupt mitotic spindle orientation during mitosis (Jaffe et al., 2008), which could suggest that keratins have a polarization-regulating role during morphogenesis.

6.4 Apoptosis and differentiation

It has been observed that loss of K8 *in vivo*, causes apoptotic resistance in the colonic epithelium while K8-loss in hepatocytes causes increased sensitivity against apoptosis (Habtezion et al., 2011). Our hypothesis was that a similar colonic phenotype would be observed in 2D culture and accentuated in 3D culture. Antibodies against caspase 7 and its cleaved form was used to elucidate any pro-apoptotic stimuli, and whether it translates into more cell death. Unfortunately, the antibodies did not work sufficiently for IF and WB. Nevertheless, there was significant increase in cleaved caspase 7 for the K18 shRNA spheroids. (fig. 17B). Cleavage of caspase 7 was also observed in 2D but insignificant by quantification (fig. 17E). The pro-apoptotic signaling could potentially be a consequence of the K8/K80-positive aggregates, but this would require further assessment and whether there were more cell deaths among the K18 shRNA cells.

One of the fundamental thoughts of the project was to study the role of K8 by culturing spheroids from CRISPR K8 KO Caco-2 cells and organoids from conditional K8 knockout models. The K8 loss *in vivo* mouse colon manifest by several phenotypes such as epithelial hyperplasia, diarrhea and inflammation (Asghar et al., 2015). On a molecular level, Notch1 levels are decreased which consequently skews maturing cells into the secretory cell fate (Lähdeniemi et al., 2017). Thus, causing a decrease in colonocytes and increase in goblet cells. The differentiation in the Caco-2 K8 KO was assessed by looking at morphology and differentiation markers (such as enterocyte marker villin and goblet cell marker mucin 2). The expectation was to observe a higher proportion of villin-positive enterocytes in K8 WT and conversely a higher proportion of mucin 2-positive cells in the K8 KO spheroids. However, no expressions were acquired for mucin 2 and villin levels were ambiguous as they were downregulated in 2D and upregulated in 3D for the K8 KO spheroids. The increased villin levels in 3D could suggest that the ECM is promoting differentiation. By blotting for Notch 1, we were able to get bands for FLN1 and cleaved NECD, which suggest that Notch activity

was higher in the K8 WT compared with the K8 KO (in both 2D and 3D culture). Therefore, Notch signaling in these cells seems to be in concordance with what has been observed in mice (Lähdeniemi et al., 2017). The targeting of villin and mucin 2 via IF-stains did not work sufficiently for neither the K18 shRNA spheroids nor K8 KO organoids (fig. 18). On the other hand, the degree of differentiation can largely be assessed by looking at the spheroid morphology. Apical-basal polarization and a prominent single cell-layered epithelium represents morphological characteristics of differentiation, which thought to be the standard morphology for the Caco-2 cell line (Jaffe et al., 2008; Magudia et al., 2012). In our 3D-cultures, we observed that the K18 shRNA spheroids developed significantly smaller, rounder and less rough spheroids (fig. 16). In addition, a subpopulation of the spheroids grew larger with clear lumens and neatly arranged simple cell layer, which suggests that some K18 shRNA spheroids would be more differentiated compared to the controls. Although there are significant differences in morphological parameters for the K8 WT and K8 KO spheroids, it is difficult to conclude which genotype would be more differentiated. One may also have to consider differentiation as a spectrum from low-grade dysplasia to highly anaplastic cells rather than searching for terminally differentiated cells. Furthermore, many studies that utilizes Caco-2 cells are rather ambiguous when it comes to differentiation of these cells. Some studies suggest that Caco-2 cells are de-differentiated in standard cell culture dishes and can differentiate when they are cultured for 14 days on polycarbonate membranes (Kaur and Moreau, 2021), others that they are already differentiated in 2D culture solely (Wanes et al., 2021). In summary, addition of a biologically relevant ECM is detrimental for differentiation *in vitro*, it might be overly ambitious to expect a cancer cell line to possess terminally differentiated cell types.

6.5 Limitations of the experimental design

Both the Caco-2 cells and the organoids were difficult to implement in 3D culture, as getting equal amounts of material to each well was difficult. Furthermore, the cells were problematic to work with, as they were reluctant to take up some of the stains. Further optimization of staining protocols for both live-cell stains and IF-staining protocol would be required before proceeding with the project. From a scientific perspective, one would need to show similar observations in other colorectal-derived

cell lines to give credibility to one's observation rather than just using one single cell line. In addition, one must acknowledge that the used Caco-2 cells are heterogeneous and exist in several different clones in various laboratories. The spheroids were stained for Ki-67 to assess proliferation, but the Ki-67 staining showed a staining pattern that looks like unspecific binding of the antibody. The K8 KO spheroids were smaller than the K8 WT, although K8 KO cells cultured in 2D showed a higher proliferation, at least in terms of confluency (fig. 20C). The proliferative capacity would likely have been better to assess at an earlier stage (e.g. day 5 or 7) of the 3D culture experiment. All things considered, comparing the non-cancerous *in vivo* colonic tissue lacking K8 with cancer cells in *in vitro* culture after K8 removal is substantially different. This could be the reason why the *in vitro* results differ from what has been observed *in vivo* (Asghar et al., 2015).

6.6 Future

In terms of the methodology, the miniaturized imaging platform has been an adequate and successful system for morphological analysis of several prostate and breast cancer cell lines (Härmä et al., 2014). Combining the platform with our spheroids/organoids was problematic regarding uptake of stains during live-cell imaging and doing IF-stains. One could possibly solve the problems by scavenging for a dye that works for Caco-2 cells and further optimize the IF-staining protocol.

The next step in this project would be to take alternative approaches to utilize the two Caco-2 cell lines (K18 shRNA/K8 KO). For example, the chorioallantoic membrane (CAM) model is a cost-effective and easy-to-use *in vivo*-like model (Nowak-Sliwinska et al., 2014). Fertilized eggs from chickens are opened, which exposes the vascular-rich membrane of the chicken embryo. By transplanting Caco-2 cells onto the membrane, one could study tumorigenesis in vicinity of vasculature and potentially epithelial-to-mesenchymal transition or other phenotypic differences between the cell lines. Furthermore, one could potentially expose the spheroids to various kinds of stress to reveal any potential vulnerabilities. It could also be advantageous to study K8/K18 loss in more aggressive colon cancer cell lines, such as HT-29 and HCT116.

Although Magin et al. already have concluded that K18 KO mice do not possess a colonic phenotype (Magin et al., 1998), one could hypothesize that these mice could potentially develop K8-positive aggregates upon tumor development in the colon, especially as keratin aggregation has been seen clinically in cancer patients (Nishibori et al., 1996). Therefore, treating K18 KO mice with carcinogenic AOM (azoxymethane) could potentially be insightful. Moreover, tight junction marker ZO-1 was downregulated in the K8 KO spheroids. A similar phenotype has been observed in K18 S230T mutant HT-29 cells where ZO-1 had a diffuse distribution and suggest to compromise tight junction function (Zupancic et al., 2014).

Considering the clinical relevance of compromised K8 in the colon, there are few clinical studies that have been conducted to study the correlation between mutated K8 and IBD. Owens et al. screened for K8 mutations in IBD patients and found that 5.2% of the IBD patients possessed previously described, heterozygous K8 miss-sense mutations (Owens et al., 2004). Therefore, there is still a need for studies that investigate the link K8 to IBD, and perhaps CRC as well (Misiorek et al., 2016). Here is a practical example of how *in vitro* 3D cultures could be utilized clinically. Patient-derived organoids could be collected by biopsy and used for diagnostics, personalized treatment and research. Organoid/spheroid biobanks would also allow further use of patient material in the future (Benam et al., 2015). This approach would be the most optimal for disease modelling, as it is done *in vitro* and representative of human biology rather than utilizing 2D culture of immortalized cell lines or animal models.

Molecular phenotype (compared to control cells)	Transgenic Caco-2 cells grown in 2D culture		Figure
	K18 shRNA	**K8 KO**	
Various keratin levels/ phenotypes	K8 - K18 ↓ (***) K7 ↓ (***) K19 ↑ (**) K80 ↓ (*) N.B! K8/K80-aggregates	K8 ↓ (***) K18 ↓ (***) K7 ↓ (**) K19 ↓ (***) K80 ↓ (***)	Fig. 17 & 19
Viability	No difference	No difference (not shown)	Fig. 13
Proliferation	Confluency ↓ (***) phos-Rb – No diff.	Confluency ↑ (***)	Fig. 13 & supplemental fig. 2
Morphology	Smaller area?	No difference	
Rate of apoptosis	Cleaved caspase 7 ↑ (n.s.)	?	Fig. 17
Differentiation	Villin ↑ (**)	Villin – No diff. Notch 1 – No diff. Cleaved Notch1 ↓	Fig. 17 & 19

Table 1. Summary table for the transgenic Caco-2 cells grown in 2D culture. Molecular phenotypes observed in K18 shRNA cells and K8 KO compared to respective control cell line. No diff. ↔ no difference. ↑ = Upregulation; ↓ = Downregulation; *** $P < 0.001$; ** $P > 0.01$; * $P < 0.05$; n.s. = not significant.

Molecular phenotype (compared to controls)		Transgenic Caco-2 cells grown in 3D culture (Spheroids)		Organoids (conditional K8 KO)	Figure
		K18 shRNA	K8 KO		
Various keratin levels/ phenotypes		K7 ↑ (*) K8 - K18 ↓ (**) K19 ↑ (*) K20 - K80 -	K7 ↓ (n.s.) K8 ↓ (**) K18 ↓ (*) K19 ↓ (***)	K8 ↓ (IF)	Fig. 17 & 19
Viability		↓ (***)	No difference	?	Fig. 16B & 20B
Proliferation		↓ (**)	?	?	Fig. 17
Morphology	**Area**	↓ (***)	↓ (**)	?	Fig. 16 & 20
	Roundness	↑ (***)	↑ (*)	?	
	Roughness	↓ (***)	Not shown	?	
	Hollowness	↓ (***) (High variation)	↓ (***)	?	
Rate of apoptosis		↑	?	?	Fig. 17
Differentiation		Villin ↑ (*)	Villin – no diff. Notch 1 – no diff. Cleaved Notch 1 - ↓ (*)	?	Fig. 17 & 19

Table 2. Summary table for the transgenic Caco-2 cells and K8 KO organoids grown in 3D-culture. Molecular phenotypes observed in K18 shRNA cells and K8 KO compared to respective control cell line. No diff. ↔ no difference. ↑ = Upregulation; ↓ = Downregulation; *** $P < 0.001$; ** $P > 0.01$; * $P < 0.05$; n.s. = not significant.

7. Conclusions

In this project, we have studied the phenotypical impact of knocking down or knocking out K18 or K8 in Caco-2 cells. Mutation or loss of K8 gives rise to multiple colonic phenotypes in mouse colon (hyperplasia, decreased cell death, diarrhea and inflammation)(Asghar et al., 2015), while no *in vivo* phenotypes in K18 KO mice colon have yet been documented (Magin et al., 1998). Therefore, we opted for using *in vitro* 3D cultures as a better approach, as it is more authentic than conventional 2D culture and more ethical than usage of mice. In addition, we took the opportunity to study the keratin composition in Caco-2 cells and how it is altered upon loss of K18/K8.

For the project, we utilized an imaging platform which allows real-time monitoring of both 2D and 3D culture using Incucyte imaging system. At the end of each experiment, the viability was examined using WST-8 assay and automated confocal microscopy of stained structures to study morphology. In addition, we used immunoblotting and immunofluorescent stains to assess several cellular mechanisms.

We showed here that downregulation of K18 in Caco-2 cells caused multiple phenotypical differences compared to control: decreased viability (2D/3D), decreased proliferation and a prominent morphological difference between the genotypes in 3D culture. In addition, loss of K18 caused cytoplasmic aggregates containing K8 and less described K80. One would assume that the K8-positive aggregation would directly cause all the differences, but it is still unknown whether MDBs have a cytoprotective function, pathological role or just an innocent bystander (Zatloukal et al., 2007). Therefore, one cannot say with certainty that the aggregates caused the observed phenotypes. On the other hand, K8-positive aggregates have been observed in hepatocytes of old K18 KO mice, which could suggest there could be more to the role of K18 in the colon.

Conversely, loss of K8 caused no difference in viability (3D), aggregation or any apparent morphological phenotype in 3D culture. K8 was shown to be less redundant than K18, as K8 causes a more substantial downregulation of other keratins compared to K18. The results suggest that there is at least partial differentiation of the Caco-2 spheroids, based on the morphology and expression of differentiation markers (Notch1

and villin). In addition, the results suggest that the K8 KO spheroids are phenotypically similar to *in vivo* according to Notch 1-activity (Lähdeniemi et al., 2017). Further studies would be needed to study the role of the K8/K80-positive aggregates and what is behind the phenotypical differences caused by loss of K18. As the K8 KO spheroids showed no prominent differences, exposure to stress (e.g. heat or hypoxia) could potentially reveal any concealed vulnerabilities.

Although this project had some practical complications, the results suggest that 3D culture is the superior culture technique relative to conventional 2D culture. The 3D experiments provided showed apparent differences in viability, proliferation and morphology, which were not as prominent in 2D culture. All in all, *in vitro* 3D cultures are still in their infancy but have the potential to be a realm for further methodological advancements in drug testing and disease modelling. There are also possibilities within the clinic, as patient-derived organoids could be utilized for diagnostics and personalized treatments (Jensen and Teng, 2020).

8. Acknowledgements

I want to express my greatest gratitude to my two main supervisors Diana & Malin, who had the confidence in me to take on this project and basically allowed me to roam the lab corridors by myself. Thanks for all the insightful input and wisdoms along the way.

Thanks to Mina for teaching me a lot of the hands-on stuff in when I first came to the lab and all help throughout these last couple of years. Best of luck with the on-going projects and hope to attend your thesis defense in the near future.

Thanks to the past and current the members of the Epithelial Biology Lab and Nees Lab. It is inspiring and fun to work alongside hard-working members of both labs. Thanks for all the jokes, coffee breaks and keeping up a great work atmosphere. A special recognition to Jesse Mattsson for all the help with AMIDA and R-studio, I would never have managed that by myself.

Thanks to the technical personnel at Cell Imaging and Cytometry Core at Bioscience Centre and Åbo Akademi University for the occasional technical support.

Lastly, a big thanks to friends and family for all the support throughout these last two years.

9. Summary in Swedish (Svensk sammanfattning)

Fenotypisk påverkan av keratin 8/18 nedreglering i *in vitro* 3D modeller av tjocktarmen

Prevalensen av inflammatorisk tarmsjukdom och tjocktarmscancer har stadigt ökat under de senaste årtiondena i västvärlden. Den först nämnda sjukdomen har ett multifaktoriellt sjukdomsförlopp som kännetecknas av kronisk inflammation av både tunn- och tjocktarm. Den bakomliggande etiologin till hur sjukdomstillståndet uppstår är fortfarande okänd, men tidigare forskning hänvisar till försvagning av epitel, onormal immunrespons och rubbing av tjocktarmens bakterieflora som bidragande faktorer. Långvarig inflammation i tjocktarmen är dessutom en riskfaktor för vidareutveckling till tjocktarmscancer. Tjocktarmscancer är den fjärde vanligaste cancertypen och har den tredje största dödligheten.

Keratiner (K) är en familj av proteiner som tillsammans med mikrofilament, mikrotubuli och septiner bygger upp cellens cytoskelett. De bygger upp ett nätverk av fibrer inuti cellens cytoplasma och är kända för att bidra med mekanisk stabilitet och ger epitelet skydd mot mekanisk påfrestning. Enskilda keratinprotein byggs upp till hetero-polymeriska fibrer, där exempelvis K8 (typ II) och K18–20 (typ I) förekommer i människans tjocktarmsepitel. De har dessutom en mångsidig roll där de är involverade i cellulära processer som exempelvis tillväxt, differentiering, signalering och försvar mot olika typer av stress. I tjocktarmen har det visat sig att K8 har en betydande funktion, varvid muterat eller förlorat K8 bidrar till ökad tillväxt av tjocktarmsepitelet, diarré och inflammation i transgena musmodeller. Förlust av K8 i samband med olika tjocktarmscancermodeller i möss har även visat sig bidra till ökad tumörbildning. Förlust av K18, en av de viktigaste keratinpartnerna till K8, har däremot ingen identifierad fenotyp i mustjocktarmen. Förlust av K18 i möss manifestar sig enbart i gamla möss, som K8-positiva aggregat i leverns hepatocyter. Gedigen forskning pågår för att påvisa den kliniska betydelsen av keratiner i tjocktarmshälsan, men dessvärre är det inte etiskt hållbart att utföra forskning på försöksdjur samtidigt som det förekommer en brist på adekvata *in vitro* modeller för att studera keratinernas mångfacetterade roll i tjocktarmen.

Målsättningen med denna pro gradu projekt är att framställa standardiserade 3D modeller och undersöka fenotypiska skillnader av förlust av K18 respektive K8 i cancerceller (Caco-2) samt K8 i tjocktarms-organoider. Cellerna odlades i traditionell 2D kultur och 3D kultur som inbegriper cellodling i en artificiell extracellulär matris. Extracellulära matris simulerar den cellulära mikromiljö som förekommer *in vivo*, vilket gör att cellerna övergår till en tredimensionell morfologi. 2D och 3D experiment studerades med hjälp av Incucyte (ett system som kontinuerligt fotograferar odlingarna under tillväxten) samt konfokalmikroskopering med färgning i slutet av experimentet för att samla bilder som sedan kan undergå digital morfologisk analys. Den morfologiska analysen utförs av AMIDA, ett automatiserat program som identifierar och kvantifierar ett flertal morfologiska parametrar av varje enskild spheroid (3D-kultur av cancerceller) eller organoid. Fenotypiska parametrar som undersöktes var morfologiska skillnader, tillväxt och celldifferentiering. Dessutom undersöktes livsduglighet och celldöd, samt förändringar i keratinkompositionen vid förlust av K18 respektive K8. Proteinnivåer av keratiner, differentieringsmarkörer, viabilitets- samt apoptosmarkörer approximerades och kvantifierades med hjälp av western blot, en immunologisk metod som används för att detektera och kvantifiera proteiner. Fixering och immunofluorescens färgning av 2D och 3D kulturer utfördes för att lokalisera av de olika proteinerna.

Nedreglering av K18 i Caco-2 resulterade i en svag nedreglering av K8 medan K19 verkar kompensera för K18 i både 2D och 3D kulturer. Dessutom upptäcktes en försvagad tillväxt vid förlust av K18 som sammanfaller med förekomst av K8- och K80-positiva aggregat. 3D kultur av K18-negativa celler påvisade en påtaglig morfologisk fenotyp i jämförelse med kontroll cellerna. Däremot påvisade K8-negativa celler ingen distinkt skillnad i morfologi eller livsduglighet, varken i 2D eller 3D kultur. Resultaten är anmärkningsvärda med tanke på att förlust av K18 verkar ha flera cytologiska effekter än förlust av K8. Särskilt förekomsten av K8- och K80-positiva aggregat, med tanke på att ingen fenotyp har observerats i tjocktarm av K18-negativa möss. Tidigare har K8-positiva aggregat enbart observerats i levern av gamla K18-negativa möss. Experimenten är utförda på cancerceller *in vitro*, men resultaten kan potentiellt tyda på en ej tidigare karaktäriserad funktion av K18 *in vivo*, likväl ett framsteg för att studera keratiner *ex vivo*. Trots att K8-negativa celler inte visade en påtaglig fenotyp kan fortsatt utveckling av modellen vara motiverat för att uppnå ett

adekvat 3D-modell. Användningen av *in vitro* 3D-modeller är på framfart inom biomedicinsk forskning och kan öppna upp för ny metodik inom grundforskning och diagnostik.

10. References

Aisenbrey, E.A., Murphy, W.L., 2020. Synthetic alternatives to Matrigel. Nat. Rev. Mater. 5, 539–551. https://doi.org/10.1038/s41578-020-0199-8

Åkerfelt, M., Bayramoglu, N., Robinson, S., Toriseva, M., Schukov, H.-P., Härmä, V., Virtanen, J., Sormunen, R., Kaakinen, M., Kannala, J., Eklund, L., Heikkilä, J., Nees, M., 2015. Automated tracking of tumor-stroma morphology in microtissues identifies functional targets within the tumor microenvironment for therapeutic intervention. Oncotarget 6, 30035–30056. https://doi.org/10.18632/oncotarget.5046

Asghar, M.N., Priyamvada, S., Nyström, J.H., Anbazhagan, A.N., Dudeja, P.K., Toivola, D.M., 2016. Keratin 8 knockdown leads to loss of the chloride transporter DRA in the colon. Am. J. Physiol. Gastrointest. Liver Physiol. 310, G1147-1154. https://doi.org/10.1152/ajpgi.00354.2015

Asghar, M.N., Silvander, J.S.G., Helenius, T.O., Lähdeniemi, I.A.K., Alam, C., Fortelius, L.E., Holmsten, R.O., Toivola, D.M., 2015. The Amount of Keratins Matters for Stress Protection of the Colonic Epithelium. PLoS ONE 10. https://doi.org/10.1371/journal.pone.0127436

Baribault, H., Penner, J., Iozzo, R.V., Wilson-Heiner, M., 1994. Colorectal hyperplasia and inflammation in keratin 8-deficient FVB/N mice. Genes Dev. 8, 2964–2973. https://doi.org/10.1101/gad.8.24.2964

Barker, N., van de Wetering, M., Clevers, H., 2008. The intestinal stem cell. Genes Dev. 22, 1856–1864. https://doi.org/10.1101/gad.1674008

Barker, N., van Es, J.H., Kuipers, J., Kujala, P., van den Born, M., Cozijnsen, M., Haegebarth, A., Korving, J., Begthel, H., Peters, P.J., Clevers, H., 2007. Identification of stem cells in small intestine and colon by marker gene Lgr5. Nature 449, 1003–1007. https://doi.org/10.1038/nature06196

Benam, K.H., Dauth, S., Hassell, B., Herland, A., Jain, A., Jang, K.-J., Karalis, K., Kim, H.J., MacQueen, L., Mahmoodian, R., Musah, S., Torisawa, Y., van der Meer, A.D., Villenave, R., Yadid, M., Parker, K.K., Ingber, D.E., 2015. Engineered in vitro

disease models. Annu. Rev. Pathol. 10, 195–262. https://doi.org/10.1146/annurev-pathol-012414-040418

Beumer, J., Clevers, H., 2021. Cell fate specification and differentiation in the adult mammalian intestine. Nat. Rev. Mol. Cell Biol. 22, 39–53. https://doi.org/10.1038/s41580-020-0278-0

Bray, F., Ferlay, J., Soerjomataram, I., Siegel, R.L., Torre, L.A., Jemal, A., 2018. Global cancer statistics 2018: GLOBOCAN estimates of incidence and mortality worldwide for 36 cancers in 185 countries. CA. Cancer J. Clin. 68, 394–424. https://doi.org/10.3322/caac.21492

Brenner, H., Kloor, M., Pox, C.P., 2014. Colorectal cancer. Lancet Lond. Engl. 383, 1490–1502. https://doi.org/10.1016/S0140-6736(13)61649-9

Cho, J.H., Brant, S.R., 2011. Recent insights into the genetics of inflammatory bowel disease. Gastroenterology 140, 1704–1712. https://doi.org/10.1053/j.gastro.2011.02.046

Clevers, H., Nusse, R., 2012. Wnt/β-Catenin Signaling and Disease. Cell 149, 1192–1205. https://doi.org/10.1016/j.cell.2012.05.012

Corrò, C., Novellasdemunt, L., Li, V.S.W., 2020. A brief history of organoids. Am. J. Physiol. - Cell Physiol. 319, C151–C165. https://doi.org/10.1152/ajpcell.00120.2020

Debnath, J., Brugge, J.S., 2005. Modelling glandular epithelial cancers in three-dimensional cultures. Nat. Rev. Cancer 5, 675–688. https://doi.org/10.1038/nrc1695

Debnath, J., Muthuswamy, S.K., Brugge, J.S., 2003. Morphogenesis and oncogenesis of MCF-10A mammary epithelial acini grown in three-dimensional basement membrane cultures. Methods San Diego Calif 30, 256–268. https://doi.org/10.1016/s1046-2023(03)00032-x

Drost, J., Clevers, H., 2018. Organoids in cancer research. Nat. Rev. Cancer 18, 407–418. https://doi.org/10.1038/s41568-018-0007-6

Edmondson, R., Broglie, J.J., Adcock, A.F., Yang, L., 2014. Three-Dimensional Cell Culture Systems and Their Applications in Drug Discovery and Cell-Based Biosensors. Assay Drug Dev. Technol. 12, 207–218. https://doi.org/10.1089/adt.2014.573

Eriksson, J.E., Dechat, T., Grin, B., Helfand, B., Mendez, M., Pallari, H.-M., Goldman, R.D., 2009. Introducing intermediate filaments: from discovery to disease. J. Clin. Invest. 119, 1763–1771. https://doi.org/10.1172/JCI38339

Etienne-Manneville, S., 2018. Cytoplasmic Intermediate Filaments in Cell Biology. Annu. Rev. Cell Dev. Biol. 34, 1–28. https://doi.org/10.1146/annurev-cellbio-100617-062534

Fletcher, D.A., Mullins, R.D., 2010. Cell mechanics and the cytoskeleton. Nature 463, 485–492. https://doi.org/10.1038/nature08908

Gerbe, F., Jay, P., 2016. Intestinal tuft cells: epithelial sentinels linking luminal cues to the immune system. Mucosal Immunol. 9, 1353–1359. https://doi.org/10.1038/mi.2016.68

Gilbert, S., Loranger, A., Daigle, N., Marceau, N., 2001. Simple epithelium keratins 8 and 18 provide resistance to Fas-mediated apoptosis. The protection occurs through a receptor-targeting modulation. J. Cell Biol. 154, 763–774. https://doi.org/10.1083/jcb.200102130

Golob-Schwarzl, N., Bettermann, K., Mehta, A.K., Kessler, S.M., Unterluggauer, J., Krassnig, S., Kojima, K., Chen, X., Hoshida, Y., Bardeesy, N.M., Müller, H., Svendova, V., Schimek, M.G., Diwoky, C., Lipfert, A., Mahajan, V., Stumptner, C., Thüringer, A., Fröhlich, L.F., Stojakovic, T., Nilsson, K.P.R., Kolbe, T., Rülicke, T., Magin, T.M., Strnad, P., Kiemer, A.K., Moriggl, R., Haybaeck, J., 2018. High Keratin 8/18 Ratio Predicts Aggressive Hepatocellular Cancer Phenotype. Transl. Oncol. 12, 256–268. https://doi.org/10.1016/j.tranon.2018.10.010

Goulielmos, G., Gounari, F., Remington, S., Müller, S., Häner, M., Aebi, U., Georgatos, S.D., 1996. Filensin and phakinin form a novel type of beaded intermediate filaments and coassemble de novo in cultured cells. J. Cell Biol. 132, 643–655. https://doi.org/10.1083/jcb.132.4.643

Grumati, P., Dikic, I., 2018. Ubiquitin signaling and autophagy. J. Biol. Chem. 293, 5404–5413. https://doi.org/10.1074/jbc.TM117.000117

Guan, Q., 2019. A Comprehensive Review and Update on the Pathogenesis of Inflammatory Bowel Disease. J. Immunol. Res. 2019, 7247238. https://doi.org/10.1155/2019/7247238

Habtezion, A., Toivola, D.M., Asghar, M.N., Kronmal, G.S., Brooks, J.D., Butcher, E.C., Omary, M.B., 2011. Absence of keratin 8 confers a paradoxical microflora-dependent resistance to apoptosis in the colon. Proc. Natl. Acad. Sci. U. S. A. 108, 1445–1450. https://doi.org/10.1073/pnas.1010833108

Habtezion, A., Toivola, D.M., Butcher, E.C., Omary, M.B., 2005. Keratin-8-deficient mice develop chronic spontaneous Th2 colitis amenable to antibiotic treatment. J. Cell Sci. 118, 1971–1980. https://doi.org/10.1242/jcs.02316

Hanahan, D., Weinberg, R.A., 2011. Hallmarks of cancer: the next generation. Cell 144, 646–674. https://doi.org/10.1016/j.cell.2011.02.013

Harada, N., Tamai, Y., Ishikawa, T., Sauer, B., Takaku, K., Oshima, M., Taketo, M.M., 1999. Intestinal polyposis in mice with a dominant stable mutation of the beta-catenin gene. EMBO J. 18, 5931–5942. https://doi.org/10.1093/emboj/18.21.5931

Härmä, V., Schukov, H.-P., Happonen, A., Ahonen, I., Virtanen, J., Siitari, H., Åkerfelt, M., Lötjönen, J., Nees, M., 2014. Quantification of Dynamic Morphological Drug Responses in 3D Organotypic Cell Cultures by Automated Image Analysis. PLoS ONE 9. https://doi.org/10.1371/journal.pone.0096426

Härmä, V., Virtanen, J., Mäkelä, R., Happonen, A., Mpindi, J.-P., Knuuttila, M., Kohonen, P., Lötjönen, J., Kallioniemi, O., Nees, M., 2010. A comprehensive panel of three-dimensional models for studies of prostate cancer growth, invasion and drug responses. PloS One 5, e10431. https://doi.org/10.1371/journal.pone.0010431

Jaffe, A.B., Kaji, N., Durgan, J., Hall, A., 2008. Cdc42 controls spindle orientation to position the apical surface during epithelial morphogenesis. J. Cell Biol. 183, 625–633. https://doi.org/10.1083/jcb.200807121

Jensen, C., Teng, Y., 2020. Is It Time to Start Transitioning From 2D to 3D Cell Culture? Front. Mol. Biosci. 7. https://doi.org/10.3389/fmolb.2020.00033

Kasendra, M., Tovaglieri, A., Sontheimer-Phelps, A., Jalili-Firoozinezhad, S., Bein, A., Chalkiadaki, A., Scholl, W., Zhang, C., Rickner, H., Richmond, C.A., Li, H., Breault, D.T., Ingber, D.E., 2018. Development of a primary human Small Intestine-on-a-Chip using biopsy-derived organoids. Sci. Rep. 8, 2871. https://doi.org/10.1038/s41598-018-21201-7

Kaur, H., Moreau, R., 2021. mTORC1 silencing during intestinal epithelial Caco-2 cell differentiation is mediated by the activation of the AMPK/TSC2 pathway. Biochem. Biophys. Res. Commun. 545, 183–188. https://doi.org/10.1016/j.bbrc.2021.01.070

Kierszenbaum, A.L., Tres, L.L., 2016. Histology and cell biology: an introduction to pathology, Fourth edition. ed. Elsevier.

Kim, Y.S., Ho, S.B., 2010. Intestinal Goblet Cells and Mucins in Health and Disease: Recent Insights and Progress. Curr. Gastroenterol. Rep. 12, 319–330. https://doi.org/10.1007/s11894-010-0131-2

Kodach, L.L., Wiercinska, E., de Miranda, N.F.C.C., Bleuming, S.A., Musler, A.R., Peppelenbosch, M.P., Dekker, E., van den Brink, G.R., van Noesel, C.J.M., Morreau, H., Hommes, D.W., Ten Dijke, P., Offerhaus, G.J.A., Hardwick, J.C.H., 2008. The bone morphogenetic protein pathway is inactivated in the majority of sporadic colorectal cancers. Gastroenterology 134, 1332–1341. https://doi.org/10.1053/j.gastro.2008.02.059

Kreplak, L., Bär, H., Leterrier, J.F., Herrmann, H., Aebi, U., 2005. Exploring the mechanical behavior of single intermediate filaments. J. Mol. Biol. 354, 569–577. https://doi.org/10.1016/j.jmb.2005.09.092

Ku, N.-O., Omary, M.B., 2006. A disease- and phosphorylation-related nonmechanical function for keratin 8. J. Cell Biol. 174, 115–125. https://doi.org/10.1083/jcb.200602146

Kumar, V., Abbas, A.K., Aster, J.C., 2018. Robbins: Basic Pathology, 10th ed. Elsevier.

Kunzelmann, K., Mall, M., 2002. Electrolyte Transport in the Mammalian Colon: Mechanisms and Implications for Disease. Physiol. Rev. 82, 245–289. https://doi.org/10.1152/physrev.00026.2001

Lagies, S., Schlimpert, M., Neumann, S., Wäldin, A., Kammerer, B., Borner, C., Peintner, L., 2020. Cells grown in three-dimensional spheroids mirror in vivo metabolic response of epithelial cells. Commun. Biol. 3, 1–10. https://doi.org/10.1038/s42003-020-0973-6

Lähdeniemi, I.A.K., Misiorek, J.O., Antila, C.J.M., Landor, S.K.-J., Stenvall, C.-G.A., Fortelius, L.E., Bergström, L.K., Sahlgren, C., Toivola, D.M., 2017. Keratins regulate colonic epithelial cell differentiation through the Notch1 signalling pathway. Cell Death Differ. 24, 984–996. https://doi.org/10.1038/cdd.2017.28

Li, C., Liu, Xisheng, Liu, Y., Liu, Xueni, Wang, R., Liao, J., Wu, S., Fan, J., Peng, Z., Li, B., Wang, Z., 2018. Keratin 80 promotes migration and invasion of colorectal carcinoma by interacting with PRKDC via activating the AKT pathway. Cell Death Dis. 9, 1009. https://doi.org/10.1038/s41419-018-1030-y

Liao, J., Omary, M.B., 1996. 14-3-3 proteins associate with phosphorylated simple epithelial keratins during cell cycle progression and act as a solubility cofactor. J. Cell Biol. 133, 345–357. https://doi.org/10.1083/jcb.133.2.345

Loschke, F., Seltmann, K., Bouameur, J.-E., Magin, T.M., 2015. Regulation of keratin network organization. Curr. Opin. Cell Biol. 32, 56–64. https://doi.org/10.1016/j.ceb.2014.12.006

Luca, A.C., Mersch, S., Deenen, R., Schmidt, S., Messner, I., Schäfer, K.-L., Baldus, S.E., Huckenbeck, W., Piekorz, R.P., Knoefel, W.T., Krieg, A., Stoecklein, N.H., 2013. Impact of the 3D Microenvironment on Phenotype, Gene Expression, and EGFR Inhibition of Colorectal Cancer Cell Lines. PLoS ONE 8, e59689. https://doi.org/10.1371/journal.pone.0059689

MacDonald, B.T., Tamai, K., He, X., 2009. Wnt/β-catenin signaling: components, mechanisms, and diseases. Dev. Cell 17, 9–26. https://doi.org/10.1016/j.devcel.2009.06.016

Magin, T.M., Schröder, R., Leitgeb, S., Wanninger, F., Zatloukal, K., Grund, C., Melton, D.W., 1998. Lessons from keratin 18 knockout mice: formation of novel keratin filaments, secondary loss of keratin 7 and accumulation of liver-specific keratin 8-positive aggregates. J. Cell Biol. 140, 1441–1451. https://doi.org/10.1083/jcb.140.6.1441

Magudia, K., Lahoz, A., Hall, A., 2012. K-Ras and B-Raf oncogenes inhibit colon epithelial polarity establishment through up-regulation of c-myc. J. Cell Biol. 198, 185–194. https://doi.org/10.1083/jcb.201202108

Misiorek, J.O., Lähdeniemi, I.A.K., Nyström, J.H., Paramonov, V.M., Gullmets, J.A., Saarento, H., Rivero-Müller, A., Husøy, T., Taimen, P., Toivola, D.M., 2016. Keratin 8-deletion induced colitis predisposes to murine colorectal cancer enforced by the inflammasome and IL-22 pathway. Carcinogenesis 37, 777–786. https://doi.org/10.1093/carcin/bgw063

Moll, R., Divo, M., Langbein, L., 2008. The human keratins: biology and pathology. Histochem. Cell Biol. 129, 705–733. https://doi.org/10.1007/s00418-008-0435-6

Molodecky, N.A., Soon, I.S., Rabi, D.M., Ghali, W.A., Ferris, M., Chernoff, G., Benchimol, E.I., Panaccione, R., Ghosh, S., Barkema, H.W., Kaplan, G.G., 2012. Increasing incidence and prevalence of the inflammatory bowel diseases with time, based on systematic review. Gastroenterology 142, 46-54.e42; quiz e30. https://doi.org/10.1053/j.gastro.2011.10.001

Nishibori, H., Matsuno, Y., Iwaya, M., Osada, T., Kubomura, N., Iwamatsu, A., Kohno, H., Sato, S., Kitajima, M., Hirohashi, S., 1996. Human colorectal carcinomas specifically accumulate Mr 42,000 ubiquitin-conjugated cytokeratin 8 fragments. Cancer Res. 56, 2752–2757.

Nowak-Sliwinska, P., Segura, T., Iruela-Arispe, M.L., 2014. The chicken chorioallantoic membrane model in biology, medicine and bioengineering. Angiogenesis 17, 779–804. https://doi.org/10.1007/s10456-014-9440-7

Omary, M.B., Ku, N.-O., Strnad, P., Hanada, S., 2009. Toward unraveling the complexity of simple epithelial keratins in human disease. J. Clin. Invest. 119, 1794–1805. https://doi.org/10.1172/JCI37762

Owens, D.W., Lane, E.B., 2004. Keratin mutations and intestinal pathology. J. Pathol. 204, 377–385. https://doi.org/10.1002/path.1646

Owens, D.W., Wilson, N.J., Hill, A.J.M., Rugg, E.L., Porter, R.M., Hutcheson, A.M., Quinlan, R.A., van Heel, D., Parkes, M., Jewell, D.P., Campbell, S.S., Ghosh, S., Satsangi, J., Lane, E.B., 2004. Human keratin 8 mutations that disturb filament assembly observed in inflammatory bowel disease patients. J. Cell Sci. 117, 1989–1999. https://doi.org/10.1242/jcs.01043

Patankar, M., Eskelinen, S., Tuomisto, A., Mäkinen, M.J., Karttunen, T.J., 2019. KRAS and BRAF mutations induce anoikis resistance and characteristic 3D

phenotypes in Caco-2 cells. Mol. Med. Rep. 20, 4634–4644. https://doi.org/10.3892/mmr.2019.10693

Polari, L., Alam, C.M., Nyström, J.H., Heikkilä, T., Tayyab, M., Baghestani, S., Toivola, D.M., 2020. Keratin intermediate filaments in the colon: guardians of epithelial homeostasis. Int. J. Biochem. Cell Biol. 129, 105878. https://doi.org/10.1016/j.biocel.2020.105878

Puschhof, J., Pleguezuelos-Manzano, C., Martinez-Silgado, A., Akkerman, N., Saftien, A., Boot, C., de Waal, A., Beumer, J., Dutta, D., Heo, I., Clevers, H., 2021. Intestinal organoid cocultures with microbes. Nat. Protoc. 16, 4633–4649. https://doi.org/10.1038/s41596-021-00589-z

Reidy, E., Leonard, N.A., Treacy, O., Ryan, A.E., 2021. A 3D View of Colorectal Cancer Models in Predicting Therapeutic Responses and Resistance. Cancers 13, 227. https://doi.org/10.3390/cancers13020227

Rousset, M., 1986. The human colon carcinoma cell lines HT-29 and Caco-2: two in vitro models for the study of intestinal differentiation. Biochimie 68, 1035–1040. https://doi.org/10.1016/s0300-9084(86)80177-8

Saladin, K.S., 2008. Human anatomy, 2nd edition. ed.

Sasaki, N., Sachs, N., Wiebrands, K., Ellenbroek, S.I.J., Fumagalli, A., Lyubimova, A., Begthel, H., van den Born, M., van Es, J.H., Karthaus, W.R., Li, V.S.W., López-Iglesias, C., Peters, P.J., van Rheenen, J., van Oudenaarden, A., Clevers, H., 2016. Reg4+ deep crypt secretory cells function as epithelial niche for Lgr5+ stem cells in colon. Proc. Natl. Acad. Sci. U. S. A. 113, E5399-5407. https://doi.org/10.1073/pnas.1607327113

Sato, T., Stange, D.E., Ferrante, M., Vries, R.G.J., Van Es, J.H., Van den Brink, S., Van Houdt, W.J., Pronk, A., Van Gorp, J., Siersema, P.D., Clevers, H., 2011. Long-term expansion of epithelial organoids from human colon, adenoma, adenocarcinoma, and Barrett's epithelium. Gastroenterology 141, 1762–1772. https://doi.org/10.1053/j.gastro.2011.07.050

Sato, T., Vries, R.G., Snippert, H.J., van de Wetering, M., Barker, N., Stange, D.E., van Es, J.H., Abo, A., Kujala, P., Peters, P.J., Clevers, H., 2009. Single Lgr5 stem cells

build crypt-villus structures in vitro without a mesenchymal niche. Nature 459, 262–265. https://doi.org/10.1038/nature07935

Schneikert, J., Behrens, J., 2007. The canonical Wnt signalling pathway and its APC partner in colon cancer development. Gut 56, 417–425. https://doi.org/10.1136/gut.2006.093310

Siebel, C., Lendahl, U., 2017. Notch Signaling in Development, Tissue Homeostasis, and Disease. Physiol. Rev. 97, 1235–1294. https://doi.org/10.1152/physrev.00005.2017

Simian, M., Bissell, M.J., 2017. Organoids: A historical perspective of thinking in three dimensions. J. Cell Biol. 216, 31–40. https://doi.org/10.1083/jcb.201610056

Sinicrope, F.A., 2018. Lynch Syndrome-Associated Colorectal Cancer. N. Engl. J. Med. 379, 764–773. https://doi.org/10.1056/NEJMcp1714533

Sjöqvist, M., Andersson, E.R., 2019. Do as I say, Not(ch) as I do: Lateral control of cell fate. Dev. Biol., Signaling pathways in development 447, 58–70. https://doi.org/10.1016/j.ydbio.2017.09.032

Snider, N.T., Omary, M.B., 2014. Post-translational modifications of intermediate filament proteins: mechanisms and functions. Nat. Rev. Mol. Cell Biol. 15, 163–177. https://doi.org/10.1038/nrm3753

Sontheimer-Phelps, A., Chou, D.B., Tovaglieri, A., Ferrante, T.C., Duckworth, T., Fadel, C., Frismantas, V., Sutherland, A.D., Jalili-Firoozinezhad, S., Kasendra, M., Stas, E., Weaver, J.C., Richmond, C.A., Levy, O., Prantil-Baun, R., Breault, D.T., Ingber, D.E., 2020. Human Colon-on-a-Chip Enables Continuous In Vitro Analysis of Colon Mucus Layer Accumulation and Physiology. Cell. Mol. Gastroenterol. Hepatol. 9, 507–526. https://doi.org/10.1016/j.jcmgh.2019.11.008

Steinhart, Z., Angers, S., 2018. Wnt signaling in development and tissue homeostasis. Development 145. https://doi.org/10.1242/dev.146589

Stenvall, C.-G.A., Tayyab, M., Grönroos, T.J., Ilomäki, M.A., Viiri, K., Ridge, K.M., Polari, L., Toivola, D.M., 2021. Targeted deletion of keratin 8 in intestinal epithelial cells disrupts tissue integrity and predisposes to tumorigenesis in the colon. Cell. Mol. Life Sci. CMLS 79, 10. https://doi.org/10.1007/s00018-021-04081-5

Sugimoto, S., Ohta, Y., Fujii, M., Matano, M., Shimokawa, M., Nanki, K., Date, S., Nishikori, S., Nakazato, Y., Nakamura, T., Kanai, T., Sato, T., 2018. Reconstruction of the Human Colon Epithelium In Vivo. Cell Stem Cell 22, 171-176.e5. https://doi.org/10.1016/j.stem.2017.11.012

Sung, H., Ferlay, J., Siegel, R.L., Laversanne, M., Soerjomataram, I., Jemal, A., Bray, F., 2021. Global Cancer Statistics 2020: GLOBOCAN Estimates of Incidence and Mortality Worldwide for 36 Cancers in 185 Countries. CA. Cancer J. Clin. 71, 209–249. https://doi.org/10.3322/caac.21660

Toivola, D.M., Boor, P., Alam, C., Strnad, P., 2015. Keratins in health and disease. Curr. Opin. Cell Biol. 32, 73–81. https://doi.org/10.1016/j.ceb.2014.12.008

Toivola, D.M., Strnad, P., Habtezion, A., Omary, M.B., 2010. Intermediate filaments take the heat as stress proteins. Trends Cell Biol. 20, 79–91. https://doi.org/10.1016/j.tcb.2009.11.004

Wanes, D., Naim, H.Y., Dengler, F., 2021. Proliferation and Differentiation of Intestinal Caco-2 Cells Are Maintained in Culture with Human Platelet Lysate Instead of Fetal Calf Serum. Cells 10, 3038. https://doi.org/10.3390/cells10113038

Wang, R.N., Green, J., Wang, Z., Deng, Y., Qiao, M., Peabody, M., Zhang, Q., Ye, J., Yan, Z., Denduluri, S., Idowu, O., Li, M., Shen, C., Hu, A., Haydon, R.C., Kang, R., Mok, J., Lee, M.J., Luu, H.L., Shi, L.L., 2014. Bone Morphogenetic Protein (BMP) signaling in development and human diseases. Genes Dis. 1, 87–105. https://doi.org/10.1016/j.gendis.2014.07.005

Wiznerowicz, M., Trono, D., 2003. Conditional suppression of cellular genes: lentivirus vector-mediated drug-inducible RNA interference. J. Virol. 77, 8957–8961. https://doi.org/10.1128/jvi.77.16.8957-8951.2003

Woods, B.L., Gladfelter, A.S., 2021. The state of the septin cytoskeleton from assembly to function. Curr. Opin. Cell Biol. 68, 105–112. https://doi.org/10.1016/j.ceb.2020.10.007

Wu, C., Zhu, X., Liu, W., Ruan, T., Tao, K., 2017. Hedgehog signaling pathway in colorectal cancer: function, mechanism, and therapy. OncoTargets Ther. 10, 3249–3259. https://doi.org/10.2147/OTT.S139639

Wu, N., Sun, H., Zhao, X., Zhang, Y., Tan, J., Qi, Y., Wang, Q., Ng, M., Liu, Zhaoyuan, He, L., Niu, X., Chen, L., Liu, Zhiduo, Li, H.-B., Zeng, Y.A., Roulis, M., Liu, D., Cheng, J., Zhou, B., Ng, L.G., Zou, D., Ye, Y., Flavell, R.A., Ginhoux, F., Su, B., 2021. MAP3K2-regulated intestinal stromal cells define a distinct stem cell niche. Nature 592, 606–610. https://doi.org/10.1038/s41586-021-03283-y

Xie, W., Burke, B., 2016. Lamins. Curr. Biol. CB 26, R348-350. https://doi.org/10.1016/j.cub.2016.01.055

Yeung, T.M., Gandhi, S.C., Wilding, J.L., Muschel, R., Bodmer, W.F., 2010. Cancer stem cells from colorectal cancer-derived cell lines. Proc. Natl. Acad. Sci. U. S. A. 107, 3722–3727. https://doi.org/10.1073/pnas.0915135107

Yu, Y., Yang, W., Li, Y., Cong, Y., 2020. Enteroendocrine Cells: Sensing Gut Microbiota and Regulating Inflammatory Bowel Diseases. Inflamm. Bowel Dis. 26, 11–20. https://doi.org/10.1093/ibd/izz217

Zatloukal, K., French, S.W., Stumptner, C., Strnad, P., Harada, M., Toivola, D.M., Cadrin, M., Omary, M.B., 2007. From Mallory to Mallory-Denk bodies: what, how and why? Exp. Cell Res. 313, 2033–2049. https://doi.org/10.1016/j.yexcr.2007.04.024

Zhang, Y.-Z., Li, Y.-Y., 2014. Inflammatory bowel disease: Pathogenesis. World J. Gastroenterol. WJG 20, 91–99. https://doi.org/10.3748/wjg.v20.i1.91

Zhou, Q., Toivola, D.M., Feng, N., Greenberg, H.B., Franke, W.W., Omary, M.B., 2003. Keratin 20 Helps Maintain Intermediate Filament Organization in Intestinal Epithelia. Mol. Biol. Cell 14, 2959–2971. https://doi.org/10.1091/mbc.E03-02-0059

Zupancic, T., Stojan, J., Lane, E.B., Komel, R., Bedina-Zavec, A., Liovic, M., 2014. Intestinal Cell Barrier Function In Vitro Is Severely Compromised by Keratin 8 and 18 Mutations Identified in Patients with Inflammatory Bowel Disease. PLOS ONE 9, e99398. https://doi.org/10.1371/journal.pone.0099398

11. Supplemental figures

Primary antibodies	Dilutions (WB/2D IF/3D IF)	Host	Manufacturer	Catalog number
Keratin 7	1:1,000/-/-	Rabbit	Abcam	181598
Keratin 8	1:1,000/ 1:200/1:100	Rat	DSHB	TROMA-I
Keratin 18	1:1,000/1:200/1:100	Mouse	Progen	61028
Keratin 19	1:1,000/-/-	Mouse	Sigma-Aldrich	C7159
Keratin 20	1:3,000/-/-	Guinea pig	Progen	GP-K20
Keratin 23	1:1,000/-/-	Rabbit	Abcam	156569
Keratin 80	1:1,000/1:200/-	Rabbit	Proteintech	16835-1-AP
Pan-cytokeratin	1:1,000/-/-	Mouse	Abcam	86734
B-tubulin	1:1,000/-/-	Mouse	Sigma-Aldrich	T8328
Caspase 7	1:1,000/1:200/1:100	Rabbit	Cell Signaling Technology	9492
Cleaved caspase 7 (Asp198)	1:1,000/1:200/1:100	Rabbit	Cell Signaling Technology	94915
Hsc70	1:1,000/-/-	Rat	Enzo Life Sciences	ADI-SPA-815F
Ki-67	1:1,000/1:200/1:100	Mouse	Abcam	16667
Mucin 2	1:1,000/1:100/1:50	Rabbit	Abcam	272692
Notch 1	1:1,000/-/-	Rabbit	Cell Signaling Technology	3608
Cleaved Notch 1 (Val1744)	1:1,000/-/-	Rabbit	Cell Signaling Technology	D3B8
Rb	1:1,000/-/-	Rabbit	Abcam	181616
Phos-Rb (Ser807/811)	1:1,000/-/-	Rabbit	Cell Signaling Technology	D20B12
Synaptophysin	1:1,000/1:100/-	Rabbit	Thermo Fischer Scientific	MA5-14532
Villin	1:1,000/1:100/1:50	Rabbit	Thermo Fischer Scientific	PA5-17290
ZO-1	-/-/1:100	Mouse	Invitrogen	33-9100

Supplemental table 1. List of primary antibodies used for the project.

Secondary antibodies	Dilutions (WB/2D IF/3D IF)	Manufacturer
Anti-rat IgG-HRP	1:10,000/-/-	Cell signaling
Anti-mouse IgG-HRP	1:10,000/-/-	GE Healthcare
Anti-rabbit IgG-HRP	1:10,000/-/-	Promega
Anti-guinea pig 488	1:10,000/1:200/-	Invitrogen
Anti-rat 488	-/1:200/1:100	Invitrogen
Anti-rat 568	-/1:200/1:100	Invitrogen
Anti-rat 647	-/1:200/1:100	Invitrogen
Anti-mouse Alexa Fluor 488	-/1:200/1:100	Invitrogen
Anti-rabbit Alexa Fluor 488	-/1:200/1:100	Invitrogen
Anti-rabbit 568	-/1:200/1:100	Invitrogen

Supplemental table 2. Secondary antibodies used for the project.

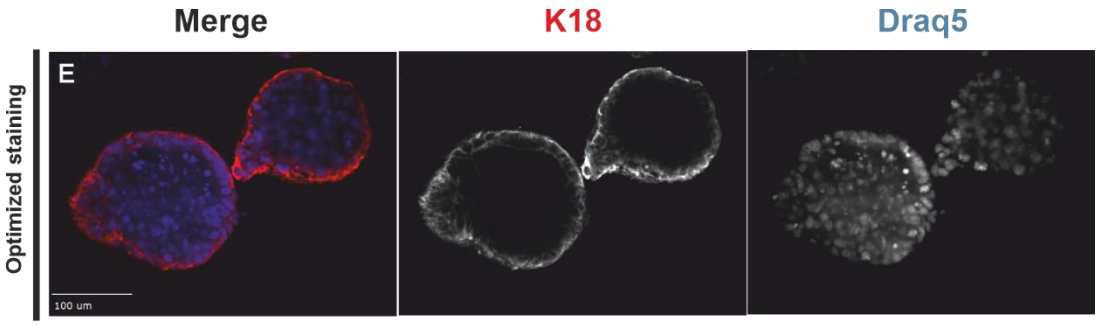

Supplemental figure 1. The Caco-2 spheroids display morphological heterogenicity in both Scramble and K18 shRNA spheroids. Caco-2 spheroids were cultured in the 3D platform for approximately 15 days and fixed using 4% formaldehyde. Immunofluorescent staining and confocal microscopy were used to study the morphologies. Phalloidin (stains filamentous actin) and anti-pankeratin antibody was used to study both large spheroids with prominent lumen formation (**A**) and spheroids with more promiscuous/unorganized structure (**B**) among the Scramble spheroids. The heterogenicity is also prevalent among the K18 shRNA spheroids as there are larger hollow spheroids (**C**) and smaller spheroids with eccentric and multiple lumens (**D**). All images are normalized for comparability and scale bars are 50 μm.

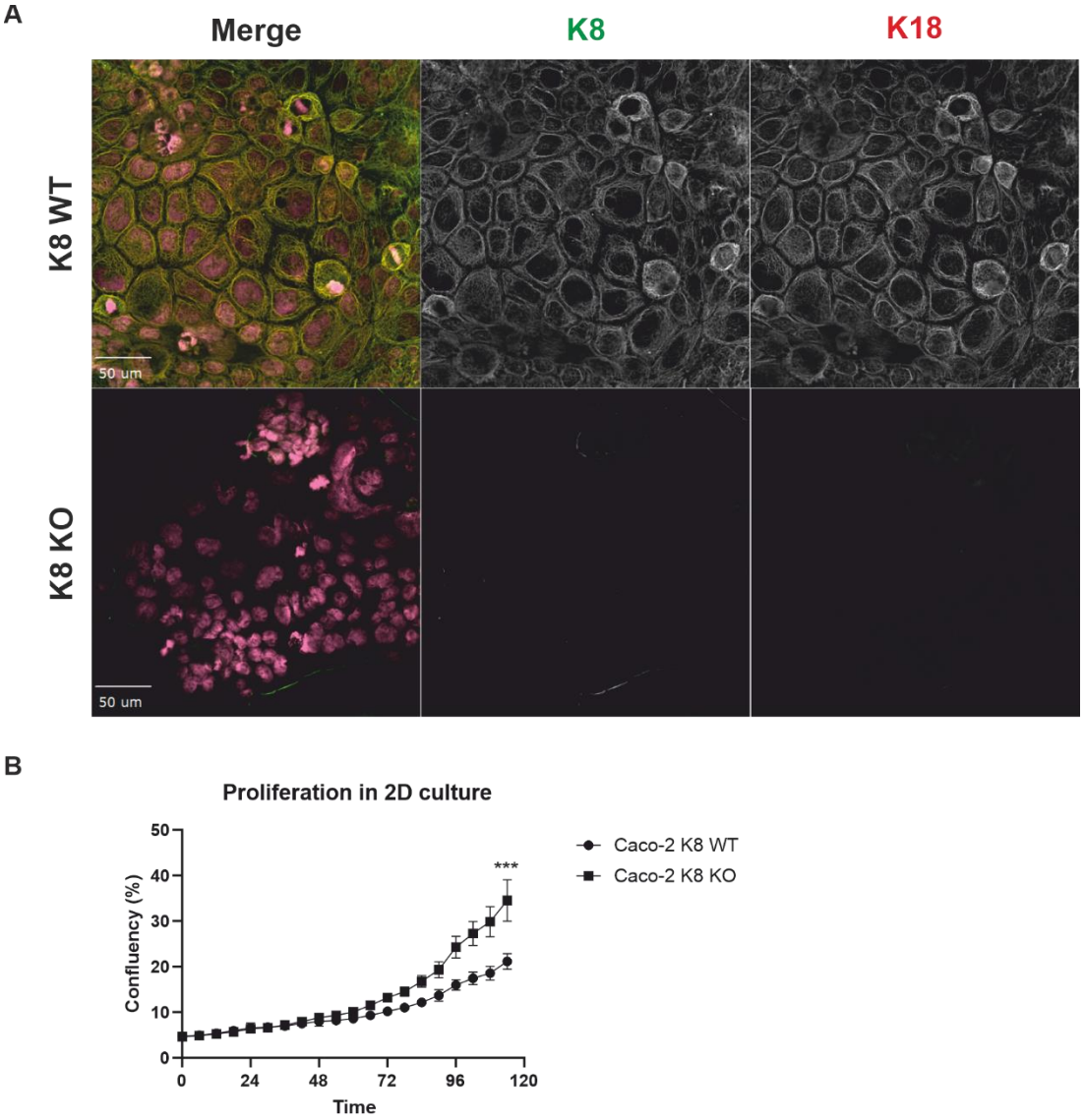

Supplemental figure 2. Keratin staining and 2D proliferation. (**A**) CRISPR K8 WT and K8 KO cells were stained for K8 (green) and K18 (red) coupled with a merged channel with Draq5 nuclear stain. (**B**) Proliferation curves of Caco-2 CRISPR K8 WT and K8 KO cell lines show a faster growth for the K8 KO. The curves show the average confluency of 15 wells/cell line imaged for five days. The confluency was calculated based on the analysis tool included in the Incucyte S3 software. Two-way analysis of variance (ANOVA) was used to assess the statistical significance. (P*** < 0.001).

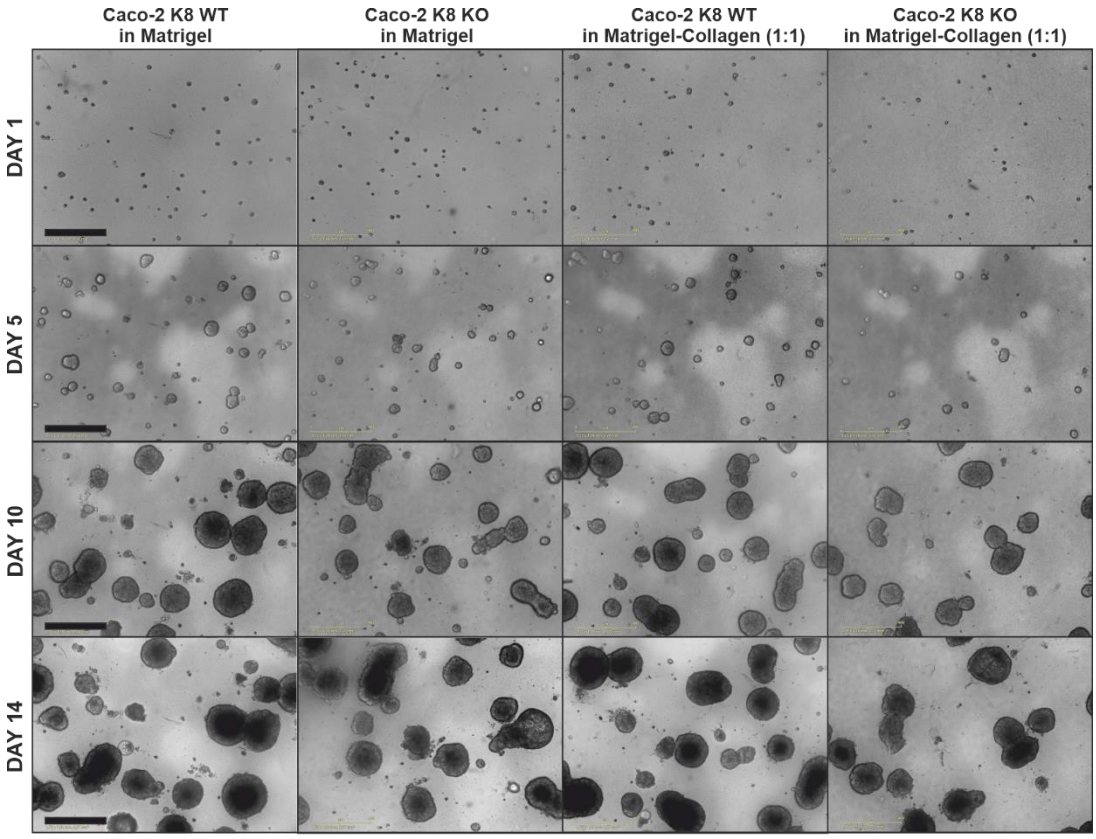

Supplemental figure 3. Incucyte data of 3D-growth of Caco-2 K8 KO spheroids grown for 14 days. Caco-2 K8 WT and K8 KO cells were plated in Matrigel and mixed Matrigel-Collagen (1:1). The scale bars are 400 μm.

12. Buffers and recipes

Cell culture

1 ml Collagen stock solution (3 mg/ml)

0.8 ml collagen (3.8 mg/ml)

0.1 ml 10x RPMI

0.1 ml Buffer: 40 ul 1 M HEPES

30 ul 7.5% $NaHCO_3$

16 ul 1 M NaOH

14 ul 1x PBS

Immunostaining

Paraformaldehyde

40 g PFA is dissolved in 1,000 ml 1x PBS

4-6 drops of 1 M NaOH

Dissolved during heating and stirring, filtration with coffee filter

Stored in -20 ºC before use

Wash buffer

0.2% Triton X-100

0.05% Tween20 dissolved in 1x PBS

Permeabilization solution

0.5-0.7% Triton X-100 dissolved in 1x PBS

Blocking solution

2.5% Bovine serum albumin

2% Donkey serum

2% Goat serum dissolved in 1x PBS

Western blotting

Homogenization buffer

0.0187 M (pH 6.8) Tris-HCl

5 mM EDTA

10% Ammonium persulfate (APS)

1 g APS dissolved in 10 ml distilled H_2O

Running gel stock (pH 8.8)

90.75 g Tris-Base dissolved in 100 ml distilled H_2O

pH is adjusted to 8.8 and diluted to 500 ml with distilled H_2O

Stacking gel stock (pH 6.8)

30.25 g Tris-Base dissolved in 100 ml distilled H_2O

pH is adjusted to 6.8 and diluted to 500 ml with distilled H_2O

3x Laemmli sample buffer

30% Glycerol

3% SDS

0.015% Bromphenol blue

3% B-mercaptoethanol (added prior to use)

0.1875 M Tris-HCl pH 6.8

20% SDS

20 g SDS dissolved in 1,000 ml distilled H_2O

Running gel

Recipe for two 1 mm gels				
Acrylamide concentration	*6%*	*8%*	*10%*	*15%*
Lower gel stock (pH 8.8)	*2.25 ml*	*2.25 ml*	*2.25 ml*	*2.25 ml*
20% SDS	*0.045 ml*	*0.045 ml*	*0.045 ml*	*0.045 ml*
Acrylamide	*1.8 ml*	*2.4 ml*	*3.0 ml*	*4.5 ml*
Distilled H_2O	*4.95 ml*	*4.4 ml*	*3.75 ml*	*2.205 ml*
10% APS	*0.06 ml*	*0.06 ml*	*0.06 ml*	*0.06 ml*
TEMED	*0.006 ml*	*0.006 ml*	*0.006 ml*	*0.006 ml*

Stacking gel

Recipe for two 1 mm gels	
Upper gel stock (pH 6.8)	*1.25 ml*
20% SDS	*0.025 ml*
Acrylamide	*0.75 ml*
Distilled H_2O	*3.0 ml*
10% APS	*0.02 ml*
TEMED	*0.01 ml*

10 x Running buffer

60 g Tris-Base

288 g Glycine dissolved in 2,000 ml distilled H_2O

Running buffer

140 ml 10x Running buffer

10 ml 20% SDS

Distilled H_2O added up to 1,400 ml

Transfer buffer

160 ml 10x Running buffer

10 ml 20% SDS

400 ml Methanol

Distilled H_2O added up to 1,600 ml

Wash buffer

4 ml Tween20 is dissolved in 2,000 ml 1x PBS